Technische Universität München

Fakultät für Medizin

Regulation of immune effector cells by myeloid cells in solid and hematological tumors

Tobias Manuel Baumann

Vollständiger Abdruck der von der Fakultät der Medizin der Technischen Universität München zur Erlangung des akademischen Grades eines Doktors der Naturwissenschaften (Dr. rer. nat.) genehmigten Dissertation

Vorsitzender: Prof. Dr. Radu Roland Rad

Prüfende der Dissertation:
1. Prof. Dr. Percy A. Knolle
2. apl. Prof. Dr. Farhah Assaad-Gerbert
3. Prof. Dr. Thomas Brocker

Die Dissertation wurde am 01.04.2021 bei der Technischen Universität München eingereicht und durch die Fakultät für Medizin am 10.08.2021 angenommen.

Table of Contents

Zusammenfassung

Neue Krebs Behandlungen wie die Immun-Checkpoint-Blockade (ICB) zielen darauf ab die Immunität gegen den Tumor wiederherzustellen und wurden während des letzten Jahrzehnts erfolgreich zur klinischen Anwendung gebracht. Jedoch wurde das Vorhandensein regulatorischer Zellen, die als MDSCs (engl. Myeloid-derived suppressor cells) bezeichnet werden, im Tumorgewebe mit Therapieversagen assoziiert. In dieser Dissertation wurde die Inhibition zytotoxischer $CD8^+$ T Zellen durch MDSCs untersucht. MDSCS übertrugen das reaktive Dicarbonyl Methylglyoxal (MGO), welches durch die enzymatische Aktivität der SSAO (engl. semicarbazide-sensitive amine oxidase) angereichert wurde, in direktem Zell-Kontakt auf $CD8^+$ T Zellen. Durch den MGO Transfer wurden $CD8^+$ T Zellen paralysiert, das bedeutet sie waren nach Stimulation mit CD3/28 nicht in der Lage mit der Aktivierung assoziierte metabolische Merkmale hochzuregulieren, zu proliferieren oder entzündungs-fördernde Zytokine (Botenstoffe) zu bilden. Die Neutralisierung von MGO durch Dimethylbiguanid (DMBG) schützte $CD8^+$ T Zellen vor der Suppression durch MDSCs. Folglich ermöglichte die Ergänzung einer ICB Behandlung (anti-PD-1) mit DMBG die Ausbildung einer T Zell Immunität und zeitweise Tumorkontrolle in einem Mausmodell des Melanoms. Diese Experimente enthüllen einen bislang unerkannten Suppressions-Mechanismus, welcher entscheidend für eine erfolgreiche Immunbehandlung in soliden Tumoren ist, und identifizieren MGO und SSAO als neue funktionelle Biomarker für MDSCs.

In weitergehenden Experimenten wurde der Fokus der Forschung auf hämatologischen Krebs ausgeweitet. Hier konnten wir zeigen, dass zirkulierende Zellen der akuten myeloischen Leukämie (AML-Blasten) in der Lage sind NK Zellen in ihrer Effektor-Funktion zu inhibieren. AML-Blasten von Patienten mit diversen Genotypen, mit unterschiedlichen zytomorphologischen Ausprägungen (klassifiziert nach dem French-American-British System, FAB), bei Erstdiagnose als auch nach Rezidiv wirkten gleichermaßen suppressiv auf NK Zellen in co-Kultur. Mechanistisch zeigte sich, dass von AML-Blasten sezerniertes Prostaglandin E2 (PGE2) die Effektor-Funktionen der NK Zellen beeinträchtigte. Die Blockierung der PGE2 Produktion mittels eines Wirkstoffs, der die Cyclooxygenase hemmt (Celecoxib), konnte folglich den suppressiven Effekt der AML-Blasten auf NK Zell Funktionen *in vitro* vermindern.

Zusammengenommen tragen die in dieser Dissertation präsentierten Ergebnisse zu einem besseren Verständnis der Immunsuppression in soliden und hämatologischen Tumoren bei und eröffnen neue therapeutische Ansätze, welche in künftige Immuntherapien implementiert werden können.

Summary

New cancer treatments like immune checkpoint blockade (ICB) aim to restore anti-tumor immunity and have successfully been translated into clinics within the last decade. However, the presence of regulatory cells denoted as myeloid-derived suppressor cells (MDSCs) in the tumor microenvironment (TME) was associated with failure of such immune therapies. In this thesis, the suppression of cytotoxic $CD8^+$ T cells by MDSCs was investigated. MDSCs transferred the reactive dicarbonyl methylglyoxal (MGO), which was accumulated by the enzymatic activity of semicarbazide-sensitive amine oxidase (SSAO), in direct cell-contact to $CD8^+$ T cells. Because of MGO transfer, $CD8^+$ T cells were paralyzed, i.e. they were unable to up-regulate metabolic features associated with activation, to proliferate or to produce pro-inflammatory cytokines in response to CD3/28 stimulation. Neutralization of MGO via dimethylbiguanide (DMBG) protected $CD8^+$ T cells from MDSC-mediated suppression. Accordingly, the complementation of an ICB treatment (anti-PD-1) with DMBG enabled T cell immunity and temporary tumor control in a mouse melanoma model. These experiments reveal a so far unrecognized mechanism of suppression that is critical for successful immunotherapy and identify MGO and SSAO as new functional biomarkers for MDSCs.

In further experiments the research focus was expanded to hematological cancer. Here we were able to show that acute myeloid leukemia cells (AML blasts), circulating in AML patients during acute disease, inhibited the effector function of NK cells. This inhibitory effect on NK ells was detected in co-culture with AML blasts from patients with diverse genotypes, with diverse cell morphology (classified according to the French-American-British system, FAB), at first diagnosis and after relapse. Mechanistically, prostaglandin E2 (PGE2) that was secreted by AML blasts impaired the effector functions of NK cells. Accordingly, blocking PGE2 production via a drug targeting cyclooxygenase (celecoxib) diminished the suppressive effect of AML blasts on NK cell functions *in vitro*.

Together, the experiments presented in this thesis contribute to a better understanding of immune suppression in solid and hematological tumors and offer new therapeutic approaches that can be translated into clinic and implemented into future immunotherapies.

1. Introduction

Cancer is the second leading cause of death globally with more than 9.9 million deaths in 2020, according to the WHO (World Health Organization, 2020). Most frequently cancer is treated by surgery, radiotherapy or chemotherapy. Besides intensive side effects, the down-side of radio- and chemotherapy is an increased risk to develop a second cancer of the hematopoietic system initiated by the treatment (Shallis et al., 2019). Additionally, recurrence with established treatments is still frequent in many cancer entities (Mahvi et al., 2018).

In recent decades, the potential of immune cells to recognize and destroy tumor cells was in the focus of new anti-cancer therapies (Robert, 2020). The overall goal of immunotherapies is to restore or induce the ability of certain immune cell types to orchestrate the immune destruction of tumors with surgical precision, at the same time sparing healthy tissue from deleterious side effects. While chemotherapies are suited to affect dividing cells and therefore often lack to eradicate dormant cancer cells, the immune system does not underlie such limitations. Additionally, immune memory might prevent recurrence of tumor growth long after discontinuation of treatment. In advanced/metastatic malignant melanoma, one of the most aggressive types of cancer, durable long-term remission after discontinuation of immune treatment has been observed in a minority of patients, raising hope to cure previously incurable cancer in future (Robert et al., 2017).

Immunotherapies such as the application of monoclonal antibodies, immune checkpoint blockade therapies (ICB) or the treatment with autologous chimeric antigen receptor (CAR) T cells are prominent examples that successfully translated into clinics (Khalil et al., 2016). A breakthrough in the field of immunotherapy that brought this field of research to broad attention in the science community and into public awareness was the development of immune checkpoint blockade (ICB) therapies, starting with the FDA approval of ipilimumab (anti-CTLA-4) in 2011 (Robert, 2020). In principle, activated immune cells up-regulate checkpoint receptors like cytotoxic T-lymphocyte-associated protein 4 (CTLA-4) and programmed death protein 1 (PD-1) that upon recognition of its cognate ligands render T cells unresponsive to further stimulation and are meant to prevent excessive immune damage. Tumor cells and tumor-associated cells hijack this mechanism and frequently express checkpoint ligands like PD-L1, that upon recognition by activated $CD8^+$ T cells dampen its anti-tumor effector functions. In ICB therapies, antibodies against CTLA-4, PD-1 or PD-L1 are applied, which take away this break from the

immune system (Hargadon et al., 2018). Immune checkpoint inhibitors have been approved for the treatment of multiple solid cancer entities (Hargadon et al., 2018).

However, only a fraction (20-40%) of patients responds to ICB therapy whereas others do not benefit (Gauci et al., 2019; Park and Youn, 2019). Infiltration of tumors with helper type 1 (T_H1) $CD4^+$ T cells, cytotoxic $CD8^+$ T cells, γδ T cells, natural killer (NK) cells and conventional type 1 dendritic cells (cDC1) is generally associated with anti-cancer immunity and favorable prognosis in many cancer types (Böttcher and Reis e Sousa, 2018; Fridman et al., 2012; Gentles et al., 2015). Accordingly, patients with favorable immune cell infiltration and high tumor mutational burden (TMB), possibly representing more immunogenic tumors, are more likely to respond to immune treatment (Barry et al., 2018; Binnewies et al., 2018; Salmon et al., 2016; Schumacher et al., 2019). In contrast, immune suppressive mediators like prostaglandin E2 (Bonavita et al., 2020), the infiltration of regulatory T cells (Treg) (Tanaka and Sakaguchi, 2017) or myeloid-derived suppressor cells (MDSCs) (Gebhardt et al., 2015; Martens et al., 2016; Meyer et al., 2014; Sade-Feldman et al., 2016; Weber et al., 2016) is hindering the induction of successful anti-cancer immunity and associated with non-responsiveness to immune therapy.

It is therefore of urgent need to better understand the immune suppressive mechanisms employed by tumor cells and tumor-associated regulatory cells to improve and complement existing immune therapies in the future.

1.1 Anti-tumor immunity

1.1.1 Orchestration of anti-cancer immunity

The immune-mediated clearance of a tumor cells is a multistep process that depends on the successful interplay of several immune cell types. Of upmost importance in anti-cancer immunity is the interplay of NK cells, cDC1, cytotoxic $CD8^+$ T cells and conventional helper $CD4^+$ T cells and excluding or suppressing one or several of these players might decide between tumor growth and tumor regression (Bonavita et al., 2020; Böttcher et al., 2018). NK cells and other innate immune cells are found in tumors early and represent the first line of defense. Activation of NK cells by perception of stimulating ligands on tumor cells leads to the secretion of cDC1-attracting chemokines CCL5 and XCL1 (Böttcher et al., 2018). cDC1s recruited to the tumor microenvironment (TME) take up antigens released from dying tumor cells and migrate to the draining lymph node, where initial priming of cytotoxic $CD8^+$ T cells and

helper CD4⁺ T cells commence by cross-presentation of exogenous antigens on MHC class I or classical presentation on MHC class II, respectively. In a second priming step, CD8⁺ T cell stimulation is further amplified by the assistance of helper CD4⁺ T cells. Activated CD4⁺ T cells aid stimulating CD8⁺ T cells by enhancing the expression of co-stimulatory ligands on cDC1 in a CD40-CD40L mediated process referred to as DC licensing and by secretion of the stimulatory cytokines IL-2 and IL-21 (Ahrends and Borst, 2018). Priming of CD8⁺ T cells by licensed cDC1 lowers the threshold for the interaction strength of the TCR with its cognate peptide presented on the dendritic cell, thereby broadening the repertoire of tumor-specific cytotoxic CD8⁺ T cell clones (Surman et al., 2000; Wong et al., 2008). Additionally, licensing is considered a critical step for the establishment of T cell memory (Ahrends and Borst, 2018). DC-mediated priming of CD8⁺ T cells causes the clonal amplification and differentiation into fully armed effector CD8+ T cells, which are attracted to the tumor via cDC1-derived chemokines CXCL9 and CXCL10 to launch a cytotoxic response against cancer cells. Pro-inflammatory cytokines like IFN-γ and IL-12 released from effector T cells, NK cells and cDC1 further support anti-cancer immunity (Figure 1) (Böttcher and Reis e Sousa, 2018). However, to initiate successful anti-cancer immunity, not only a favorable composition of immune cells is necessary but also the metabolic environment is strongly implicated in immune cell survival, activation, proliferation, and cytokine production.

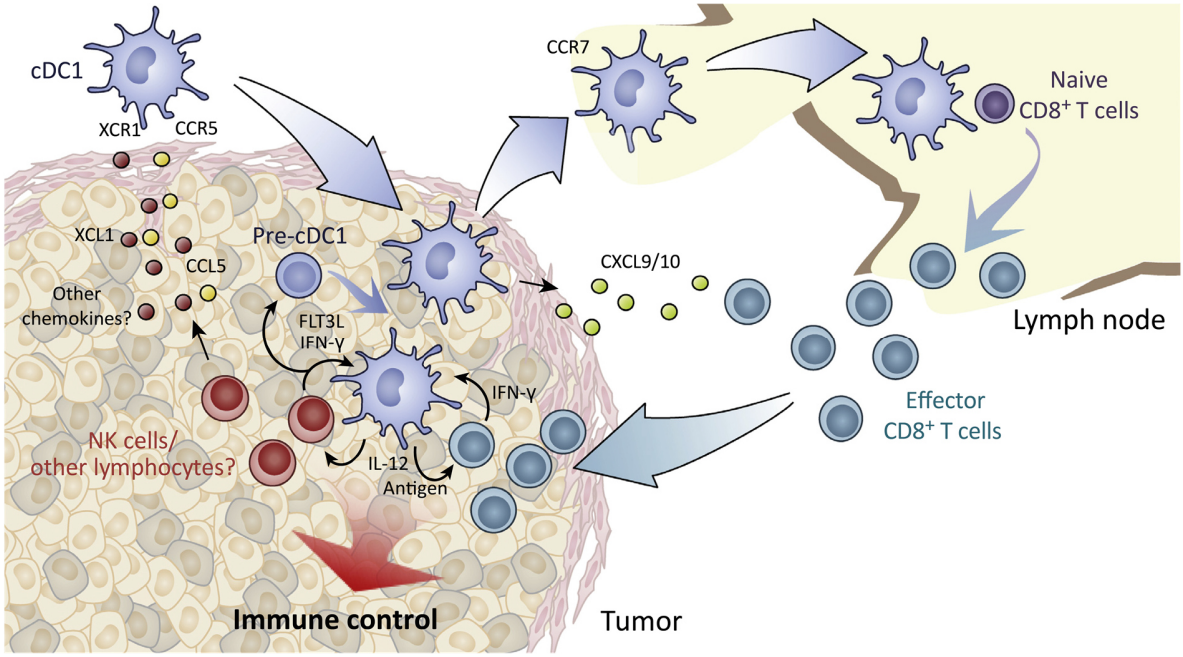

Figure 1: Interplay of immune cells in anti-cancer immunity. NK cells and possibly other lymphocytes present at the site of tumor attract cDC1 via secretion of the chemokines XCL1 and CCL5 and support DC maturation via secretion of the growth factor FLT3L. Tumor antigens are taken up by cDC1 and transported to tumor draining lymph nodes. Cross-presentation of tumor antigens primes naïve CD8⁺ T cells and initiates clonal proliferation. Amplified effector CD8⁺ T cells are recruited to the

tumor via cDC1-derived chemokines CXCL9/10. Local re-stimulation of effector $CD8^+$ T cells and IL-12 secretion by cDC1 further boosts anti-tumor immunity. Figure from: Böttcher and Reis e Sousa, *The Role of Type 1 Conventional Dendritic Cells in Cancer Immunity*, Trends in Cancer 4(11):784-792, 2018, ©Elsevier.

1.1.2 Immunometabolism

Most immune cells undergo substantial metabolic re-programming upon activation and distinct T cell subsets have various metabolic demands depending on the state of activation and differentiation (Pearce et al., 2013). The main metabolic pathways that have been studied in immune cells are glycolysis, amino acid metabolism, the tricarboxylic acid (TCA) cycle, fatty acid oxidation (FAO), fatty acid synthesis (FAS) and the pentose phosphate pathway (PPP) (O'Neill et al., 2016). Resting, naïve $CD8^+$ T cells are metabolically quiescent and mainly engage in mitochondrial oxidative phosphorylation (OXPHOS) to produce energy for homeostasis (Pearce et al., 2013). During oxidative phosphorylation, acetyl-CoA derived from the glycolytic product pyruvate or from oxidized fatty acids is used to fuel the TCA cycle under consumption of oxygen. The cells energy currency is adenosine triphosphate (ATP) and one molecule of glucose yields app. 30 molecules of ATP when metabolized completely in the TCA cycle to H_2O and CO_2 (Alberts et al., 2008). Even though yielding much less ATP (2 ATP molecules per molecule glucose), activated effector T cells switch to a metabolic program called aerobic glycolysis, which describes a metabolic configuration in which most glucose is diverted into glycolytic intermediates or lactate and not feeded into the TCA cycle even in the presence of oxygen (Pearce et al., 2013). Carbon intermediates of glycolysis serve as building blocks for amino acids, lipids and nucleotides and enable clonal proliferation and cytokine production. In memory T cells, FAO provides energy for longevity and upon encounter of the same antigen glycolysis can rapidly be upregulated to allow macromolecule synthesis and clonal proliferation (Figure 2) (Guerra et al., 2020). Also among $CD4^+$ T cells, different subsets (T_H1, T_H2, T_H17, Treg) require unique metabolic pathways to serve their functions (Guerra et al., 2020). In analogy, myeloid cells use distinct metabolic programs depending on their polarization. Pro-inflammatory M1 macrophages are more glycolytic and have a unique mitochondrial configuration that assists in the production of nitric oxygen (NO), the antimicrobial itaconate and the cytokine IL-1β whereas anti-inflammatory M2 macrophages use metabolic intermediates for post-translational modifications (PTM) and epigenetic modifications connected to M2 function (Mehta et al., 2017; Moon et al., 2015).

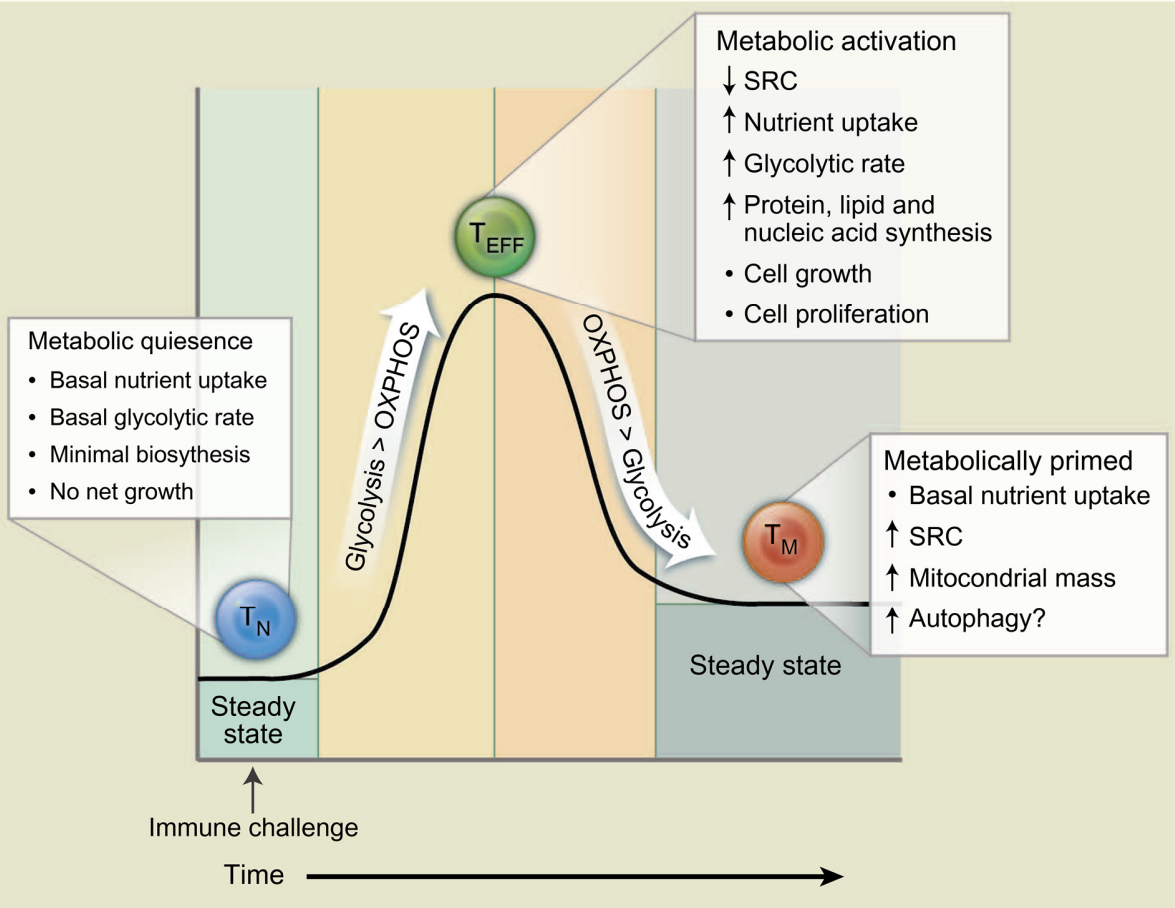

Figure 2: Metabolic reprogramming of T cells during an immune response. Metabolically quiescent naïve T cells (T_N) take up low amounts of nutrients and use OXPHOS to provide ATP for survival. Activation of T cells induces up-regulation of nutrient transporter and increased uptake of amino acids and glucose to enable clonal proliferation. The mitochondrial spare respiratory capacity (SRC), indicative of OXPHOS, is decreased in effector T cells (T_{EFF}) and glucose is the primary fuel for energy production. During transition of T_{EFF} into memory T cells (T_M) nutrient uptake is reduced and fatty acid oxidation is the primary source of energy to ensure longevity. T_M are metabolically primed as indicated by higher mitochondrial mass and can rapidly upregulate glycolysis upon second antigen exposure. Figure from: Pearce et al., *Fueling Immunity: Insights into Metabolism and Lymphocyte Function*, Science 342, 1242454, 2013. Reprinted with permission from AAAS.

Furthermore, direct connections between the metabolic configuration and effector functions of cells exist. In a study from 2013, Chang and colleagues demonstrated that the glycolytic enzyme glyceraldehyde 3-phosphate dehydrogenase (GAPDH) is directly implicated in T cell cytokine production. In resting state, GAPDH is bound to the 3' untranslated region (UTR) of the IFN-γ and IL-2 mRNAs, thereby preventing its translation. Upon activation, the glycolytic flux of T cells is up-regulated, leading to the dissociation of the GAPDH-mRNA complex and initiation of cytokine translation (Chang et al., 2013). With the same mechanism the cytokines IL-2, IFN-γ and TNF are controlled by lactate dehydrogenase (LDH) in T cells (Menk et al., 2018) and TNF translation by GAPDH in monocytes (Millet et al.). Both, the glycolytic enzyme pyruvate kinase M2 (PKM2) and the TCA cycle metabolite succinate

control IL-1β transcription in macrophages (Palsson-McDermott et al., 2015; Tannahill et al., 2013). The expression of the Treg-defining transcription factor forkhead box P3 (FOXP3) is controlled by the glycolytic enzyme enolase-1 (De Rosa et al., 2015) and the glycolytic metabolite phosphoenolpyruvate (PEP) is involved in sustained Ca^{2+} signaling in activated T cells (Ho et al., 2015).

In glucose deprived conditions, T cells produce less cytotoxic molecules perforin and granzyme B and less IFN-γ (Cham et al., 2008). L-tryptophan deprivation sensitizes T cells to apoptosis mediated by the death receptor FAS (Lee et al., 2002) and L-arginine starvation limits the expression of the T cell receptor (TCR) signaling element CD3-ζ chain and proliferation of activated $CD8^+$ T cells *in vitro* (Rodriguez et al., 2002, 2007). Moreover, the rapid uptake of glutamine by activated T cells is indispensable for proliferation, cytokine production and the transition of $CD4^+$ T cells into pro-inflammatory T_H1 and T_H17 cells (Carr et al., 2010; Nakaya et al., 2014). Accordingly, the function and differentiation or polarization of immune cells is intrinsically tied to the metabolic configuration. On the one hand, activation of immune cells alters the demand for glucose, fatty acids, amino acids and oxygen. On the other hand, changes in the nutrient concentration of an environment directly affects the activity of immune cells, as outlined in the following section.

1.2 Immune dysfunction in cancer

In cancer diseases, an emerging hallmark of tumor cells is immune evasion (Hanahan and Weinberg, 2011) and frequently dysfunctional or exhausted immune cells are observed in the microenvironment of tumors. Diverse mechanisms exploited by tumor cells and cells of the tumor stroma to suppress immune cell activation, survival or migration have been described. These mechanisms can be broadly divided into four categories: (1) metabolic restrictions of the tumor microenvironment (TME) due to the metabolic competition of immune cells with tumor cells and enzymatic depletion of amino acids; (2) the release of immunomodulatory small molecules and peptides / proteins interfering with immune cell activation; (3) receptor-ligand mediated suppression of immune cells (“immune checkpoints”) and (4) the accumulation of regulatory immune cells in the TME.

1.2.1 Metabolic restrictions in the tumor microenvironment

The TME is an environment densely packed with rapidly dividing tumor cells and scarce in oxygen, glucose and amino acids. Excessive lactate produced by tumor cells is exported via monocarboxylate transporters (MCTs) and acidifies the environment. Consequently, the TME is hypoxic, acidic, and

nutrient depleted and hostile to infiltrating immune cells. Furthermore, reactive oxygen species (ROS) produced by tumor cells induce oxidative stress to immune cells (Figure 3).

Tumor cells are metabolically adapted to survive in the TME and reprogram towards a state of aerobic glycolysis (DeBerardinis and Chandel, 2020). Using glucose as primary fuel for energy production allows for survival and proliferation in hypoxic regions of the tumor. Additionally, intermediates of glycolysis are used to produce amino acids, lipids and nucleotides, thus supporting the synthesis of macromolecules and assisting cellular division. Stabilization and overexpression of hypoxia inducible factor 1 alpha (HIF1α) facilitates the shift from OXPHOS to glycolysis by upregulation of glycolytic genes. Both, hypoxia and oncogenes like RAS increase HIF1α levels. Additionally, the expression of glucose transporter is increased in many tumors to outcompete non-tumor cells in glucose depleted environments (Hanahan and Weinberg, 2011). Within tumors, metabolic heterogeneity assures survival in regions of various oxygen and nutrient levels. In some tumors, subpopulations of tumor cells are locally separated and grow in symbiotic relationship. One subpopulation converts glucose to lactate in hypoxic regions and a second population fuels parts of the TCA cycle with lactate in oxygen rich regions (Kim and DeBerardinis, 2019).

Immune cells on the other hand are not as well adapted to nutrient depleted, acidic and hypoxic environments, and often fail to elicit appropriate immune responses against tumor cells in the TME. Cheng and colleagues showed in a mouse sarcoma model that tumor infiltrating lymphocytes (TIL) compete with tumor cells for glucose and that glucose deprivation dampens IFN-γ secretion, glycolytic activity and mTOR signaling in $CD8^+$ T cells (Chang et al., 2015). Lactic acidosis derived from excessive glycolysis induces mitochondrial dysfunction in tumor-resident NK cells and diminishes IFN-γ production and cytolytic activity (Harmon et al., 2019; Husain et al., 2013; Pötzl et al., 2017). Additionally, lactate interferes with NK and T cell activation and correlates with reduced survival in melanoma patients (Brand et al., 2016). On a functional level, pathologic concentrations of lactate prevented the up-regulation of nuclear factor of activated T cells (NFAT) in T and NK cells and diminished IFN-γ production (Brand et al., 2016). L-arginine is a critical amino acid in $CD8^+$ T cells that promoted the development of central memory-like T cells with high survival capacity and strong anti-tumor response in a mouse model (Geiger et al., 2016). However, arginine is heavily depleted in the TME via arginase 1 (ARG1)- and inducible nitric oxide synthase (iNOS) mediated enzymatic catabolism, which is mostly expressed by tolerogenic myeloid cells of the TME (Bronte et al., 2003). Similarly, L-tryptophan is degraded by indoleamine-2,3-oxygenase (IDO) activity expressed by certain tumor

types and regulatory cells (Opitz et al., 2011). IDO activity results in L-kynurenine accumulation, a metabolite further limiting effector T and NK cell proliferation (Frumento et al., 2002), promoting Treg generation (Mezrich et al., 2010) and impairing NK cell cytotoxicity via down-regulation of activating receptors (Chiesa et al., 2006). Besides, limitation of amino acids prevents the activation of the signaling complex mammalian target of rapamycin complex 1 (mTORC1) and stabilization of the transcription factor MYC, which are key regulator of metabolic re-programming in activated $CD8^+$ T cells and NK cells (O'Brien and Finlay, 2019; Shyer et al., 2020). Hypoxia induces the down-regulation of multiple stimulatory receptors and cytotoxic molecules and impairs cytotoxicity of NK cells (Balsamo et al., 2013; Fink et al., 2003; Sarkar et al., 2013). And even though moderate intracellular concentrations of ROS serve signaling functions mandatory for T cell activation, high concentrations of environmental ROS often found in tumors impair metabolic reprogramming and development of T effector cells (Guerra et al., 2020).

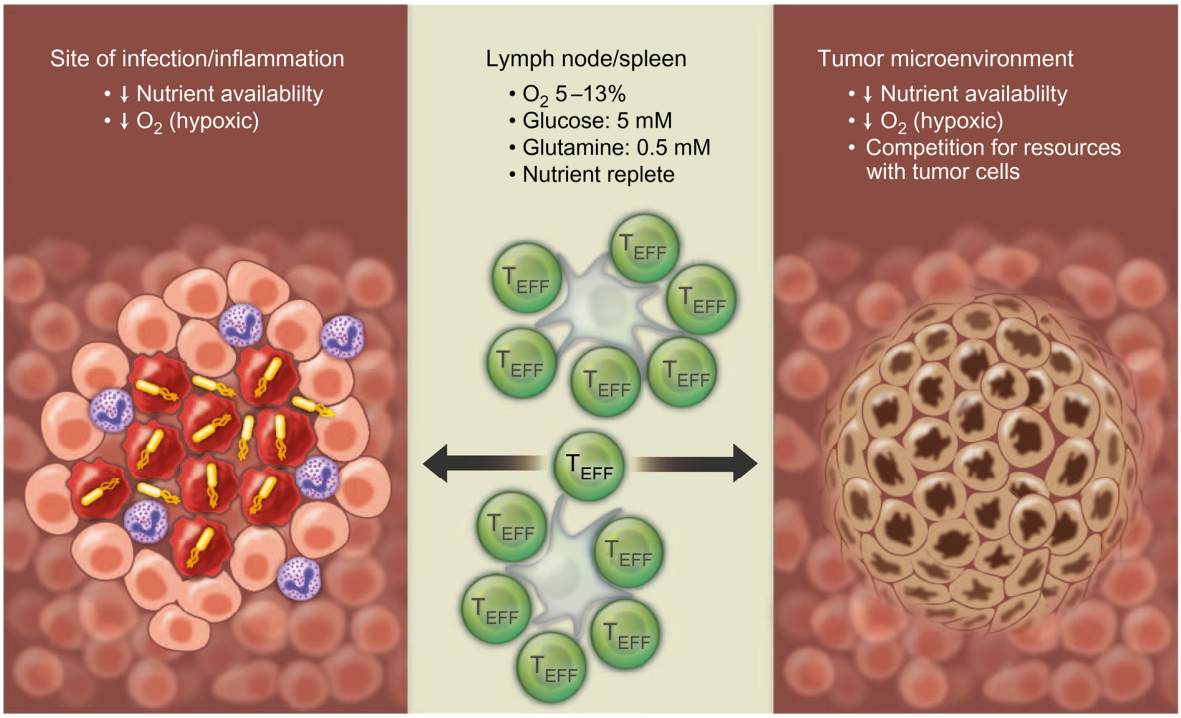

Figure 3: T cells are exposed to diverse metabolic environments. Lymphoid tissue is considered nutrient replete and oxygen rich, allowing for optimal immune cell activation and proliferation. At sites of chronic inflammation (infection or tumor microenvironment) nutrient availability is limited. Neutrophils consume high amounts of oxygen and tumor cells compete with immune cells for amino acids and glucose. Furthermore, tumor vasculature is often insufficient to distribute oxygen evenly within tumors. Immune cells need to adapt to nutrient depleted environments or fail to elicit appropriate immune control. Figure from: Pearce et al., *Fueling Immunity: Insights into Metabolism and Lymphocyte Function*, Science 342, 1242454, 2013. Reprinted with permission from AAAS.

It has become evident, that the TME is a highly competitive environment in which tumor cells are often superior in adaptation to the microenvironment. There are multiple examples, how these adaptions simultaneously can help tumor cells to survive and proliferate while preventing on the other side immune cell activity. Accordingly, many strategies have been proposed or are currently tested to shift the hostile TME towards a more favorable environment for anti-tumor immunity (Guerra et al., 2020).

1.2.2 Secretion of immunomodulatory molecules

A second route to suppress immune cell activity in the TME is the release of soluble mediators, comprising mainly anti-inflammatory cytokines, metabolites and soluble ligands or receptors.

For example, the anti-inflammatory cytokine TGF-β is frequently found concentrated in the TME and induces the down-regulation of major genes involved in cytotoxicity (coding for granzyme A/B, perforin and FasL) and IFN-γ in cytotoxic T cells (Thomas and Massagué, 2005). Furthermore, conventional helper $CD4^+$ T cells are converted into regulatory T cells (Treg) under the influence of TME-derived TGF-β1 (Liu et al., 2007b). Systemic TGF-β1 neutralization or T cell specific blocking of TGF-β signaling enabled T cell dependent immune control in mouse models of thymoma and melanoma (Gorelik and Flavell, 2001; Thomas and Massagué, 2005). Platelets are a dominant source of activated TGF-β in the TME and contribute to the suppression of T cell proliferation and IFN-γ secretion (Rachidi et al., 2017). Accordingly, genetic deletion of a gene involved in TGF-β activation in platelets enabled tumor control by adoptively transferred T cells in mouse models of colon cancer and melanoma (Metelli et al., 2018; Rachidi et al., 2017). In NK cells, TGF-β1 induces the down-regulation of the activating receptors natural killer group 2D (NKG2D) and natural cytotoxicity triggering receptor 3 (NKp30) (Castriconi et al., 2003; Crane et al., 2010; Park et al., 2011). It blocks the cytokine-induced up-regulation of glycolysis and OXPHOS in NK cells and impairs effector functions like target cell killing and IFN-γ secretion (Viel et al., 2016; Zaiatz-Bittencourt et al., 2018). TGF-β1 is elevated in the plasma of human cancer patients and can be expressed membrane-bound on regulatory myeloid cells, thereby suppressing NK cell anti-cancer activity (Crane et al., 2010; Lee et al., 2004; Li et al., 2009). Together, TGF-β1 is an immune suppressive cytokine frequently found in tumors that inhibits multiple levels of anti-cancer immunity.

A second suppressive mediator with especially broad and strong immune modulating power is prostaglandin E2 (PGE2). The enzyme cyclooxygenase 2 (COX2) is a rate-limiting enzyme in the synthesis of PGE2 and frequently expressed by tumor cells or cells of the TME (Hashemi Goradel et al., 2019; Park et al., 2018). PGE2 is perceived by T cells, cDC1 and NK cells via receptors EP1-4, thereby

interfering with chemotaxis and effector functions. PGE2 inhibits IL-2 and IFN-γ production in $CD4^+$ T cells and impairs γδ T cell cytotoxicity (Martinet et al., 2010; Snijdewint et al., 1993). Furthermore, it promotes FOXP3 expression and regulatory activity of Tregs (Sharma et al., 2005). In melanoma mouse models, PGE2 has been shown to impair cDC1 responsiveness to chemo attractants and NK cell survival (Böttcher et al., 2018). PGE2 down-regulates the expression of activating receptors and inhibits functional maturation, cytotoxicity and IFN-γ secretion of NK cells (Martinet et al., 2010; Park et al., 2018). In a recent study, Bonavita and colleagues demonstrated that PGE2-mediated inhibition of IFN-γ secretion by NK cells shapes the tumor niche into an anti-inflammatory environment that fails to control tumor growth. Importantly, a molecular signature associated with PGE2 had independent prognostic utility in cancer and predicted unresponsiveness to ICB therapy with higher sensitivity compared to other established biomarkers (Bonavita et al., 2020).

1.2.3 Checkpoint inhibition

Apart from the release of soluble mediators, surface bound ligands and receptors add up to the suppressive machinery of tumor cells and stromal cells of the TME. To activate T cells successfully, TCR stimulation needs to be accompanied by a second co-stimulatory signal provided by antigen presenting cells (APCs). Usually, this is binding of CD28 on T cells to CD80/86 on APCs. Upon activation, T cells translocate so-called checkpoint molecules like programmed death protein 1 (PD-1) and cytotoxic T-lymphocyte-associated protein 4 (CTLA-4) to the cell surface. Perception of cognate ligands on APCs (PD-L1 / PD-L2 for PD-1 and CD80/86 for CTLA-4) dampens proliferation and effector functions of T cells to prevent overshooting immune damage in tissues (Khalil et al., 2016). Engagement of CTLA-4 on anti-CD3/28 stimulated T cells inhibits cell cycle progression and IL-2 accumulation (Krummel and Allison, 1996). Similarly, PD-L1 and PD-L2 inhibit proliferation and cytokine production of TCR stimulated T cells (Butte et al., 2007; Freeman et al., 2000; Latchman et al., 2001) and both receptors (CTLA-4 and PD-1) suppress glucose metabolism and AKT kinase signaling (Parry et al., 2005). Underlining the strong regulatory potential of immune checkpoint receptors, mice devoid of PD-1 develop signs of autoimmune diseases (Nishimura et al., 1999, 2001) and deletion of CTLA-4 causes fatal multi-organ destruction by self-reactive T cells (Tivol et al., 1995; Waterhouse et al., 1995).

However, tumor cells and tumor stroma cells hijack this regulatory mechanism to impair immune-mediated tumor clearance. Accordingly, tumor-associated PD-L1 expression is prognostic for several cancer entities, including renal cell, stomach, ovary, esophagus, pancreas and urothelial carcinoma (Okazaki and Honjo, 2007).

1.2.4 Regulatory cells

Immune effector cells are not only directly inhibited by tumor cells, but also regulatory immune cells accumulating in the tumor microenvironment strongly contribute to immune suppression. Among those, regulatory T cells (Treg) and myeloid-derived suppressor cells (MDSCs) are best studied. High frequencies of intratumoral Treg cells are usually associated with bad prognosis and several modes of Treg-mediated immune suppression have been described (Tanaka and Sakaguchi, 2017). Tregs express high levels of CTLA-4, thereby competing with conventional T cells for co-stimulation and inducing down-regulation of CD80/86 on APCs upon binding (Sethna et al., 1994; Takahashi et al., 2000). Tregs express the high affinity IL-2 receptor α chain (CD25) and induce proliferation stop and apoptosis of conventional T cells via IL-2 deprivation (Pandiyan et al., 2007). Additionally, Tregs transfer the immune-modulatory second messenger cyclic adenosine monophosphate (cAMP) to $CD4^+$ T cells and DCs, thereby suppressing IL-2 expression or co-stimulation, respectively (Bopp et al., 2007; Weber et al., 2013). Furthermore, the anti-inflammatory cytokines IL-10 and TGF-β1 have been associated with Treg-mediated suppression of conventional T cells (Asseman et al., 1999; Worthington et al., 2015).

The second group of regulatory cells frequently present in the tumor microenvironment are myeloid-derived suppressor cells (MDSCs), which have been recognized as major obstacle in the induction of successful anti-cancer immunity (Gabrilovich, 2017).

1.3 Myeloid-derived suppressor cells

Myeloid-derived suppressor cells (MDSCs) are myeloid cells with immune suppressive functions commonly found in the TME. It has become increasingly aware that MDSCs are main players in the defense of tumor cells against the immune system and substantial research has been made to identify drugs that target MDSCs in the TME (Gabrilovich et al., 2012). MDSCs have been found increased in the circulation of patients with hepatocellular carcinoma (Hoechst et al., 2008), pancreatic cancer (Porembka et al., 2012), gastric cancer (Wang et al., 2013a), prostate cancer (Vuk-Pavlović et al., 2010), colorectal carcinoma (OuYang et al., 2015), multiple myeloma (Brimnes et al., 2010), non-small-cell lung cancer (Liu et al., 2010), melanoma (Jordan et al., 2013) and many other solid tumors (Diaz-Montero et al., 2009).

The origin of MDSCs is often attributed to abnormal, sustained myelopoiesis in chronic inflammation or plastic adaptation of myeloid cells entering a chronically inflamed environment. Multiple growth

factors have been connected to MDSC generation in the bone marrow and attraction to the TME including vascular endothelial growth factor (VEGF), granulocyte colony stimulating factor (G-CSF) and granulocyte macrophage colony stimulating factor (GM-CSF). Other cytokines like IL-6 and IL-1β, damage-associated molecular patterns (DAMPs) like HMGB1 and S100A8/9 and metabolites like PGE2 are related to the suppressive function and survival of MDSCs in the TME (Ostrand-Rosenberg and Fenselau, 2018). However, our picture of the origin of MDSCs and adaptation to the microenvironment is likely still incomplete.

1.3.1 Phenotype and subtypes of myeloid-derived suppressor cells

For several decades immune suppressive myeloid cells in the TME have been described as null cells, natural suppressor, myeloid suppressor cells, immature myeloid cells or $GR1^+$ myeloid cells with diverse phenotypic definition (Talmadge and Gabrilovich, 2013). Today, most publications use the term MDSC and discriminate between two major subsets with distinct morphological and phenotypic traits: polymorphonuclear or granulocytic MDSCs (PMN-MDSCs / G-MDSCs) and monocytic MDSCs (M-MDSCs).

Whereas PMN-MDSCs are defined as $CD11b^+CD14^-CD66b^+$ or $CD11b^+CD14^-CD15^+$ in humans and $CD11b^+Ly6C^{low}Ly6G^+$ in mice, M-MDSCs are $CD11b^+CD14^+HLA\text{-}DR^{-/low}$ in humans and $CD11b^+Ly6C^{hi}Ly6G^-$ in mice (Bronte et al., 2016). However, currently applied gating strategies based on surface markers lack specificity to identify MDSCs unequivocally. Also, separation of PMN-MDSCs from granulocytes via density gradient centrifugation does not allow a clear discrimination (Bronte et al., 2016; Moses and Brandau). To date, only combinations of phenotypic and functional analysis allow definitive identification of MDSCs. To test for MDSC function, the suppressive effect of MDSCs on T cells is considered the gold standard, comprising the measurement of T cell proliferation or cytokine production in response to antigen- or anti-CD3/CD28-stimulation in the presence of MDSCs (Bronte et al., 2016).

One major goal in the field of MDSC biology is a specific, phenotypic identification of MDSCs in mixed populations of pro- and anti-inflammatory myeloid cells, for example in peripheral blood samples of cancer patients. Additionally, the staining of MDSCs and discrimination from monocytes, neutrophils and other myeloid cells in immunohistochemistry (IHC) is not possible to date (Bronte et al., 2016).

1.3.2 Known suppressive mechanism

Many suppressive mechanisms have been proposed for different MDSC subsets in various settings, including the production of molecular radicals, amino acid deprivation, induction of Tregs and interference with T cell homing. Main targets of MDSC-mediated suppression are NK cells (Hoechst et al., 2009; Li et al., 2009; Liu et al., 2007a) and T cells.

Two enzymes and their reaction products are frequently associated with MDSCs, ARG1 and iNOS. Both enzymes catalyze the degradation of L-arginine under production of reactive oxygen species (ROS, e.g. H_2O_2 or O^{2-}) and nitric oxide (NO), respectively. ARG1, iNOS, ROS and NO are independently associated with MDSC-mediated suppression of T cells (Donkor et al., 2009; Goh et al., 2016; Kusmartsev et al., 2004; Mazzoni et al., 2002; Rodriguez et al., 2005; Young et al., 1996). Additionally, ARG1 and iNOS together generate the radical species peroxynitrite, which covalently binds to the TCR complex, thereby preventing antigen recognition on MHC (Kusmartsev et al., 2000; Lu et al., 2011; Nagaraj et al., 2007). Furthermore, cysteine deprivation is connected to MDSC, thereby limiting the supply of T cells with an amino acid needed for glutathione synthesis, detoxification and redox balance (Srivastava et al., 2010). MDSCs support the accumulation of Tregs in tumor-bearing hosts (Huang et al., 2006; Schlecker et al., 2012; Serafini et al., 2008) and *in vitro* co-culture of conventional $CD4^+$ T cells with MDSCs induced the trans-differentiation into Tregs in a mechanism dependent on TGF-β1 and retinoic acid (Hoechst et al., 2008, 2011). Last, impaired homing of T cells to lymphoid tissue via shedding of L-selectin (CD62L) from naïve T cells is associated with MDSCs (Hanson et al., 2009; Ku et al., 2016).

1.3.3 MDSCs in cancer

Due to their versatile and strong suppressive effect on immune effector cells, MDSCs have emerged as a major prognostic factor in cancer. The numbers of MDSCs in the circulation and TME of patients are correlating with disease stage and survival in pancreatic adenocarcinoma (Porembka et al., 2012), gastric cancer (Wang et al., 2013a), melanoma (Jordan et al., 2013; Weide et al., 2014), colorectal carcinoma (OuYang et al., 2015) and diverse other solid tumor entities (Diaz-Montero et al., 2009). Also in a meta-analysis of 16 studies with 1864 cancer patients, MDSC frequencies were found to be a prognostic marker for disease-free and overall survival (Ai et al., 2018).

Importantly, MDSC frequencies are associated with therapy resistance to ICB. Meyer and co-workers identified the high frequency of M-MDSCs in the blood of melanoma patients as confounding factor

for the therapy resistance to anti-CTLA-4 (ipilimumab) in a subpopulation of patients (Meyer et al., 2014). These results have been confirmed for anti-CTLA-4 and anti-PD-1 by several other studies to date (Gebhardt et al., 2015; Martens et al., 2016; Sade-Feldman et al., 2016; Weber et al., 2016). Many clinical trials combining ICB therapy and drugs targeting MDSCs are ongoing to overcome MDSC mediated non-responsiveness (Park and Youn, 2019; Weber et al., 2018).

It is consensus, that future treatment strategies against cancer need to combine checkpoint inhibitors with drugs aiming to disarm other regulatory mechanism of the TME and/or drugs directly targeting the tumor cells to have best chances to control the disease.

1.4 Research topic and scientific approach

MDSCs have been termed the "Queen Bee of the TME" (Tesi, 2019) due to its strong suppressive effect and abundance in the tumor microenvironment of diverse tumor entities. MDSCs are a major obstacle in anti-cancer immune therapies and treatments aiming to disarm or deplete MDSCs in the TME as well as specific and easy to measure MDSC markers are urgently needed to identify patient cohorts that benefit most from MDSC-targeting therapies.

To this end, the research presented in this thesis aimed to better understand the molecular mechanism leading to MDSC-mediated $CD8^+$ T cell suppression and to identify possible drugs counteracting MDSC-mediated immune suppression. Additionally, a method for identification of MDSCs in immunohistochemistry is proposed. Collaboratively collected data within the group and by cooperation partners was integrated into a publication and several figures from this publication are depicted within this thesis (Baumann et al., Knolle and Höchst, *Regulatory myeloid cells paralyze T cells through cell–cell transfer of the metabolite methylglyoxal*, Nature Immunology 21(5):555-566, May 2020).

In a second step, the focus of research was expanded to hematological malignancies. Being aware of strong immune suppression in acute myeloid leukemia (AML), the suppressive effect of leukemia blasts on natural killer cells was investigated and treatments to alleviate the suppression were tested in an *in vitro* model (manuscript in preparation).

Together, these studies exemplify roadblocks in immune-mediated tumor eradication and will help to improve and complement existing immune therapies in the future.

2. Materials and Methods

2.1 Materials

2.1.1 Antibodies (anti-human)

Target	Clone	Manufacturer
Surface		
CD1c	L161	Biolegend or Sony Biotechnology
CD3	OKT3	Thermo Fisher Scientific
CD3	HIT3a	Biolegend or Sony Biotechnology
CD4	OKT4	Biolegend or Sony Biotechnology
CD8	SK1	Biolegend or Sony Biotechnology
CD11c	3.9	Biolegend or Sony Biotechnology
CD14	63D3	Biolegend or Sony Biotechnology
CD16	3G8	Biolegend or Sony Biotechnology
CD19	HIB19	Biolegend or Sony Biotechnology
CD20	2H7	Biolegend or Sony Biotechnology
CD24	ML5	Biolegend or Sony Biotechnology
CD25	BC96	Biolegend or Sony Biotechnology
CD27	M-T271	Biolegend or Sony Biotechnology
CD33	P67.6	Thermo Fisher Scientific
CD38	HB-7	Biolegend or Sony Biotechnology
CD40	5C3	Biolegend or Sony Biotechnology
CD45	HI30	Biolegend or Sony Biotechnology
CD45RA	HI100	Biolegend or Sony Biotechnology
CD45RO	UCHL1	Biolegend or Sony Biotechnology
CD56	HCD56	Biolegend or Sony Biotechnology
CD56	5.1H11	Biolegend or Sony Biotechnology
CD62L	REG-56	Biolegend or Sony Biotechnology
CD69	FN50	Biolegend or Sony Biotechnology
CD95	DX2	Biolegend or Sony Biotechnology
CD98	MEM-108	Life Technologies
CD107a	H4A3	Biolegend or Sony Biotechnology
CD123	6H6	Biolegend or Sony Biotechnology
CD127	A019D5	Biolegend or Sony Biotechnology
CD158/KIR	HP-MA4	Biolegend or Sony Biotechnology
CD197	G43H7	Biolegend or Sony Biotechnology
CD226/DNAM	11A8	Biolegend or Sony Biotechnology
CD274	19E.2A3	Biolegend or Sony Biotechnology
CD303	201A	Biolegend or Sony Biotechnology

CD314/NKG2D	1D11	Biolegend or Sony Biotechnology
CD335/NKp46	9E2	Biolegend or Sony Biotechnology
CD337/NKp30	AF29-4D12	Miltenyi Biotech
CX3CR1	2A9-1	Biolegend or Sony Biotechnology
Glut-1	polyclonal	Novus Biologicals
HLA-DR	L243	Biolegend or Sony Biotechnology
IgG	HP6017	Biolegend or Sony Biotechnology
IgM	MHM-88	Biolegend or Sony Biotechnology
LAP	FMLAP	Thermo Fisher Scientific
Intracellular		
c-myc	polyclonal	Cell Signaling Technologies
GzmB	GB11	Thermo Fisher Scientific
IFN-γ	4S.B3	Thermo Fisher Scientific
TNF	Mab11	Biolegend or Sony Biotechnology
Phospho-Antibodies		
p-AKT (Ser473)	SDRNR	Thermo Fisher Scientific
p-ERK1/2 (Thr202, Tyr204)	MILAN8R	Thermo Fisher Scientific
p-Lck (Tyr505)	SRRCHA	Thermo Fisher Scientific
p-mTOR (Ser2448)	MRRBY	Thermo Fisher Scientific
p-S6 (Ser235, Ser236)	cupk43k	Thermo Fisher Scientific
p-ZAP70/Syk (Tyr319, Tyr352)	n3kobu5	Thermo Fisher Scientific
Secondary		
Goat anti-Rabbit IgG Fab2	polyclonal	Cell Signaling Technologies
Blocking		
Anti-TGF-β	1D11	Thermo Fisher Scientific
Anti-PD-1	EH12.2H7	Thermo Fisher Scientific
Anti-PD-L1	MIH1	Thermo Fisher Scientific
Immunohistochemistry		
MG-H1	3D11	Cell Biolabs
SSAO / VAP-1	EPR10027	Abcam
Rabbit anti-Mouse IgG	M111-2	Abcam

2.1.2 Antibodies (anti-mouse)

Target	Clone	Manufacturer
Surface		
B7-H1	10F.9G2	Biolegend or Sony Biotechnology
CD3	145-2C11	Biolegend or Sony Biotechnology
CD4	RM4-5	Biolegend or Sony Biotechnology
CD8	53-6.7	Biolegend or Sony Biotechnology
CD11b	M1/70	Biolegend or Sony Biotechnology

CD11c	N418	Biolegend or Sony Biotechnology
CD25	PC61	Biolegend or Sony Biotechnology
CD44	IM7	Biolegend or Sony Biotechnology
CD45.1	A20	Biolegend or Sony Biotechnology
CD45.2	104	Biolegend or Sony Biotechnology
CD62L	MEL-14	Biolegend or Sony Biotechnology
F4/80	BM8	Biolegend or Sony Biotechnology
I-A/I-E	M5/114.15.2	Biolegend or Sony Biotechnology
Ly6C	4K1.4	Biolegend or Sony Biotechnology
Ly6G	1A8	Biolegend or Sony Biotechnology
MerTK	2B10C42	Biolegend or Sony Biotechnology
NK1.1	PK136	Biolegend or Sony Biotechnology
Intracellular		
Foxp3	FJK16S	Biolegend or Sony Biotechnology
IFN-γ	XM61.2	Biolegend or Sony Biotechnology
TNF	MP6-XT22	Biolegend or Sony Biotechnology
In vivo		
Anti-PD-1	29.F1A12	

2.1.3 Reagents

Reagent	Supplier
Cytokines	
Proleukin S (rhIL-2)	Novartis
rhTGF-β	Peprotech
rhu G-CSF	Peprotech
rhu IL-3	Peprotech
rhu thrombopoietin	Peprotech
Cell culture / In vitro co-culture	
12 well flat bottom tissue culture plate	Corning
24 well flat bottom tissue culture plate	TPP
2-mercaptoethanol	Sigma-Aldrich
96 well round bottom tissue culture plate	TPP
Dimethyl sufoxide (DMSO)	Serva Electrophoresis
DMEM medium	Thermo Fisher Scientific
FBS (fetal bovine serum)	PAN-Biotech
G418	Thermo Fisher Scientific
Horse serum	Sigma-Aldrich
L-Glutamine (100X)	Thermo Fisher Scientific
Penicillin/Streptomycin (100X)	Thermo Fisher Scientific
Poly-L-Lysine	Thermo Fisher Scientific

RPMI 1640 medium	Thermo Fisher Scientific
Transwell plate, 3 µm pore size	Corning
αMEM medium	PAN Biotech
Dyes for flow cytometry	
2-NBDG (2-N-(7-Nitrobenz-2-oxa-1,3-diazol-4yl)-Amino)-2-Deoxyglucose)	Cayman Chemicals
7-AAD (7-Aminoactinomycin D)	Thermo Fisher Scientific
Calcein-AM	Thermo Fisher Scientific
Cell proliferation dye eFluor 450	Thermo Fisher Scientific
Cell proliferation dye eFluor 670	Thermo Fisher Scientific
CFSE (carboxyfluorescein succinimidyl ester) proliferation dye	Thermo Fisher Scientific
DilC1(5)	Thermo Fisher Scientific
ER Tracker green	Thermo Fisher Scientific
Fixable viability dye AF488	Thermo Fisher Scientific
Fixable viability dye APC-eF780	Thermo Fisher Scientific
Fixable viability dye eFluor 450	Thermo Fisher Scientific
MBo (methyl diaminobenzene-BODIPY)	Gift from David Spiegel, Yale University
MitoTracker green	Thermo Fisher Scientific
PI (Propidium Iodide)	Thermo Fisher Scientific
Assay Kits	
Anti-PGE2 ELISA kit monoclonal	Cayman Chemicals
Anti-TGF-β1 ELISA	Thermo Fisher Scientific
ATP assay kit	Sigma-Aldrich
Bio-Rad DC Protein asasy	Bio-Rad Laboratories
Glyoxylase I activity assay kit	Sigma-Aldrich
GSH/GSSG-Glo assay kit	Promega
Hexokinase colorimetric assay kit	Sigma-Aldrich
Cell isolation from blood and tissue	
Bicoll	Biochrome
CD11b MicroBeads, mouse	Miltenyi Biotech
CD14 MicroBeads, human	Miltenyi Biotech
CD8 MicroBeads, human	Miltenyi Biotech
CD8a MicroBeads, mouse	Miltenyi Biotech
Collagenase IV	Sigma-Aldrich
Collagenase IV	Sigma-Aldrich
Human Pan T Cell Isolation Kit	Miltenyi Biotech
MagniSort human NK cell enrichment Kit	Thermo Fisher Scientific
Pancoll	PAN Biotech
Percoll	Thermo Fisher Scientific
RNA isolation and qPCR	

No Rox SYBR ® MasterMix dTTP Blue	Takyon
NucleoSpin RNA XS	Machery-Nagel
SensiFAST™ cDNA Synthesis Kit	Bioline
Flow cytometry staining	
Brefeldin A	Thermo Fisher Scientific
CountBright counting beads	Invitrongen
Foxp3 Fixation/Permeabilization Concentrate and Diluent	Thermo Fisher Scientific
IC fixation buffer	Thermo Fisher Scientific
Monensin	Thermo Fisher Scientific
Permeabilization buffer (10X)	Thermo Fisher Scientific
Seahorse / Extracellular Flux Analysis	
2-DG (2-deoxy-D-glucose)	Sigma-Aldrich
Antimycin A	Sigma-Aldrich
CCCP (carbonyl cyanide 3chlorophenylhydrazone)	Sigma-Aldrich
Glucose	AppliChem
Oligomycin	Sigma-Aldrich
Rotenone	Sigma-Aldrich
XF base medium minimal DMEM (wo phenol red)	Agilent
XF base medium minimal RPMI (wo phenol red)	Agilent
XF calibrant buffer	Agilent
XF96 cell culture microplate	Agilent
XF96 extracellular flux assay kit	Agilent
Chemical Agonists / Antagonists and other reagents	
Adenosine	Sigma-Aldrich
Anti-CD3/CD28 Dynabeads, human	Thermo Fisher Scientific
Celecoxib (COX2 inhibitor)	Cayman Chemicals
Dimethylbiguanide (DMBG / Metformin)	Sigma-Aldrich
L-161,982 (EP4 inhibitor)	Cayman Chemicals
L-NMMA (NOS inhibitor)	Cayman Chemicals
Methylglyoxal (MGO)	Sigma-Aldrich
Nor-NOHA (Arginase inhibitor)	Cayman Chemicals
PF 04418948 (EP2 inhibitor)	Cayman Chemicals
Prostaglandine E2 (PGE2)	Cayman Chemicals
Rapamycin (Raptor / mTORC1 inhibitor)	Biomol
SCH 58261 (Adensoine receptor A2AR inhibitor)	Cayman Chemicals
In vivo experiments	

CpG-oligonucleotide 1668	TIB MOLBIOL
Ovalbumin	Sigma-Aldrich
αgalactosylceramide	Axxora

2.1.4 Cell lines

Cell line	Description	Medium
K562	Cell line established from a 53-year-old female chronic myelogenous leukemia patient	T cell medium
LX2	Human myofibrbolast cell line generated by immmortalization of primary human hepatic stellate cells with the SV40 large T antigen	LX2 medium
MS-5 (feeder cell line for AML blasts)	Murine bone marrow stromal cell line	AML blast medium
B16-OVA	Mouse melanoma cell line expressing the ovalbumin (OVA) antigen	T cell medium + 400 µg/ml G418

2.1.5 Mouse lines

Line	Description	Origin
C57Bl/6	Wildtype	Janvier
OT-I	C57Bl/6, TCR transgenic animals restricted to the ovalbumin antigen SIINFEKL 257-264	Own breeding

2.1.6 Media and buffer

Buffer	Receipt
MACS/FACS buffer	PBS
	2 mM EDTA
	1% FBS
T cell medium (TCM)	RPMI 1640
	10% FBS
	2 mM Glutamine
	P/S (100 U/ml penicillin + 100 µg/ml streptomycin)
Seahorse RPMI medium	XF base medium minimal RPMI (wo phenol red)
	2 mM Glutamine
	10 mM Glucose
	pH adjusted to 7.4 with KOH
	filtered
Seahorse DMEM medium	XF base medium minimal DMEM (wo phenol red)
	2 mM Glutamine

	pH adjusted to 7.4 with KOH
	filtered
LX2 medium	DMEM
	10% FBS
	2 mM Glutamine
	P/S (100 U/ml penicillin + 100 µg/ml streptomycin)
AML blast medium (for pre-culture)	αMEM
	12.5% FBS
	12.5% horse serum
	2 mM Glutamine
	P/S (100 U/ml penicillin + 100 µg/ml streptomycin)
	20 ng/ml rhu G-CSF
	20 ng/ml rhu IL3
	20 ng/ml rhu Thrombopoietin
	57.2 µM 2-mercaptoethanol

2.1.7 Devices

Device	Manufacturer
AutoMACS Separator	Miltenyi Biotech
Infinite M1 1000 PRO	Tecan
LightCycler® 480 II	Roche
SA3800 Spectral Analyzer	SONY Biotechnology
Seahorse XF96 Analyzer	Agilent Technologies
SH800 Cell Sorter	SONY Biotechnology
SP6800 Spectral Analyzer	SONY Biotechnology

2.2 Methods

Methods described in this section were published in (Baumann et al., 2020). Experimental procedures written by collaborators are marked as such.

2.2.1 Animal models and treatments

All animal experiments were performed according to the federal German law regarding the protection of animals (ROB-55.2-2532.Vet_02-193 and ROB-55.2-2532.Vet_02-17-234). C57Bl/6J mice and OT-I were bred according to the Federation of European Laboratory Animal Science Associations guidelines. For tumor implantation, 5×10^5 B16-OVA melanoma cells were injected subcutaneously into the left flank. Tumor size was measured using a digital caliper, and tumor volume was calculated using the ellipsoid formula $V = \frac{4}{3}\pi r^2$. After 10 d, mice were vaccinated using 200 µg ovalbumin with 20 µg CpG-oligonucleotide 1668 and 0.2 µg α-galactosylceramide in 100 µl PBS. DMBG was administrated via drinking water (40 mM) and anti-PD-1 (clone 29.F1A12) was applied intraperitoneally every third day (200 µg), both starting 10 d after tumor transplantation.

2.2.2 AML patient samples

AML Blasts for co-culture experiments. After written informed consent in accordance with the Declaration of Helsinki and approval by the Institutional Review Board of the Ludwig-Maximilians-University (Munich, Germany), peripheral blood or bone marrow samples were collected from patients with AML at primary diagnosis or relapse. At primary diagnosis or relapse, samples were analyzed at the Laboratory for Leukemia Diagnostics of the Klinikum der Universität München as described previously (Büchner et al., 1999; Dufour et al., 2010). Patient characteristics are summarized in Table 1. Mononuclear cells from AML patients were isolated by density gradient centrifugation (Biocoll Separating Solution) and cryopreserved at <-80°C in 80% fetal calf serum and 20 % dimethyl sulfoxide. After thawing of primary AML samples, T cells were depleted by a Pan-T cell isolation kit. Remaining primary AML cells were precultured for 72h in 12 well flat bottom culture plates in αMEM supplemented with 12.5 % fetal calf serum, 12.5% horse serum, 2mM Glutamine and Penicillin/Streptomycin. The medium was supplemented with 20 ng/ml recombinant human (rhu) granulocyte-colony stimulating factor (G-CSF), rhu interleukin 3 (IL-3), rhu thrombopoietin and 57.2 µM 2-mercaptoethanol as previously described (van Gosliga et al., 2007). To improve the viability of

primary AML cells, a feeder layer of irradiated MS-5 cells was used. *Text written and cells kindly provided by Bettina Brauchle, research group of Marion Subklewe, LMU Munich, Germany.*

Table 1: AML Patient characteristics. ID: initial diagnosis; Rel: relapse; F: female; M: male; nd: not determined; tAML: therapy related AML; sAML: secondary AML; + : mutated; - : not mutated.

#	Diagnosis	Sex	Age	Cyto-genetics	FAB	ELN 2017	% blasts	FLT3-ITD mut	FLT3-TKD mut	NPM1 mut
1	ID	F	27	46 XX	nd	Intermediate	96	+	-	+
2	ID	F	50	46 XX	M1	Intermediate	87	+	-	+
3	ID	F	26	46 XX	M1	adverse	47	-	-	-
4	ID	M	32	46 XY	M4	intermediate	81	+	-	+
5	ID	F	63	aberrant/ normal	tAML	adverse	31	-	-	-
6	ID	F	31	46 XX	M1	favorable	83	+	-	+
7	ID	M	86	46 XY	M0	nd	55	-	-	nd
8	ID	F	75	46 XX	nd	nd	nd	nd	nd	nd
9	ID	F	72	46 XX	M4	favorable	80	+	-	+
10	ID	F	71	46 XX	sAML	nd	69	-	-	+
11	ID	F	59	aberrant/ normal	M4	favorable	79	-	-	+
12	ID	M	43	aberrant/ normal	M2	favorable	50	-	-	nd
13	ID	F	77	46XX	M1	nd	84	+	-	-
14	ID	M	45	46 XY	nd	intermdiate	nd	+	-	+
15	ID	M	80	aberrant/ normal	nd	nd	nd	-	-	-
16	ID	M	62	aberrant/ normal	M1	nd	94	+	-	+
17	ID	M	41	46XY	nd	nd	nd	+	-	-
18	ID	M	65	46XY	nd	nd	98	+	+	-
19	ID	F	45	aberrant	M3	nd	86	+	-	nd
20	ID	M	74	nd	nd	nd	98	+	-	-
21	ID	M	58	46XY	M1	nd	77	-	+	+
22	ID	M	59	46 XY	M4	nd	84	+	-	+
23	ID	M	76	46XY	M2	nd	83	+	-	-
24	ID	M	69	46XY	sAML	nd	76	+	+	+
25	ID	M	73	aberrant/ normal	M1	favorable	61	-	-	-
26	ID	M	72	46XY	M1	intermediate	89	+	-	+
27	ID	F	38	aberrant	M1	nd	84	-	-	-
28	ID	F	69	nd	M1	nd	65	+	nd	nd
29	ID	F	50	46XX	M1	adverse	77	+	+	-

30	ID	M	54	46XY	M2	nd	70	+	-	+
31	ID	M	68	aberrant	M2	adverse	62	-	+	-
32	ID	M	46	46 XY	M2	nd	55	-	-	-
33	Rel	M	80	aberrant	M0	intermediate	85	+	-	-
34	Rel	F	36	46 XX	M4	nd	68	+	-	+
35	Rel	M	37	complex	M0	adverse	69	-	-	-
36	Rel	F	85	46XX	sAML	nd	nd	-	+	-
37	Rel	M	50	46 XY	M5	nd	nd	+	-	+
38	Rel	F	56	nd	M2	nd	69	-	-	-

2.2.3 Immune cell isolation and culture

All experiments with human blood or human liver samples were performed in accordance with the ethic votes 434/17S, 564/18SAS, 218-08 and 232/19S. Informed written consent was obtained from each patient.

Cells isolated from peripheral blood. Peripheral blood mononuclear cells were isolated from freshly drawn blood by density gradient centrifugation (pancoll gradient). Human monocytes and $CD8^+$ T cells from healthy donors were isolated via positive immunomagnetic isolation using anti-CD14 or anti-CD8 coupled microbeads and the AutoMACS device. NK cells were purified using a negative selection kit following the manufacturers recommendations. The purity of $CD56^+$ $CD3^-$ NK cells, $CD14^+$ monocytes or $CD8^+$ T cells was usually >90%. MDSCs and monocytes were isolated from patient blood PBMCs by FACS gating on $CD14^+HLA\text{-}DR^{-/low}$ or $CD14^+HLA\text{-}DR^+$ cells.

***Induction of human MDSCs from monocytes by stromal cells*.** Human monocytes (10^6) isolated from peripheral blood of healthy volunteers were cultured on a confluent layer of human stromal liver cells (that is myofibroblast cells (LX2) (Weiskirchen et al., 2013), 4×10^5 cells in poly-l-lysine coated 24-well plates in T cell medium for 3 d without medium change). Viable MDSCs were separated from myofibroblasts by FACS before use in functional assays. MDSCs generated from monocytes were characterized by downregulation of HLA-DR and their capacity to inhibit the proliferation of anti-CD3/CD28-activated $CD8^+$ T cells. If indicated, inhibitors at the specified concentration were added during the co-culture with stromal cells.

Cells isolated from human tissue. Human tumor tissue was mechanically shredded followed by enzymatic digestion with 0.1% collagenase and 0.1% DNAse in RPMI at 37 °C for 30 min. Single cells

were isolated using 40% percoll and 100% pancoll density gradient centrifugation. $CD8^+$ T cells and myeloid cells were further purified by immunomagnetic separation using anti-CD8 or anti-CD14 microbeads and AutoMACS. Primary keratinocytes and fibroblasts were kindly provided by Jana Sänger, research group of Stefanie Eyerich, TU Munich, Germany.

Cells isolated from mouse tissue. Immune cells were isolated from spleen and tumor tissues by mechanical disruption, and tumor tissue was further digested with 0.1% collagenase in RPMI for 10 min at 37 °C. Single cells were isolated using 40% percoll and 100% pancoll density gradient centrifugation. $CD8^+$ T cells and myeloid cells were further purified by immunomagnetic separation using anti-CD8 or anti-CD11b microbeads, followed by FACS gating on $CD11b^+Ly6C^+$ or $CD11b^+Ly6G^+$ cells.

Culture of NK cells with AML blasts. AML blasts were separated from MS-5 feeder layer and co-cultured with allogenic, healthy donor derived NK cells at various ratios (AML blasts:NK 0.3:1, 1:1, 3:1, 10:1) in T cell medium supplemented with 25 IU IL-2 in 96-well U-bottom plates. If not otherwise stated, co-cultures lasted overnight (20h) and allowed direct cell-cell contact. If indicated, inhibitors were added to the co-culture at the specified concentrations.

2.2.4 Flow cytometry and FACS

The phenotype of cells was analyzed by flow cytometry using a Sony SP6800 or Sony SA3800 spectral analyzer. FACS-Sorting of cells was done using a Sony SH800 cell sorter. Data were analyzed using FlowJo software.

Surface staining. For surface staining, cells were transferred to a 96-well V-bottom plate and stained with fluorochrome-coupled antibody mixtures diluted in MACS/FACS buffer for 15 min on ice. Cells were washed with MACS/FACS buffer and measured directly or stored on ice for short periods. Live/Dead staining was performed with fixable viability dyes together with surface staining or 7-AAD or PI was added shortly before starting the measurement.

Staining of cells with fluorescent dyes. K562 cells or AML blasts were stained with eF450 or CFSE before starting co-cultures with NK cells, to allow easy exclusion or identification in flow cytometry gating. Additionally, eF450 or CFSE was used to monitor cell division of $CD8^+$ T cells after anti-CD3/CD28 stimulation. MitoTracker green was used as a surrogate marker of mitochondrial mass or to measure cytosolic exchange between immune cells, as was calcein and ER Tracker. Immune cells were stained

with eF450, eF670, MitoTracker green or CFSE to discriminate different immune cell populations in confocal microscopy and to visualize cytosolic exchange. Immune cells were stained for 10 min at 37°C with dyes diluted in PBS, since serum proteins might interfere with the staining procedure. MitoTracker green was used at 200 nM, ER Tracker green at 200 nM, CFSE at 1 µM, eF450 at 4 µM, eF670 at 1 µM, and calcein at 10 nM concentrations.

Cell sorting. Immune cells were stained with antibodies and/or fluorescent dyes, as described above. Cells were re-suspended in TCM or MACS buffer and subjected to cell sorting with a Sony SH800 device. Briefly before sorting, 7-AAD or PI was added to discriminate dead cells. For mtDNA detection or metabolite analysis, cell sorting was performed in ultra purity to ascertain highest purity.

Phospho-kinase staining. Phosphorylated kinases (p-mTOR, p-ZAP70/Syk, p-AKT, p-ERK1/2, pS6, p-LCK) were stained after indicated time points using a methanol-based fixation method. Briefly, surface stained immune cells were stimulated and IC fixation buffer was added after indicated time points to freeze kinase phosphorylation. After 10 min at 37°C, cells were washed and re-suspended in ice cold (-20°C) methanol. Plates were stored at -20°C at least overnight and up to 1 week, then cells were washed and stained with anti-phospho-kinase antibodies overnight at 4°C.

Intracellular cytokine staining (ICS). Cells were subjected to surface staining (15 min on ice), then fixed and permeabilized using commercial FoxP3 fixation/permeabilization kit. Fixation was usually done overnight at 4°C, then cells were washed and intracellular antibody targets (GzmB, IFN-γ, TNF) were stained for 2h on ice in permeabilization buffer.

Methylglyoxal detection. The fluorescent sensor MBo, which specifically detects methylglyoxal (Wang et al., 2013b), was used to detect the presence of methylglyoxal at the level of single cells using flow cytometry. Cells were loaded with MBo (10 µM) for 30 min in TCM at 37 °C, washed and subjected to further cell surface antibody staining before flow cytometric evaluation.

2.2.5 Functional assays of $CD8^+$ T and NK cells

T cell proliferation assay. Isolated $CD8^+$ T cells were labeled with CFSE for quantitative determination of cell proliferation. $CD8^+$ T cells and $CD14^+$ myeloid cells were co-cultured at a ratio of 1:1 and T cells were activated with anti-CD3/CD28 Dynabeads (1 µl / 4×10^4 beads per 10^6 cells). Proliferation was determined after 3 d by dilution of CFSE and the division index was calculated using FlowJo Software. Where indicated, inhibitors were added to the co-culture at specified concentrations.

NK cytotoxicity assay. NK cells cultured alone or with AML blasts overnight were stimulated by addition of K562 to the wells in equal number (E:T = 1:1). After 2.5h, anti-CD107a and DilC1(5) (1 nM) was added to the co-culture. Surface detection of CD107a is a widely accepted method to evaluate NK cell degranulation (Lorenzo-Herrero et al., 2019). DilC1(5) indicates mitochondrial membrane potential and can be used to identify early and late apoptotic cells by the loss of DilC1(5) staining. 30 min later (3h of co-culture total), cells were washed and subjected to surface staining. Counting beads were used to assess the total number of living K562 cells. Additionally, the frequency of DilC1(5) negative (apoptotic) K562 cells was analyzed. Both readouts allowed the quantification of K562 killing by NK cells.

Cytokine production. $CD8^+$ T cells and $CD14^+$ myeloid cells were co-cultured at a ratio of 1:1 and T cells were activated as before. Brefeldin A (3 µg/ml) and Monensin (2 µM) was added to inhibit cytokine secretion. After 4h of culture, cells were subjected to surface staining, then intracellular antibody targets (GzmB, IFN-γ, TNF) were stained as described above. NK cells cultured alone or with AML blasts were stimulated by addition of K562 to the wells in equal number (E:T = 1:1) in the presence of brefeldin A (3 µg/ml) and monensin (2 µM) with identical staining procedure.

2.2.6 Analysis of cellular metabolism

***Glucose uptake assa*y.** Cells were cultured in glucose-free T cell medium and incubated with 10 µM 2-NBDG for 30 minutes followed by determination of 2-NBDG fluorescence intensity in cells by flow cytometry.

Extracellular Flux Analysis (Seahorse). (Re-)isolated immune cells were seeded on a XF96 cell culture microplate ($1x10^5$ $CD8^+$ T cells or $2x10^5$ NK cells per 96-well) in unbuffered Seahorse RPMI medium containing 10 mM glucose and 2 mM glutamine, manually adjusted to pH 7.4. For oxidative profiling, 2 µM oligomycin to block ATP synthesis, 1.5 µM CCCP to uncouple mitochondria proton pumping and 2 µM antimycin A and rotenone (each to block the electron transport chain) were injected during measurement of oxygen consumption rates (OCRs) in a Seahorse XF96 Analyzer. For glycolytic profiling, immune cells were seeded in unbuffered, glucose-free DMEM manually adjusted to pH 7.4. Glycolysis, monitored as the extracellular acidification rate (ECAR), was started after the addition of 10 mM glucose, followed by 1 µM oligomycin to block mitochondrial ATP synthesis and 20 mM 2-DG to reduce the ECAR to glycolysis unrelated levels. The glycolytic reserve was calculated as the difference between the ECAR after oligomycin injection and the baseline ECAR. ATP-linked respiration states the difference between OCRs after oligomycin injection and at baseline.

2.2.7 Measurement of specific analytes

Glyoxalase assay. The enzymatic activity of glyoxalase I was measured using the Glyoxalase I Activity Assay Kit from Sigma–Aldrich, and was based on the change of absorbance at 240 nm due to the conversion of methylglyoxal (substrate) to S-lactoylglutathione in the presence of reduced glutathione (co-substrate). Briefly, cell pellets were permeabilized in assay buffer supplemented with 0.1% Triton X for 5 min at 21 °C in an ultraviolet-transparent 96-well plate. Assay buffer containing substrate and co-substrate was added and the increase in absorbance at 240 nm within 20 min was measured to calculate the enzymatic activity. The activity was normalized to the protein concentration of the sample, as measured with a standard colorimetric protein assay (Bio-Rad Laboratories).

Hexokinase colorimetric assay. The activity of hexokinase in cellular lysates was analyzed by measuring the NADH production per time in a colorimetric assay, according to the manufacturer's protocol (Sigma-Aldrich).

Glutathione GSH/GSSG assay. Total, reduced (GSH) and oxidized (GSSG) glutathione in cell lysates was measured according to the instructions of a luminescence-based assay kit (Promega).

ATP assay. The ATP level of cells was analyzed using an ATP Assay Kit (Sigma–Aldrich), according to the manufacturer's protocol.

TGF-β1 ELISA. TGF-β1 quantification was done using an enzyme-linked immunosorbent assay (ELISA) (Thermo Fisher Scientific), according to the manufacturer's protocol.

PGE_2 ELISA. Concentrations of PGE_2 in cell culture supernatants was assessed using a competitive ELISA kit (Cayman Chemicals) according to manufacturers recommendations.

2.2.8 Mass spectrometry-based detection methods

UHPLC-TOF-DIA-MS/MS analysis. Monocytes and MDSCs were isolated or induced as described above. For the ^{13}C labeling experiments, medium containing 50% $^{13}C_6$ glucose (Merck) was used during the induction of MDSCs. Isolated cells were transferred into CK14 (0.5 ml) bead beater tubes (Bertin Technologies) containing 1.4-mm-diameter ceramic (zirconium oxide) beads. After the addition of acetonitrile (ACN)/water (250 µl; 50/50 v/v), the samples were homogenized for 3 × 30 s with 20-s breaks in between at 7,800 r.p.m. (Precellys Evolution Homogenizer; Bertin Technologies). To prevent excessive heating during homogenization, samples were cooled with liquid nitrogen using a Cryolys

cooling system (Bertin Technologies). Subsequently, samples were equilibrated for 15 min at 21 °C and centrifuged at 16,100g and 4 °C for 5 min (Centrifuge 5415R; Eppendorf) and the clear supernatant was stored at −80 °C until further analysis. For derivatization, 40 µl of the cell extract was mixed with 20 µl of a solution of 3-nitrophenylhydrazine (200 mM; 50:50 v/v; ACN/H_2O) and 20 µl of a 120-mM solution of N-(3-dimethylaminopropyl)-N′-ethylcarbodiimide in 6% pyridine (50:50 v/v; ACN/H_2O) and reacted for 30 min at 40 °C. Afterwards, the mixture was diluted with ACN/H2O (200 µl; 50:50 v/v) and used directly for UHPLC-TOF-DIA-MS/MS to acquire fragment spectra. For the analysis, an Nexera X2 UHPLC system (Shimadzu) consisting of two LC-30AD pumps, a SIL-30AC auto sampler, a CTO-30A column oven and a CBM-20A system controller was connected to a 6600 TripleTof instrument (Sciex) equipped with an IonDrive ion source (Sciex) operating in negative electrospray mode. After each fifth sample, the instrument's calibration was verified and corrected using ESI Negative Calibration solution (Sciex) and a Calibrant Delivery System (Sciex). UHPLC separation was performed on a Kinetex Phenyl-Hexyl column (100 mm × 2.1 mm; 1.7 µm; Phenomenex) using water (mobile phase A) and ACN (mobile phase B) with 0.1% formic acid in each and the following gradient program: 0 min, 36% B; 2 min, 36% B; 3.5 min, 80% B; 5 min, 100% B; 7 min, 100% B; 8 min, 36% B; and 12 min, 36% B. The total flow of the chromatography was set to 0.25 ml min^{-1} and separation was performed at 40 °C. The mass spectrometer was operated in the SWATH mode with a series of 19 consecutive experiments per 1.05-s measurement cycle. After starting with a high-resolution scan of the intact precursor ions from 50–1,000 m/z for 100 ms, fragment ions were generated by means of collision-induced fragmentation subsequently for precursor ions within 18 separate windows ranging from 50–600 m/z (window width: 30 Da each; 1 Da overlap). The resulting fragment spectra were recorded in the high-sensitivity mode (50 ms acquisition per window). The ion spray voltage was set at −4,500 V and the following source parameters were applied: curtain gas: 35 psi; gas 1: 55 psi; gas 2L 65 psi; and temperature: 500 °C. The declustering potential was set to 80 V for all experiments while the collision energy was 10 V for precursor ion scans and 35 V (including 25 V collision energy spread) for the fragmentation in the individual SWATH windows. The following compounds were measured as references: 3-phosphoglycerat, fructose-6-phosphate, fructose-1,6-diphosphate, glucose, glucose-6-phosphate, glutathione, glyoxal, lactate, lactoylglutathione, methylglyoxal, nucleotide mix, organic acid mix, phosphoenolpyruvate and pyruvate. *Text written and analysis kindly performed by Andreas Dunkel, Leibniz-Institute of Food Systems Biology, TU Munich, Germany.*

***Quantification of amino acids and AGPs by stable isotope dilution analysis (SIDA*).** The amino acids L-arginine (1), L-glutamine (2), L-methionine (3), L-asparagine (4), L-glutamic acid (5), L-tyrosine (6), L-

isoleucine (7), L-phenylalanine (8), L-lysine (9), L-serine (10), L-leucine (11), L-tryptophan (12), L-aspartic acid (13) and L-alanine (14), as well as the AGPs argpyrimidine (15), MG-H1 (16), imidazolysine (17), pyrraline (18), carboxyethyllysine (19) and carboxymethyllysine (20), were analyzed by means of two newly developed SIDA-UHPLC-MS/MS_{MRM} methods separately. To this end, the corresponding stable isotope-labeled amino acid standards L-arginine (^{13}C6-1), L-glutamine ($^{13}C_5$-2), L-methionine (methyl-d_3-3), L-asparagine ($^{15}N_2$-4), L-glutamic acid ($^{13}C_5$-^{15}N-5), L-tyrosine (ring-d_4-6), L-isoleucine ($^{13}C_6$-7), L-phenylalanine (ring-d_5-8), L-lysine ($^{13}C_6$-9), L-serine ($^{13}C_3$-10), L-leucine ($^{13}C_2$-11), L-tryptophan (indole-d_5-12), L-aspartic acid ($^{13}C_4$-^{15}N-13) and L-alanine ($^{13}C_3$-14), as well imidazolysine-$^{15}N_2$ (17-$^{15}N_2$) and MG-H1-d_3 (16-d_3) for AGP analysis, were utilized. AGPs were obtained from Iris Biotech. Stable isotope-labeled amino acids were bought from Cambridge Isotopes. The solvents used for UHPLC-MS/MS analysis were of LC-MS grade (Honeywell). Ultrapure water for UHPLC separation and mass spectrometry was purified by means of a Milli-Q water advantage A10 water system (Millipore). Millipore-grade water was used for all of the experiments unless stated otherwise.

Internal standards. Internal standards were prepared in stock solutions (500 µl) with the concentrations provided in Supplementary Table 8 of (Baumann et al., 2020) and were prepared in ACN/H_2O (10/90 v/v). Iimidazolysine-$^{15}N_2$ (12.06 mmol l^{-1}; 17-$^{15}N_2$) and MG-H1-d_3 (13.1 mmol l^{-1}; 16-d_3) were dissolved in D_2O and their exact concentrations was verified by means of quantitative NMR (qNMR) before storage at −20 °C until use. Internal standard solutions for amino acid and AGP analysis were prepared by diluting stock solutions 1:5 and 1:20 with ACN/H_2O (50/50 v/v), respectively.

Sample preparation. Cells were lysed at 0 °C using a bead beater (Precellys Evolution homogenizer; Bertin Instruments) at 7,000 r.p.m. for 6 × 20 s with a 30-s pause in between. Afterwards, lysed cells were ultrafiltrated (Amicon Ultra; Merck; 3 kDa centrifugal filters; 13,600g; 30 min; 4 °C). Filtrates were dried by vacuum centrifugation (Eppendorf Concentrator Plus; 6 h; 30 °C) and solved in 100 µl H_2O. Internal standard solutions (each 2 µl) were added and subjected to the UHPLC-MS/MS system. Recovered protein was eluted by centrifugation (1,000g; 5 min; 4 °C). According to Ahmed at al. (Ahmed et al., 2002) and Salomón et al. (Salomón et al., 2017), hydrolysis was carried out with slight modifications. Protein samples were mixed with HCl (aq, 40 mM; 50 µl), thymol solution (1 mg ml^{-1} in 40 mM HCl; 10 µl) and pepsin solution (1 mg ml^{-1} in 40 mM HCl; 10 µl) and incubated at 37 °C for 24 h in an Eppendorf Thermomixer at 400 r.p.m. Subsequently, each sample was buffered and neutralized by the addition of sodium phosphate buffer (aq.; 500 mM; 50 µl) and sodium hydroxide (aq.; 260 mM; 9 µl). Further hydrolysis was conducted using Pronase E (1 mg ml^{-1} in 10 mM sodium phosphate buffer;

10 µl) for 24 h at 37 °C in an Eppendorf Thermomixer at 400 r.p.m. In the last hydrolysis step, leucine aminopeptidase and prolidase (each 1 mg ml^{-1} in 10 mM sodium phosphate buffer; 10 µl) were added and incubation was continued at 37 °C for 48 h using an Eppendorf Thermomixer at 400 r.p.m. To each hydrolysate, internal standards of amino acids and AGPs were added (3 µl). Afterwards, samples were ultrafiltered (Amicon Ultra; 3 kDa centrifugal filters; 13,600g; 30 min; 4 °C), dried by vacuum centrifugation and reconstituted to a defined volume (150 µl) by the addition of H_2O for UHPLC-MS/MS analysis.

UHPLC-MS/MS. UHPLC-MS/MS analysis was conducted on a QTRAP 6500+ UHPLC-MS/MS system connected to an ExionLC AD (Sciex) operated in the positive ESI mode (ion spray voltage: 5,500 V): curtain gas: 35 V; temperature: 450 °C (amino acids) or 500 °C (AGPs); gas 1: 55 psi; gas 2: 65 psi; collision-activated dissociation: 2 V; entrance potential: 10 V. For compound optimization, flow injection with a syringe pump (10 µl min^{-1}) and compound solutions in ACN (0.1% FA) were used. Amino acids and AGPs were separated on a BEH Amide column (100 × 2.1 mm; 1.7 µm; Waters). Chromatography was performed using an injection volume of 1 µl (amino acids) or 2 µl (AGPs), a flow rate of 0.4 ml min^{-1} and a column temperature of 40 °C. The solvent system consisted of (A): 5 mM NH4Ac and 0.1% formic acid in water; and (B): 5 mM NH4Ac and 0.1% formic acid in ACN/water (95/5 v/v). For amino acid and AGP analysis, two separate methods were used sharing the following gradient: 0 min, 90% B; 5 min, 85% B; 8 min, 70% B; 9 min, 0% B; 11 min, 0% B; 12 min, 90% A; and 14 min, 90% B. Data acquisition and instrumental control was performed using Analyst 1.6.3 software (Sciex). Amino acids and AGPs were analyzed in the positive multiple reaction monitoring (MRM) mode following MS/MS parameters, as depicted in Supplementary Table 8 of (Baumann et al., 2020).

Calibration curve and linear range. For AGP analysis, stock solutions of standards were prepared in D_2O and each concentration was verified by means of qNMR. Thereafter, a mixture of analytes with concentrations of 132.5 µmol l^{-1} (15), 750 µmol l^{-1} (16), 300.5 µmol l^{-1} (17), 215.5 µmol l^{-1} (18), 214.5 µmol l^{-1} (19) and 118.5 µmol l^{-1} (20) were prepared and subsequently diluted by factors of 2, 5, 10, 20, 50, 100, 200, 500, 1,000, 2,000, 5,000, 10,000, 20,000, 50,000 and 100,000. Afterwards, diluted analyte mixtures were mixed with constant concentrations of internal standard MG-H1-d_3 (16-d_3; 0.655 mmol l^{-1}) and imidazolysine-$^{15}N_2$ (17-$^{15}N_2$; 0.606 mmol l^{-1}). Triplicate UHPLC-MS/MS analysis calibration curves were prepared by plotting peak area ratios of argpyrimidine (15), MG-H1 (16), pyrraline (18), carboxyethyllysine (19) and carboxymethyllysine (20) to the internal standard MG-H1-d_3 (16-d_3) against concentration ratios of the analytes to the internal standard using linear regression. The calibration

curve of imidazollysine (17) was created by plotting peak ratios to the internal standard imidazollysine-15N2 (17-$^{15}N_2$) against concentration ratios of respective analyte and internal standard. Amino acid analysis was conducted first by dilution (1:10, 1:20, 1:50, 1:100, 1:200, 1:500, 1:1,000, 1:2,000, 1:5,000 and 1:10,000) of an amino acid mix with the concentrations referred to in Supplementary Table 9 of (Baumann et al., 2020). Subsequently, to each diluted amino acid standard solution, diluted internal standard (1/20 dilution of stock solution) was added to a dilution factor of 250 (see internal standard concentrations in Supplementary Table 9). Calibration curves were created by taking triplicate UHPLC-MS/MS measurements and plotting peak area ratios of amino acids to corresponding internal standards using a linear regression model. The response was linear for each analyte (amino acids and AGPs), with correlation coefficients of >0.99 for the chosen molar ratios, and the contents of AGPs in the samples were calculated using the respective calibration function. Determination of the limit of detection at a signal-to-noise ratio of 3 and the limit of quantitation at a signal-to-noise ratio of 10 revealed the following values: limit of detection ≤ 0.0001 µM; limit of quantitation ≤ 0.0005 µM. *Text written and analysis kindly performed by Christian Schmid, Food Chemistry and Molecular Sensory Science, TU Munich, Germany.*

2.2.9 RNA and DNA-based detection methods

Quantitative PCR (qPCR). Cells used for qPCR analysis were separated by cell sorting and mRNA was isolated using a commercial kit (Macherey-Nagel). After reverse transcription (SensiFAST kit, Bioline) cDNA was amplified (No Rox SYBR, Takyon) using the following primer pairs:

Target	Species	Sequence (5'->3')
ACTG1 human for (house keeping)	human	CAC CAT TGG CAA TGA GCG GTT C
ACTG1 human rev (house keeping)	human	AGG TCT TTG CGG ATG TCC ACG T
RSP18 human for (house keeping)	human	GCA GAA TCC ACG CCA GTA CAA G
RSP18 human rev (house keeping)	human	GCT TGT TGT CCA GAC CAT TGG C
CYPA human for (house keeping)	human	ATG CTC AAC CCC ACC GTG T
CYPA human rev (house keeping)	human	TCT GCT GTC TTT GGG ACC TTG TC
TGFB1 human for	human	TAC CTG AAC CCG TGT TGC TCT C
TGFB1 human rev	human	GTT GCT GAG GTA TCG CCA GGA A
COX1 human for	human	GAT GAG CAG CTT TTC CAG ACG AC
COX1 human rev	human	AAC TGG ACA CCG AAC AGC AGC T
COX2 human for	human	CGG TGA AAC TCT GGC TAG ACA G
COX2 human rev	human	GCA AAC CGT AGA TGC TCA GGG A
AOC3 / SSAO human for	human	GGA ACC AAG TGT CAG AGC ACA C
AOC3 / SSAO human rev	human	GGA CAA AGA CCA TAT CCT CGG C

The increase of fluorescence was measured with a LC480 light cycler (Roche). ΔCp was calculated as difference of target genes and the Cp value of house keeping genes (ACTG1, RSP18 and CYPA). ΔCp vales were used to calculate the relative expression of genes ($2^{-\Delta Cp}$). Fold change is the relative expression of each sample normalized to one reference sample. Samples were recorded in technical triplicates.

Mitochondrial DNA detection. $CD8^+$ T cells (acceptors) or monocytes (donors) were purified from the blood of two non-related, healthy individuals. After 30 min of co-culture, viable $CD8^+$ T cells were separated using a SH800 cell sorter in ultra-purity mode, and whole DNA was isolated. Mitochondrial DNA was amplified via XL-PCR (single amplicon: 16,569 bp) and sequenced with an Illumina MiSeq (Illumina). Donor-specific homoplasmic single-nucleotide polymorphisms were identified and used to test for trans-cellular mitochondrial DNA transfer from donor to acceptor cells. To control for contamination with donor cells due to false sorting, donor-specific microsatellites of nuclear DNA were analyzed. No contamination was detected; the limit of detection was approximately 2%. *Analysis of mitochondrial DNA transfer was kindly executed by Uwe Ahting and Bettina Lorenz-Depiereux, research group of Thomas Meitinger, TU Munich, Germany.*

2.2.10 Confocal live cell microscopy

For live cell imaging, a PerkinElmer UltraVIEW VoX spinning disc microscope and a Nikon TiE equipped with the Hamamatsu EM-CCD ImagEM X2 camera, APO TIRF 60× NA1.49 oil immersion objective and environment control system (37 °C and 5% CO2) were used. T cells were stained with eF670 (1 µM) and monocytes with MitoTracker Green (200 nM) for 15 min and placed in 8-well glass-bottom chambered slides (Ibidi) in imaging medium (T cell medium). Chambered slides were placed on the microscope and the focus was locked in using a hardware-based autofocusing system. Then, monocytes were added to the chambers and time-lapse acquisition started. The entire three-dimensional volume of the cells was acquired by optical sectioning using a piezo z-drive step of 0.5 µm (15 steps) every 75 s for a total imaging duration of 40–60 min. eF670 and MitoTracker Green were imaged using a 640-nm laser with a 705/90 filter and a 488-nm laser with a 525/50 filter, respectively. Transmission (differential interference contrast (DIC)) images were acquired in addition.

For ultra-structural analysis during live cell imaging, an LSM 880 Airyscan and an Airyscan FAST, respectively equipped with a Plan-Apochromat 63x NA1.2 water immersion objective, were used (Carl

Zeiss Microscopy). T cells and monocytes were isolated. Monocytes were stained with MitoTracker Green (200 nM) and placed in 8-well glass-bottom chambered slides (Ibidi) in the imaging medium (T cell medium). Then, monocytes were added to the chambers and time-lapse acquisition started. The entire three-dimensional volume of cells was acquired by optical sectioning using a piezo z-drive step of 0.173 µm (45 steps; total range: 7.6 µm) every 53 s for a total imaging duration of 1 h 28 min. Cells were imaged, including nuclear staining, laser-DIC and MitoTracker Green using 405, 488 and 633 nm lasers with emission bands of 420–480 nm (nuclear staining) and 495–550 nm (MitoTracker Green), respectively. Laser-DIC was added in an additional track using a 633-nm laser for optimized penetration depth at minimal bleaching. Images were acquired at twofold optical zoom, resulting in 67.5 × 67.5 μm^2 at a pixel size of 0.04 × 0.04 μm^2. *Text was kindly written by and confocal imaging was done together with Vibor Laketa, German Center for Infection Research, Heidelberg, Germany.*

2.2.11 Immunohistochemistry (IHC)

Human or mouse liver tissue (healthy and HCC) was stained for methylglyoxal-induced protein modifications (MG-H1, methylglyoxal-derived hydroimidazolone-1) or SSAO / VAP-1 using a Leica BOND RX IHC stainer. For antigen retrieval, tissue was treated with citrate buffer for 30 min. Anti-MG-H1 was stained for 15 min at 1:500 dilution, the secondary anti-mouse IgG antibody was incubated 30 min at 1:1000 dilution. Slides were developed with DAB (3,3'-Diaminobenzidin). *Staining was kindly performed by Anne Jakob, Core Facility of Comparative Pathology, Institute of Pathology leaded by Katja Steiger, TU Munich, Germany.*

2.2.12 Statistical analysis

Statistical analyses were performed with Graph-Pad Prism 6, 7 and 8 (GraphPad Software). Differences between groups were calculated by Student's two-way unpaired or paired t-test, one or two-way analysis of variance (ANOVA) or Mantel–Cox test, dependent on the experimental design. Statistical significance is depicted as follows: p*<0.05; p**<0.01; p***<0.001; p****<0.0001.

3. Results

3.1 Preceding work

The investigation of human MDSCs is impeded by the small frequency of circulating, peripheral blood MDSCs in healthy human volunteers and the limited access to chronically inflamed tissue (e.g. primary tumors), in which MDSCs accumulate. In 2013, Bastian Höchst and co-workers developed an *in vitro* model that allowed to convert non-suppressive peripheral blood-derived monocytes upon 3 days of co-culture on activated hepatic stellate cells (HSC) or the human hepatic stellate cell line LX2 into monocytic MDSCs (M-MDSCs) that suppressed $CD8^+$ T cell proliferation (Höchst et al., 2013). Stromal-cell induced M-MDSCs can be induced in sufficient numbers for in-depth studies on the phenotype, metabolism, and function of human MDSCs. If not otherwise stated (e.g. cancer patient-derived M-MDSCs), the term MDSC refers to *in vitro* generated human stromal-cell induced M-MDSCs in this thesis.

In preceding work, metabolic features of MDSCs were comprehensively compared with monocytes from the same donors cultured 3 days without LX2. A transcriptome analysis revealed that several genes involved in glycolysis were down-regulated in MDSCs compared with non-suppressive monocytes, hinting towards a metabolic phenotype. In line, the uptake of glucose and the activity of hexokinase was reduced in stromal cell- and cancer patient-derived MDSCs. Extracellular flux analysis underpinned low glycolytic flux in MDSCs. Additionally, the mitochondrial membrane potential and baseline oxygen consumption rate (OCR) was reduced in MDSCs compared with monocytes. Together with a strongly reduced ATP content, these experiments comprehensively showed a low / dormant metabolism of MDSCs compared with donor-matched monocytes.

In a next step, the regulation of $CD8^+$ T cells by stromal-cell induced MDSCs was investigated. Early signal events (phosphorylation of kinases ZAP-70, LCK, AKT, mTOR and ERK1/2) driving activation and metabolic reprogramming of anti-CD3/28 activated $CD8^+$ T cells were abrogated upon co-culture with MDSCs. $CD8^+$ T cells activated in the presence of MDSCs had low Glut-1 (main glucose transporter for activated immune cells) surface expression, hexokinase activity and glucose uptake comparable to unstimulated T cells. On a functional level, MDSCs suppressed cytokine production and proliferation of anti-CD3/28 activated $CD8^+$ T cells. Physical separation via transwell inserts, but not the addition of L-NOHA (arginase inhibitor), L-NMMA (nitric oxide synthase inhibitor), MnTBAP (peroxynitrite

scavenger), 1-MT (indolamin-2,3-dioxygenase inhibitor) or blocking antibodies against transforming growth factor-beta (TGF-β), interleukin-10 (IL-10) or programmed cell death ligand 1 (PD-L1) counteracted the suppression of T cell proliferation. In summary, $CD8^+$ T cells acquired metabolic dormancy and functional anergy after direct co-culture with MDSCs that could not be alleviated with inhibitors targeting commonly reported mediators of immune suppression.

3.2 MDSC-mediated suppression of $CD8^+$ T cells via methylglyoxal transfer

In further experiments, the underlying mechanism leading to MDSC-induced metabolic dormancy and functional anergy of $CD8^+$ T cells was investigated. The experiments of this project were cooperatively planned, executed, and analyzed within the research group and assisted by scientific research partners. Results depicted were published in 2020 in Nature Immunology (Baumann et al., 2020) and are shown in compliance with contributing experimenter and Nature Publishing Group.

3.2.1 Cytosolic transfer from myeloid cells to $CD8^+$ T cells

To investigate the dynamics of cellular interaction, $CD14^+$ myeloid cells (that is $CD14^+HLA\text{-}DR^+$ monocytes and $CD14^+HLA\text{-}DR^{-/low}$ MDSCs) and $CD8^+$ T cells were stained with fluorescent dyes for discrimination and co-cultured cells were monitored via confocal microscopy.* Myeloid cells were stained with MitoTracker green (MT green) dye, which accumulates in mitochondria preferentially, and $CD8^+$ T cells were stained with eF670 dye, which covalently binds to primary amino-groups of cytosolic proteins. Unexpectedly, MT green staining was acquired in $CD8^+$ T cells after 30 min of co-culture with myeloid cells and only T cells that interacted with myeloid cells in proximity were MT green positive (Figure 4A). Flow cytometry measurements confirmed, that $CD8^+$ T cells acquired MT green staining in direct co-culture with myeloid cells, but physical separation (by using transwell inserts) abrogated the effect (Figure 4B). In control settings at 4°C or when using lysed myeloid cells, no transfer of dye was measured, favoring active transport of MT green dye instead of unspecific diffusion (Figure 4B). We also observed transfer of the cytosolic dye calcein and the endoplasmic reticulum (ER)-specific dye ER tracker, but not transfer of a membrane staining dye (Figure 4C). In line, surface markers characteristic for myeloid cells were not detected on $CD8^+$ T cells after direct co-culture (Figure 4D). Interestingly, we recognized that antigen-experienced $CD8^+$ T cells were targeted by the dye transfer preferentially (Figure 5A), inferring that the transfer process could be regulated by receptors or ligands that are up-

* Confocal microscopy was done in cooperation with Vibor Laketa
Department of Infectious Diseases, German Center for Infection Research, Heidelberg University, Heidelberg

regulated upon activation. Dye transfer to $CD8^+$ T cells was not only detected in co-culture with stromal cell-induced M-MDSCs and monocytes, but also in co-culture with cancer patient derived myeloid cells (Figure 4E). To test if MT green dye is also transferred from non-immune cells to T cells, human skin fibroblasts and keratinocytes were co-cultured with $CD8^+$ T cells but no remarkable transfer of MT green dye was observed (Figure 4F).

We wondered, if whole cell organelles can be transferred from myeloid cells to $CD8^+$ T cells and if this could affect the metabolism and function of recipient cells. Interestingly, several research groups reported the transfer of cell organelles, including mitochondria, between different cell types previously (Murray and Krasnodembskaya, 2019). For example, mitochondrial transfer has been observed between cells from the bone marrow microenvironment and leukemia cells (Griessinger et al., 2017) and from astrocytes to neurons (Hayakawa et al., 2016), thereby supporting chemoresistance and survival of recipient cells, respectively.

To test if whole mitochondria or mitochondria-derived sub-organelles were transferred from myeloid cells to T cells, $CD8^+$ T cells and myeloid cells were isolated from genetically distinct donors and co-cultured as before. After re-isolation of $CD8^+$ T cells, myeloid cell donor-specific mtDNA (mitochondrial DNA) single nucleotide polymorphisms (SNPs) were sequenced.* In several independent experiments, MT green dye but no donor-specific SNPs were detected in acceptor $CD8^+$ T cells, thereby excluding the transfer of intact mitochondria containing mtDNA (Figure 4G). In line, there was no increase of mitochondrial mass in $CD8^+$ T cells after co-culture with myeloid cells, as measured by quantification of TOM22 staining intensity in confocal microscopy (Figure 5B). We concluded that myeloid cells transferred cytosolic constituents containing residues of the fluorescent dyes to antigen-experienced $CD8^+$ T cells and we speculated, that this transfer interaction could be related to the suppressive effect of MDSCs on effector T cells.

* mtDNA sequencing was performed by Uwe Ahting and Bettina Lorenz-Depiereux
Institute of Human Genetics, Helmholtz Zentrum München, Munich

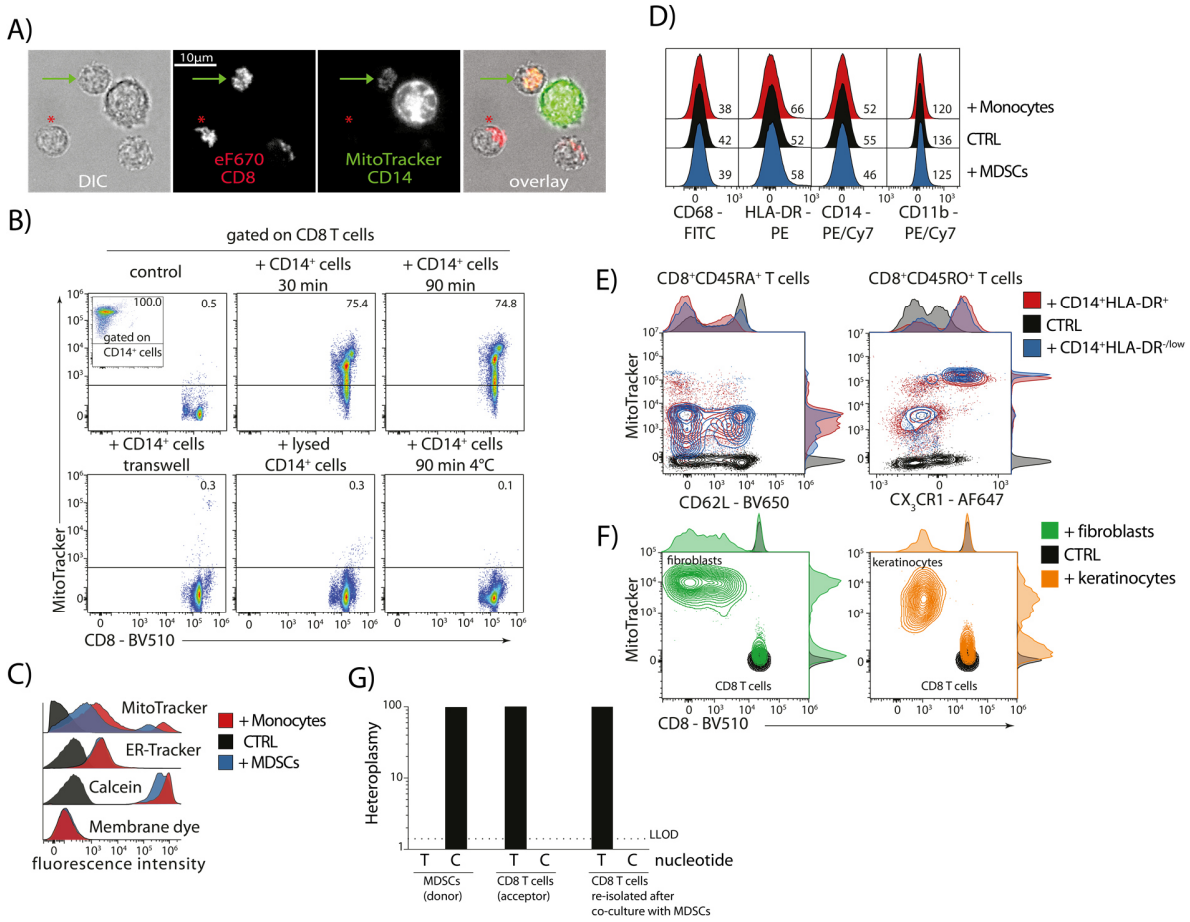

Figure 4: Transfer of cytosolic constituents from MDSCs to CD8⁺ T cells. A) Transfer of cytosolic constituents from myeloid cells (MitoTracker) to CD8⁺ T cells (eF670) after co-culture for 30 min. Green arrows point to a CD8⁺ T cell acquiring MitoTracker fluorescence. Scale bar: 10 µm (n = 4 independent biological samples). **B)** Detection of MitoTracker Green fluorescence in CD8⁺ T cells in co-culture (30 min) with MitoTracker Green–labeled MDSCs (transwell pore size 0.4 µm; MDSC lysis by hypo-osmotic shock; n = 3 independent biological samples; results shown gated for CD8⁺ T cells). **C)** Quantification of the transfer of cytosolic constituents to CD8⁺ T cells by flow cytometry for monocytes (red) and MDSCs (blue) (n = 4 independent biological samples). **D)** There was no transfer of myeloid cell surface markers to CD8⁺ T cells (n = 3 independent biological samples). **E)** Transfer of cytosolic constituents from tumor-infiltrating CD14⁺ cells of patients with cancer (that is, HLA-DR^{hi} monocytes and HLA-DR$^{-/low}$ MDSCs labeled with MitoTracker) to CD8⁺ T cells in co-culture (30 min). The results are shown gated for CD8⁺ T cells (n = 3 independent biological samples). The most pronounced transfer was into CX_3CR1^+CD45RO⁺ effector CD8⁺ T cells. **F)** There was no significant transfer of cytosolic constituents from MitoTracker-labeled primary human fibroblasts (left) or keratinocytes (right) to CD8⁺ T cells in co-culture (30 min) (n = 3 independent biological samples). **G)** There was no detection of single-nucleotide polymorphisms at position 152 of mitochondrial DNA from human MDSCs (donors) in lysates of CD8⁺ T cells (acceptors) FACS sorted after co-culture (30 min) (n = 5 independent biological samples in each experiment (that is, donor versus acceptor)), demonstrating that no mitochondrial DNA was transferred from MDSCs to CD8⁺ T cells, thus excluding the transfer of entire DNA-containing mitochondria. LLOD, lower level of detection. **Figure and description published in: Baumann et al., *Regulatory myeloid cells paralyze T cells through cell–cell transfer of the metabolite methylglyoxal*, Nature Immunology 21(5):555-566, May 2020, ©Springer Nature.**

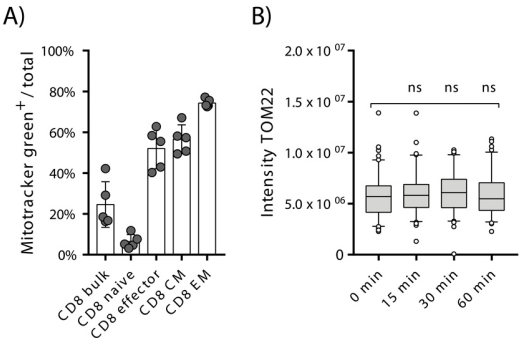

Figure 5: Cytosolic but not mitochondrial transfer from myeloid cells to CD8⁺ T cells. A) Frequency of MitoTracker green positive CD8⁺ T cells after co-culture with myeloid cells. Less naïve CD8⁺ T cells acquired MitoTracker green fluorescence compared with effecor, central memory (CM) or effector memory (EM) CD8⁺ T cells (n = 5). **B)** CD8⁺ T cells were co-cultured for 15, 30 or 60 min with myeloid cells, then stained for mitochondrial marker TOM22. Dots depict staining intensity of single CD8⁺ T cells measured via confocal microsocpy (n = 94-120 cells per condition in two independent experiments). Statistical analysis with one-way ANOVA.

3.2.2 Accumulation of the metabolite methylglyoxal in MDSCs

CD8⁺ T cells undergo metabolic reprogramming upon activation, often referred to as glycolytic switch, which is mandatory to fulfill the energetic and molecular demands of proliferation and cytokine production (Pearce and Pearce, 2013). CD8⁺ T cells in co-culture with MDSCs failed to up-regulate glycolytic metabolism upon anti-CD3/28 activation and consequently lacked nutrients to proliferate. Therefore, we attempted to restore CD8⁺ T cell functions by addition of dimethylbiguanide (DMBG) or rotenone to co-cultures with MDSCs. DMBG and rotenone are inhibitors of oxidative phosphorylation (OXPHOS), thereby forcing cells to engage in glycolysis. Both compounds target mitochondrial complex I of the respiratory chain but only DMBG restored T cell proliferation in co-culture with MDSCs, suggesting a mode of action apart from inhibition of complex I (El-Mir et al., 2000; Teeter et al., 1969; Wheaton et al., 2014) (Figure 6A).

DMBG is a drug primarily known for its anti-diabetic effects. Some of the complications associated with type 2 diabetes (T2D) are associated with advanced glycation end products (AGPs), which are built by non-enzymatic modification of proteins, lipids, and DNA with glucose or dicarbonyls (Goh and Cooper, 2008). Dicarbonyls are primarily generated by spontaneous de-phosphorylation of dihydroxyacetone phosphate (DHAP) during glycolysis but can be produced in enzyme-catalyzed reactions as well (Chakraborty et al., 2014). It was suggested, that part of the anti-diabetic effect of DMBG is covalent scavenging of reactive dicarbonyls and that this effect is dependent on the guanidine group (HN=C-(NH_2)(NHR)) of DMBG (Beisswenger and Ruggiero-Lopez, 2003; Kender et al., 2014; Kinsky et al., 2016).

In contrast to DMBG, rotenone lacks a guanidine group and is incapable to scavenge dicarbonyl metabolites.

We reasoned that dicarbonyls accumulated in MDSCs because of dysregulated metabolism and anticipated to test this hypothesis via mass spectrometry-based metabolite analysis. Strikingly, quantification of metabolites revealed that the prototypic dicarbonyl methylglyoxal (MGO) was approximately 30-fold increased in MDSCs compared with monocytes (Figure 6B-C).* To verify methylglyoxal concentrations with an alternative readout, MDSCs and monocytes were stained with the sensor dye MBo (methyl diaminobenzene-BODIPY) that covalently reacts with free MGO to a fluorescent product (Wang et al., 2013b). Flow cytometry confirmed, that MDSCs contained higher concentrations of MGO compared with monocytes (Figure 6D). Importantly, we found MBo positive cells among $CD14^{+}HLA\text{-}DR^{-/low}$ myeloid cells from cancer patients, indicating that MGO accumulation is a feature of stromal cell-induced and cancer patient-derived M-MDSCs (Figure 6E). When comparing $CD14^{+}$ myeloid cell populations collected from different anatomical compartments, most MBo positive cells were detected among intratumoral cells and low frequencies were detected in peritumoral liver tissue and blood of hepatocellular carcinoma (HCC) patients. In contrast, $CD15^{+}$ myeloid cells from all three compartments were MBo negative (Figure 6F). Treatment with DMBG strongly reduced methylglyoxal levels, as indicated by reduced MBo staining, and restored 2-NBDG uptake in MDSCs (Figure 6G-H). Underlining the MGO scavenging activity of guanidine groups, DMBG-related molecules aminoguanidine and methylguanidine reproduced MGO scavenging and 2-NBDG uptake. In contrast, the guanidine-lacking derivate robenidine failed to scavenge MGO and had no positive effect on glucose uptake (Figure 6H). Further strengthening the link between MGO and the dormant metabolism of MDSCs, DMBG treatment fully restored OXPHOS and glycolysis of MDSCs to levels comparable with monocytes, as indicated by oxygen consumption rates (OCR) and extracellular acidification rates (ECAR), respectively (Figure 6I-J).

Together, these experiments revealed accumulation of the dicarbonyl MGO that was connected to the depressed metabolic phenotype of MDSCs. In conjunction with the observation of dye transfer, we hypothesized that cytosolic fractions containing methylglyoxal were actively transported from MDSCs to $CD8^{+}$ T cells, thereby transferring metabolic dormancy and consequently functional unresponsiveness.

** Ultrahigh performance liquid chromatography with time-of-flight tandem mass spectrometry and data independent acquisition (UHPLC-TOF-DIA-MS/MS) measurement and analysis was performed by Andreas Dunkel Leibniz-Institute of Food Systems Biology, TUM, Munich*

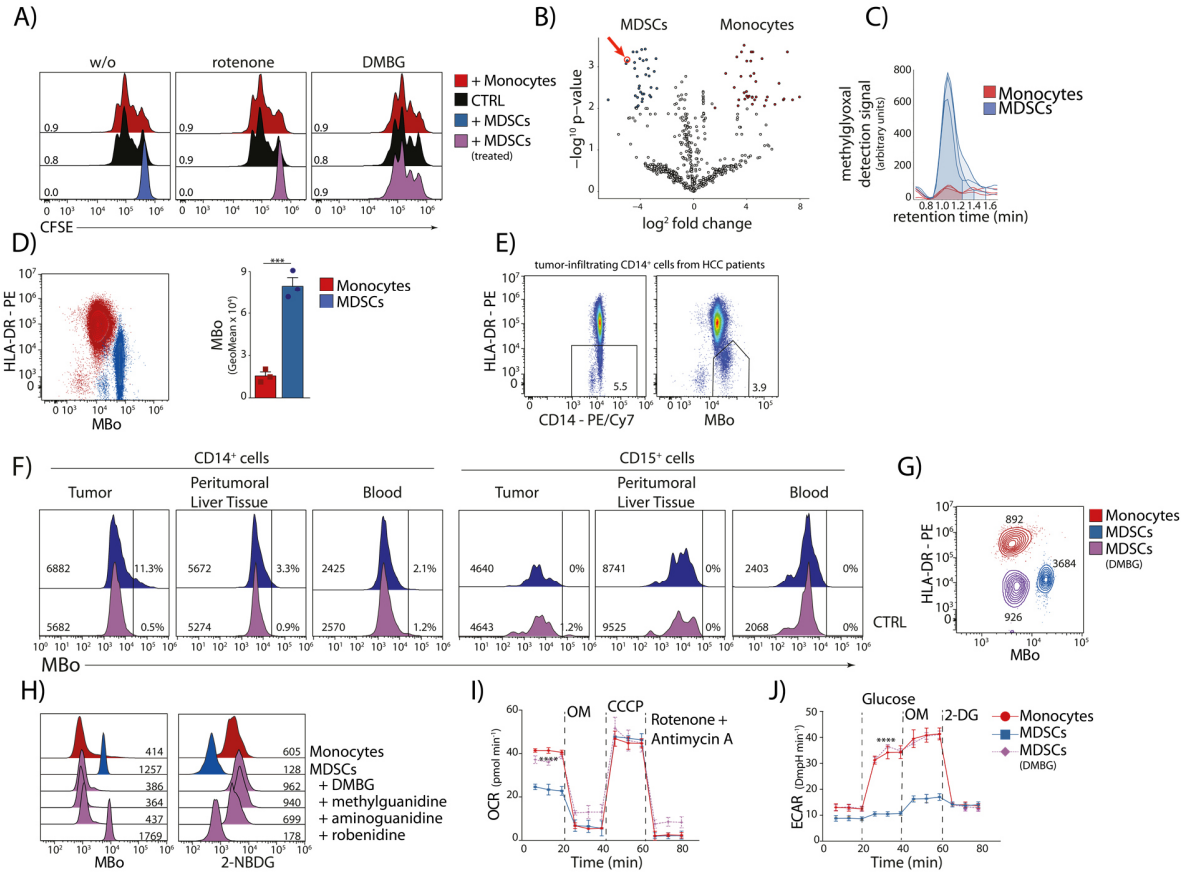

Figure 6: Accumulation of the dicarbonyl radical methylglyoxal is a metabolic marker for MDSCs and mediates their dormant metabolic phenotype. A) Proliferation profiles of activated CD8⁺ T cells after co-culture with MDSCs (blue) or MDSCs treated with rotenone (2 µM) or DMBG (200 µM) (purple) (n = 3). **B-J)** Analyses of MDSCs. **B)** Volcano plot (P value versus log_2[fold change]) of 3-nitrophenylhydrazine (3-NPH)-bound metabolites detected in MDSCs as compared with monocytes by UHPLC-TOF-DIA-MS/MS. The red arrow indicates methylglyoxal (feature ID: 67) (n = 6 independent samples). **C)** Ion chromatograms of 3-NPH-bound methylglyoxal (exact mass of 3-NPH-bound methylglyoxal: 206.0579 Da; tolerance: 0.01 Da; n = 3). **D-E)** Fluorescence intensity of the methylglyoxal-specific dye MBo in MDSCs and monocytes (**D**) and in tumor-infiltrating CD14⁺ cells isolated from patients with hepatocellular carcinoma (**E**) (n = 3). **F)** CD14⁺ or CD15⁺ cells were isolated from tumor tissue, liver tissue or blood from the same patient and examined for the expression of methylglyoxal (n = 2). **G)** MBo fluorescence intensity in MDSCs after DMBG treatment (30 min) (n = 5). **H)** MBo fluorescence (left) and glucose uptake (right) in MDSCs (with 30 min pretreatment with inhibitors). Note the absence of an effect with robenidine, which does not contain a guanidine group (n = 3 independent samples). **I-J)** OCRs (**I**) and ECARs (**J**) of MDSCs (with 30 min DMBG pretreatment) (n = 3 independent samples). ***P < 0.001 (two-way unpaired t-test); ****P < 0.0001 (two-way ANOVA). Error bars represent s.e.m. OM, oligomycin. **Figure and description published in: Baumann et al., *Regulatory myeloid cells paralyze T cells through cell–cell transfer of the metabolite methylglyoxal*, Nature Immunology 21(5):555-566, May 2020, ©Springer Nature.**

3.2.3 MDSCs generate methylglyoxal via semicarbazide-sensitive amine oxidase

We next questioned how methylglyoxal accumulates in MDSCs. MGO is dominantly produced via spontaneous de-phosphorylation of DHAP in most cell types (Chakraborty et al., 2014). Additionally, enzymatic synthesis via acetol mono-oxygenase (AMO) or semicarbazide-sensitive amine oxidase (SSAO) have been described (Chakraborty et al., 2014) (Figure 7A). To trace the origin of MGO in

3. Results

MDSCs, cells pulsed with 50% ^{13}C-labelled glucose and the molecular mass of MGO was analyzed via UHPLC-TOF-DIA-MC/MS.* If originating from glucose via spontaneous de-phosphorylation of DHAP, MGO mass would be expected to increase by three daltons in ^{13}C-glucose culture. Strikingly, MGO mass increased only by two daltons, indicating semicarbazide-sensitive amine oxidase (SSAO) mediated synthesis of MGO. SSAO catalyzes the production of MGO from glycine and acetyl-CoA, of which the latter is labelled with two ^{13}C-atoms when derived from ^{13}C-glucose (Figure 7B). Quantification of mRNA via quantitative polymerase chain reaction (q-PCR) confirmed expression of SSAO (gene AOC3) in MDSCs at higher levels compared with monocytes (Figure 7C). In line, blocking SSAO activity via the inhibitor hydralazine or PXS-4681A during the 72h induction phase on LX2 cell line prevented accumulation of MGO and down-regulation of 2-NBDG uptake in MDSCs, whereas inhibitors of unrelated amine oxidases (clorgyline, TETD) had no such effect (Figure 7D-E).

We furthermore analyzed pathways leading to the degradation of MGO. Since MGO is ubiquitously produced at low levels during glycolysis, eukaryotic cells developed an enzymatic pathway to prevent intracellular accumulation of methylglyoxal. In a first step, MGO is scavenged by reduced glutathione (GSH), then further converted to S-D-lactoylglutathione and D-lactate in two reactions catalyzed by glyoxalase I and II enzymes, respectively (Bellahcène et al., 2017). The conversion of MGO to S-D-lactoylglutathione can be monitored with an UV-spectrometer and used to determine glyoxalase I activity in cell lysates. In comparison with monocytes, MDSCs had a significantly reduced glyoxalase I activity (Figure 7F). Additionally, the concentration of the co-substrate glutathione, both in reduced form and total (reduced + oxidized), was lower in MDSCs, indicating exhausted MGO detoxification (Figure 7G). We speculated that higher glyoxalase I (gene GLO1) activity might protect CD8$^+$ T cells from suppression. Albeit glyoxalase I activity could be increased (factor 2X) by GLO1 transfection (Figure 8A), there was no significant alleviation of suppression in co-culture with MDSCs (Figure 8B). Thus, it is likely that MGO detoxification is not (only) limited by low glyoxalase I activity in CD8$^+$ T cells but also by a redox dysbalance.

In summary, low detoxification capacity of monocytes in conjunction with SSAO-mediated enzymatic production contributed to MGO accumulation and generation of MDSCs. Blocking SSAO activity during this induction period prevented the establishment of the inhibitory effects of MDSCs and their metabolic dormancy.

** Ultrahigh performance liquid chromatography with time-of-flight tandem mass spectrometry and data independent acquisition (UHPLC-TOF-DIA-MS/MS) measurement and analysis was performed by Andreas Dunkel Leibniz-Institute of Food Systems Biology, TUM, Munich*

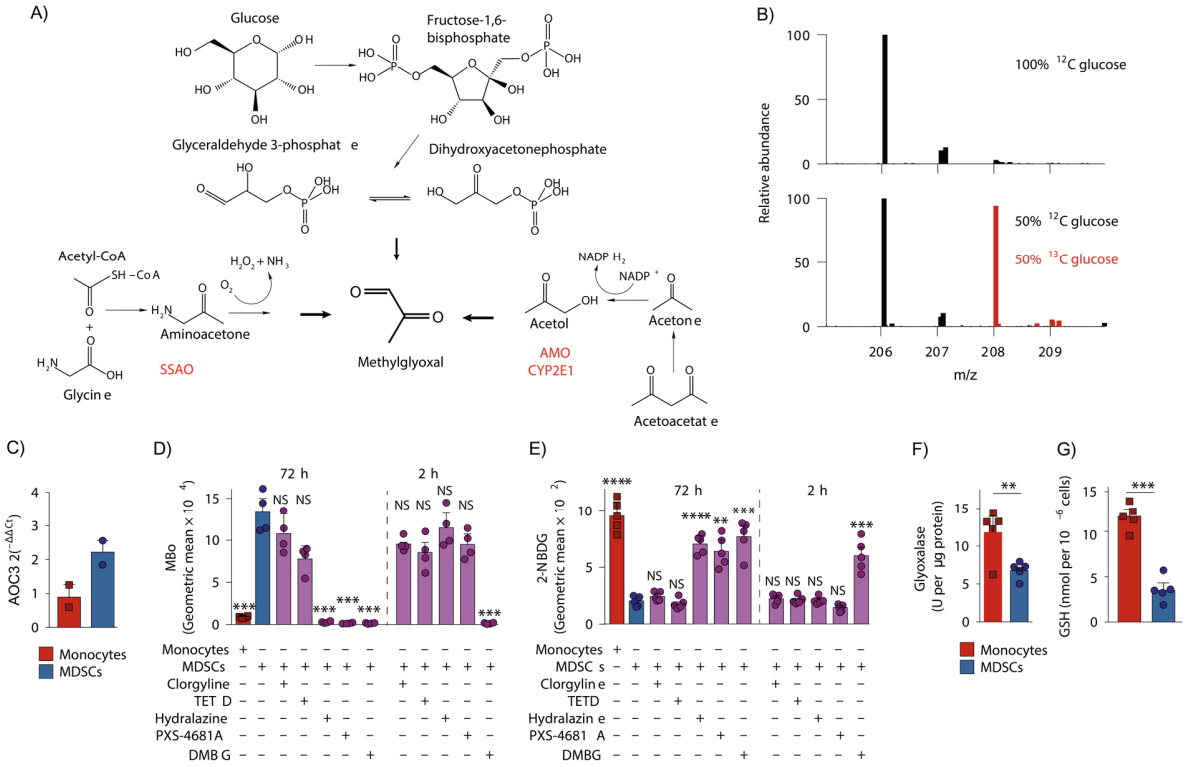

Figure 7: Methylglyoxal accumulates in MDSCs in a semicarbazide-sensitive amine oxidase-dependent fashion. A) Schematic of the different pathways for the generation of methylglyoxal in mammalian cells: spontaneous non-enzymatic dephosphorylation of glucose-derived dihydroxyacetone phosphate; AMO-mediated enzymatic generation from fatty acid-derived acetol; and SSAO-mediated generation from glucose- and amino acid-derived aminoacetone. **B-E)** Analyses of human MDSCs. **B)** Metabolic pulse (6 h) with 50% $^{13}C_6$ glucose and UHPLC-TOF-DIA-MC/MS analysis of MDSC lysates, showing the relative abundance of methylglyoxal isotopologs (technical triplicates: n = 2). **C)** AOC3 messenger RNA levels (coding for SSAO) in MDSCs and monocytes (n = 2 independent biological samples). **D)** MBo fluorescence intensity in MDSCs generated in the presence of the following inhibitors (72 h): the monoamine oxidase A inhibitor clorgyline (100 nM); the AMO inhibitor tetraethylthiuram disulfide (TETD; 1 µM); and the SSAO-specific inhibitors hydralazine (15 µM) and PXS-4681A (500 nM). Incubation of MDSCs with inhibitors for 2 h excluded direct neutralization of methylglyoxal. DMBG was used as a positive control that directly neutralized the glycation activity of methylglyoxal (n = 4 independent biological samples). **E)** Glucose uptake by MDSCs in the presence of the inhibitors described in **D)** with short incubation (2 h), demonstrating that the compounds did not have a direct effect on MDSCs (n = 5). **F)** Glyoxalase I activity (n = 5 independent biological samples). **G)** Glutathione (GSH) quantification (n = 5 independent biological samples). **P < 0.01; ***P < 0.001; ****P < 0.0001 (two-way unpaired t-test). Error bars represent s.e.m.. **Figure and description published in: Baumann et al., *Regulatory myeloid cells paralyze T cells through cell–cell transfer of the metabolite methylglyoxal*, Nature Immunology 21(5):555-566, May 2020, ©Springer Nature.**

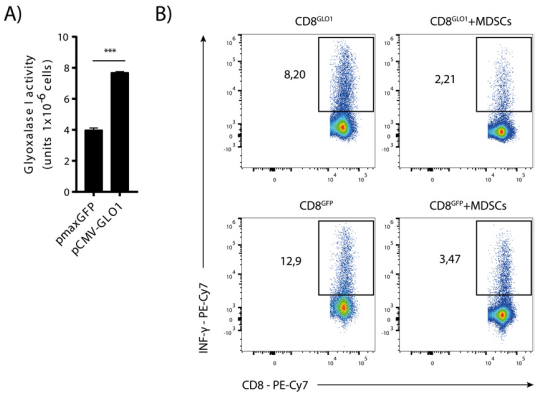

Figure 8: Increased glyoxalase I activity does not protect CD8⁺ T cells from MDSC-mediated suppression. A) Glyoxalase I activity in CD8⁺ T cells transfected with GLO1 (glyoxalase I) or GFP-coding control vector via electroporation (n = 2). **B)** GLO1 or GFP transfected CD8⁺ T cells co-cultured with or without MDSCs were stimulated for 4h with anti-CD3/28 beads, then intracellular TNF was quantified (n = 2). Gated on CD8⁺ T cells. Unpaired student t-test. *P < 0.05; **P < 0.01; ***P < 0.001; ****P < 0.0001.

3.2.4 SSAO detection in immunohistochemistry

To date, the identification of MDSCs in tissue slices via immunohistochemistry (IHC) is still challenged by the lack of specific markers. We wondered, if an IHC-based MDSC detection method could be developed based on antibody-recognition of MGO-induced protein modifications (MG-H1) or SSAO expression, respectively. Staining of tissue slices with anti-MG-H1, which is a glycation product of MGO binding to L-arginine residues in cellular peptides or proteins, yielded uniform high background in tumor and healthy tissue and could not unequivocally discriminate positive and negative cells (not shown). In contrast, anti-SSAO specifically stained the surface of endothelial cells in human HCC tissue and produced cytosolic staining of single cells scattered within the tumor tissue (Figure 10A).* To verify myeloid progeny of such cells, double staining with a myeloid marker like CD68 was attempted. Double staining could not be established yet due to technical challenges but will be subject of future efforts.

With SSAO-mediated accumulation of MGO we identified a previously unrecognized feature of MDSCs, that allows for the identification of MDSCs via flow cytometry (MBo staining) and putatively via immunohistochemistry (SSAO staining) based on a functional marker. Translation into clinical routine could facilitate the detection of MDSCs in cancer patients for diagnostic assessment and therapy decisions in future. However, further work needs to be invested to establish a double staining of SSAO with myeloid markers like CD68 and to validate the technique.

** IHC staining was established and performed by the group of Katja Steiger, Core Facility of Comparative Pathology, Institute of Pathology, TUM, Munich*

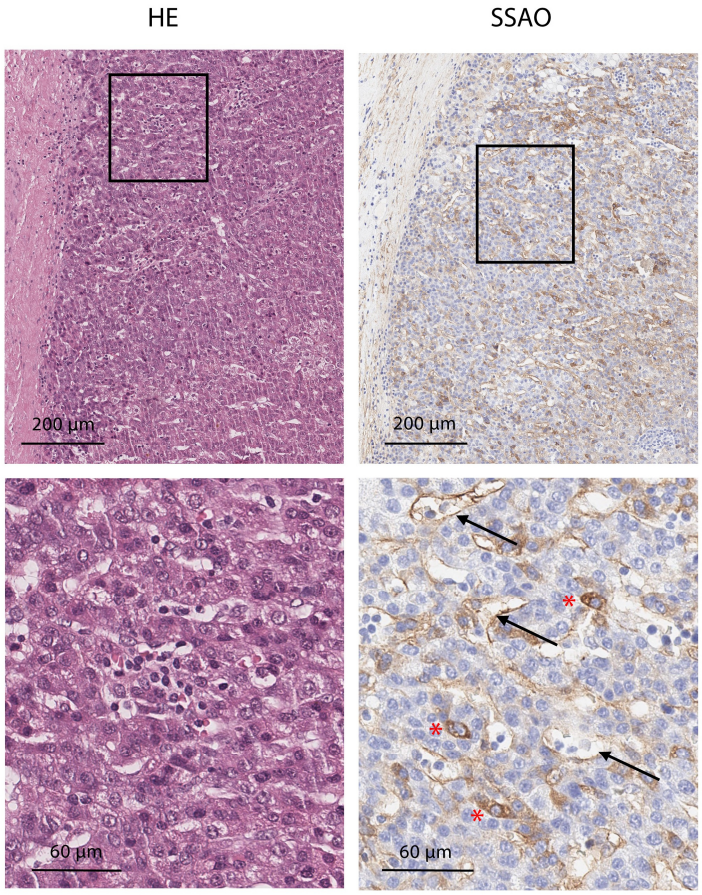

Figure 9: Detection of MDSCs via SSAO staining in immunohistochemistry. Hematoxylin and eosin (HE) stain (left) and SSAO (right) staining of liver tissue from human HCC patient. Black arrows point towards SSAO positive endothelium and red asterix mark cells, that contain intracellular SSAO. Top: 15X magnification. Bottom: 40X magnification.

3.2.5 Glycation of intracellular arginine in CD8⁺ T cells

Having established a link between MGO accumulation and the suppression of MDSC metabolism, we wanted to investigate if MGO is transferred to CD8⁺ T cells and how it interferes with CD8⁺ T cell effector functions. Increased MBo staining of CD8⁺ T cells together with depressed 2-NBDG uptake after co-culture with MDSCs suggested, that MGO is transferred from MDSCs to CD8⁺ T cells, thereby interfering with T cell glucose metabolism as observed in MDSCs (Figure 10A). Further strengthening the connection between MGO transfer and the depression of glucose uptake, 2-NBDG staining was unaffected and no MGO was detected in CD8⁺ T cells when MDSCs were pre-treated with DMBG (Figure 10A). In line with studies demonstrating a tight connection between metabolic reprogramming and effector functions of activated T cells (Chang et al., 2013; Gubser et al., 2013; Menk et al., 2018), the production of IFN-γ and TNF as well as proliferation of anti-CD3/28 stimulated CD8⁺ T cells was

suppressed by MDSCs but again treatment with DMBG and guanidine-containing derivates counteracted the inhibition (Figure 10B-C). $CD8^+$ T cells treated with exogenously added MGO were unable to proliferate, directly demonstrating a suppressive effect of MGO on T cells (Figure 11A). Re-isolated $CD8^+$ T cells recovered from MDSC-mediated suppression within 4h, but treatment with DMBG shortened this time frame to 1h (Figure 10B). In co-cultures with cancer patient-derived $CD14^+HLA\text{-}DR^{-/low}$ M-MDSCs suppression of $CD8^+$ T cell proliferation was strongest for cells originating from the tumor and lower from peritumoral liver tissue or blood, which is in line with highest frequencies of $CD14^+MBo^+$ cells in the tumor (Figure 5f). Despite, DMBG treatment alleviated the suppression of M-MDSCs originating from all three compartments, underlining the significance of MGO for suppression of T cell immunity in cancer (Figure 10D).

We wondered how MGO interferes with T cell metabolism and effector functions on a molecular level. MGO primarily reacts with guanidine groups of L-arginine residues to a variety of chemical products, and to a lesser extent with L-lysine, L-cysteine or L-tryptophan (Li et al., 2018). Reaction of L-arginine with methylglyoxal was confirmed in a cell-based assay (Figure 11B). In a control setting, L-glutamine had only little effect on the readout which is possibly explained by the reaction of MGO with free amino groups in L-glutamine (Figure 11B). L-arginine is critical for the activation of $CD8^+$ T cells (Bronte et al., 2003; Geiger et al., 2016) and L-arginine depletion could account for the suppressive effect of MGO on $CD8^+$ T cell effector functions. As expected, mass spectrometry-based quantification revealed exhaustion of intracellular L-arginine in $CD8^+$ T cells after co-culture with MDSCs (Figure 11E-F).* In line, the concentration of argpyrimidine and MG-H1 (methylglyoxal 5-hydro-5-methylimidazolones), both reaction products of L-arginine with MGO, was increased in MDSCs (Figure 11F). We also observed deprivation of intracellular L-glutamine in $CD8^+$ T cells co-cultured with M-MDSCs, which is hardly bound by MGO (Figure 11B). However, L-glutamine serves as educt for glutathione synthesis, which is bound by methylglyoxal during glyoxalase-mediated detoxification. The depletion of L-glutamine could therefore rather indicate GSH exhaustion and represent an indirect effect of MGO transfer. Summarized, we propose that the suppressive effect mediated by MDSCs on $CD8^+$ T cells is based on the intracellular depletion of L-arginine by MGO and this suppression can be counteracted by molecules containing a guanidine group, like DMBG.

** Quantification of free amino acids and derivates via stable isotope dilution analysis (SIDA) UHPLC-MS/MS_{MRM} by Christian Schmid*
Food Chemistry and Molecular Sensory Science, TUM, Munich

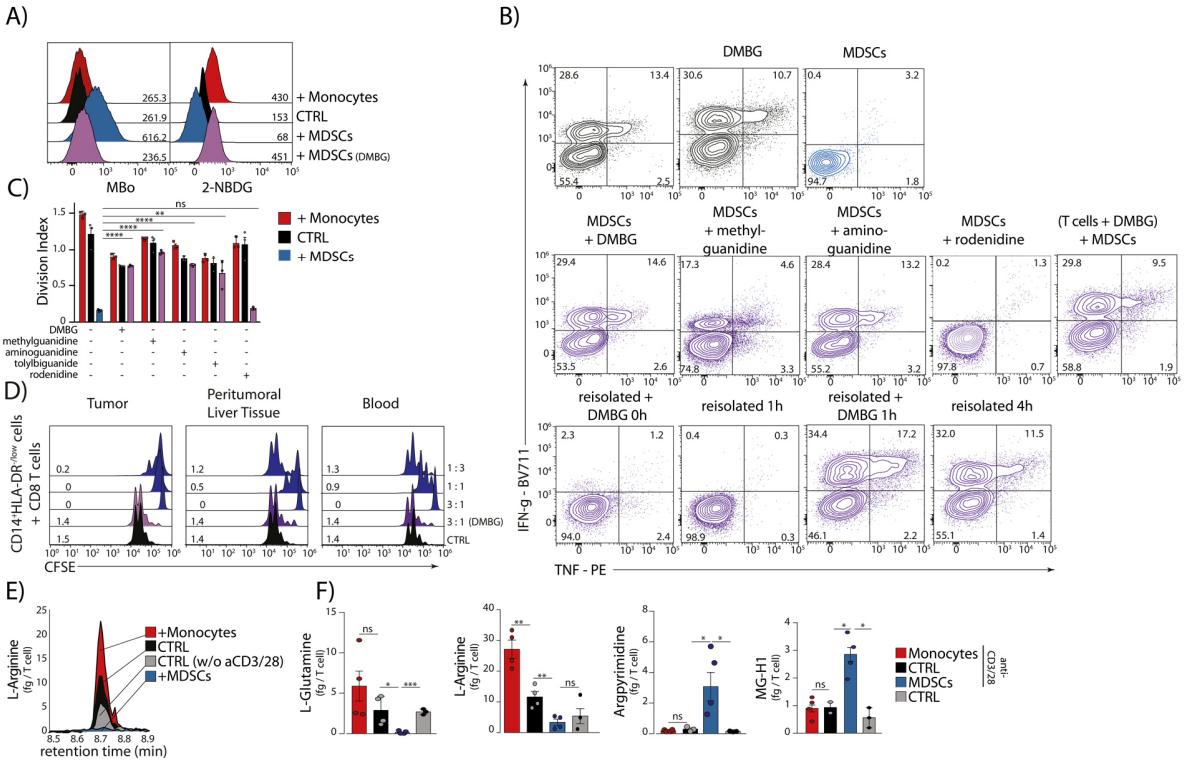

Figure 10: Guanidine treatment of MDSCs abrogates their suppressive activity on CD8+ T cell effector functions. A-F) Analyses of human activated $CD8^+$ T cells in co-culture with MDSCs. These cells were pretreated (for 30 min) with the indicated inhibitors. **A)** MBo fluorescence (left) and glucose uptake (right) in $CD8^+$ T cells after 10 min of co-culture with MDSCs or monocytes (n = 3 independent samples). **B)** Top: intracellular cytokine staining of activated $CX_3CR1^+CD45RO^+$ $CD8^+$ T cells (n = 3 independent samples). Middle: T cells were stimulated in the presence of MDSCs (pretreated with DMBG, methylguanidine, aminoguanidine or rodenidine (200 µM), as indicated). Bottom: T cells were pretreated with DMBG, re-isolated after co-culture with MDSCs and stimulated after 1 or 4 h, or treated with DMBG directly or after 1 h. **C)** Proliferation of activated $CD8^+$ T cells in co-culture with MDSCs or monocytes in the presence of the indicated compounds (CFSE dilution; numbers denote division indices) (n = 3). **D)** $CD14^+$ or $CD15^+$ cells isolated from tumor tissue, liver tissue or blood from the same patient were isolated and co-cultured with CFSE-labeled, activated $CD8^+$ T cells. Proliferation was measured by the dilution of CFSE (n = 2). **E-F)** Free amino acids and AGPs were measured using SIDA-UHPLC-MS/MS_{MRM} in $CD8^+$ T cells after co-culture with MDSCs or monocytes. **E)** Ion chromatogram of free L-arginine in $CD8^+$ T cells. **F)** Quantification of the amino acids L-glutamine and L-arginine and the glycation products argpyrimidine and MG-H1 (n = 4). *P < 0.05; **P < 0.01; ***P < 0.001; ****P < 0.0001 (two-way unpaired t-test). Error bars represent s.e.m. **Figure and description published in: Baumann et al., *Regulatory myeloid cells paralyze T cells through cell–cell transfer of the metabolite methylglyoxal*, Nature Immunology 21(5):555-566, May 2020, ©Springer Nature.**

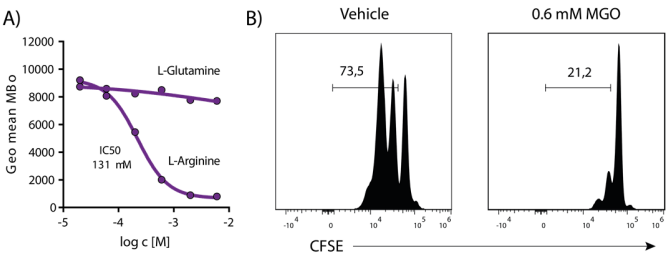

Figure 11: The effect of methylglyoxal on T cell proliferation and scavenging activity of guanidine-containing compounds. A) $CD8^+$ T cells were treated with vehicle (left) or 0.6 mM MGO (right) for 30 min at 37°C, then stimulated with anti-CD3/28 beads. Impaired proliferation upon MGO treatment indicated by low CFSE dilution after 72h culture (n = 2). **B)** Cells were

treated with increasing concentrations of L-glutamine or guanidine group containing L-arginine in the presence of 0.6 mM MGO, then stained with MBo. MGO scavenging activity of L-arginine indicated by decreasing MBo fluorescence (n = 1).

3.2.6 DMBG treatment supports ICB therapy in mice

Being aware of the pivotal role of MDSCs in the suppression of anti-cancer immunity and the correlation with non-responsiveness to ICB therapy in human cancer patients (Gebhardt et al., 2015; Martens et al., 2016; Meyer et al., 2014; Sade-Feldman et al., 2016; Weber et al., 2016), we combined DMBG with anti-PD-1 treatment in the ovalbumin (OVA) antigen expressing mouse melanoma model B16-OVA. Furthermore, we included a therapeutic vaccination consisting of OVA adjuvanted with the toll-like receptor 9 (TLR9) ligand CpG and the natural killer T (NKT) cell stimulant alpha-galactosylceramide (αGalCer) into our study. Mice were subcutaneously implanted with B16-OVA into the left flank. At day 10 after implantation, mice were vaccinated and treatment with anti-PD-1 or DMBG was initiated. All three treatments only had marginal effects on tumor growth when applied alone (Figure 12A). However, the combination of anti-PD-1 and DMBG exerted strong synergistic effects on the duration of tumor remission irrespective of vaccination (Figure 12A). As expected, tumor-derived myeloid cells (both $CD11b^+Ly6C^+$ M-MDSCs and $CD11b^+Ly6G^+$ G-MDSCs) from mice treated with vaccination or anti-PD-1 were MBo positive, had low glucose uptake and suppressed $CD8^+$ T cell proliferation *ex vivo* (Figure 12B-D). This is different to human $CD15^+$ PMN-MDSCs, which were devoid of MGO (Figure 6f). In sharp contrast, myeloid cells from animals that received DMBG via drinking water showed no sign of MGO accumulation, had normal 2-NBDG uptake and were non-suppressive (Figure 12B-D). Accordingly, only $CD8^+$ T cells from such animals were MBo negative and consumed 2-NBDG, which was most pronounced in CX_3CR1^+ effector $CD8^+$ T cells (Figure 12E-G). Furthermore, $CD8^+$ T cells isolated from mice receiving combined treatment of anti-PD-1 and DMBG were responsive to re-stimulation with OVA peptide *ex vivo*, as indicated by IFN-γ and TNF expression (Figure 12H-I). Together, these results comprehensively demonstrate a synergistic effect of anti-PD-1 and DMBG treatment in the restoration of $CD8^+$ T cell mediated anti-cancer immunity.

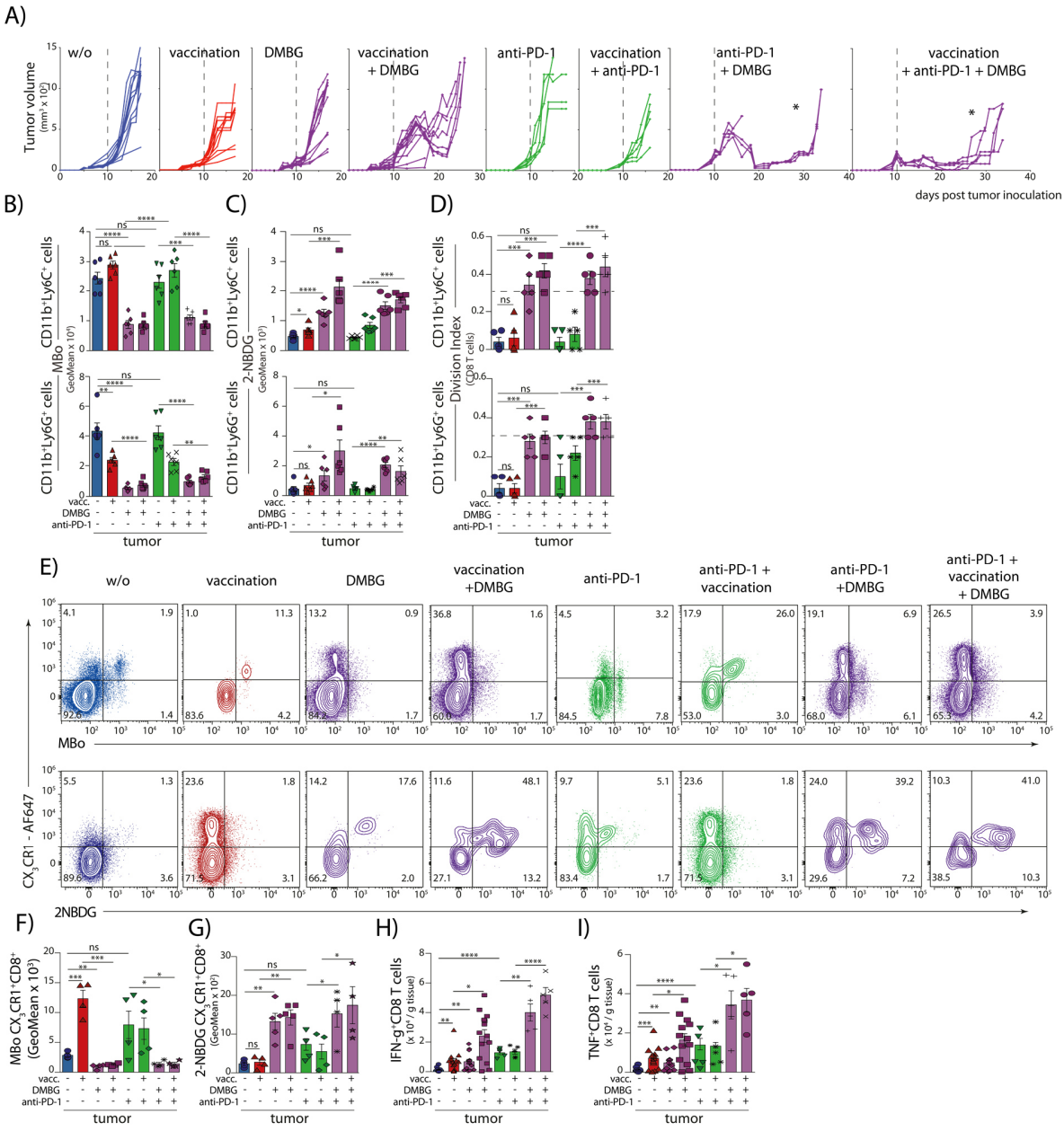

Figure 12: DMBG treatment overcomes MDSC-induced suppression of CD8⁺ T cell function during therapeutic anti-cancer vaccination. DMBG treatment overcomes MDSC-induced suppression of CD8⁺ T cell function during therapeutic anti-cancer vaccination. **A-G)** At day 10 after subcutaneour B16-OVA cancer cell inoculation, mice received ovalbumin adjuvanted with CpG/αGalCer, anti-PD-1 and/or DMBG in drinking water (40 mM). Analyses were performed at day 17 (n = 5 mice). **A)** Time kinetics of cancer growth in individual mice. **B-C)** MBo fluorescence (**B**) and glucose uptake (**C**) of CD11b⁺ cells from cancer tissue and spleen. **D)** CD8⁺ T cell proliferation (CFSE dilution) in co-culture with CD11b⁺Ly6C⁺ or CD11b⁺Ly6G⁺ cells (FACS sorted) from cancer tissue (numbers denote division indices). **E-G)** MBo fluorescence (top row in **E** and quantified in **F**) and glucose uptake (bottom row in **E** and quantified in **G**) *ex vivo* in CD8⁺ T cells from tumor tissue. **H-I)** Cytokine expression (IFN-γ (**H**) and TNF (**I**)) by CD8⁺ T cells from cancer tissue after *ex vivo* ovalbumin peptide-specific stimulation. Data are presented as means ± s.e.m. *P < 0.05; **P < 0.01; ***P < 0.001; ****P < 0.0001 (two-way unpaired t-test). **Figure and description published in: Baumann et al., *Regulatory myeloid cells paralyze T cells through cell–cell transfer of the metabolite methylglyoxal*, Nature Immunology 21(5):555-566, May 2020, ©Springer Nature.**

3.3 Functional suppression of NK cells by acute myeloid leukemia blasts

Having discovered the mechanism of methylglyoxal transfer from MDSCs to $CD8^+$ T cells in the context of solid tumors, we wondered if this mechanism also appears in hematological cancer. We chose to conduct our studies with acute myeloid leukemia (AML) cells, an aggressive type of leukemia originating from myeloid progenitor cells. In AML, therapeutic options are limited to high dose chemotherapy and hematological stem cell transfer and different signs of immune suppression have been described.

Various studies demonstrated that NK cells are important combatants in acute myeloid leukemia (Giebel et al., 2003; Hsu et al., 2005; Ruggeri et al., 2002; Savani et al., 2007). Accordingly, the cytolytic activity and cytokine production of autologous NK cells is a sensitive predictor of relapse and disease-free survival in patients achieving complete remission (Lowdell et al., 2002; Tajima et al., 1996; Tratkiewicz and Szer, 1990). However, several studies reported functional and phenotypic deficiencies of NK cells in AML. Patient NK cells are equipped with low levels of the activating receptors NKp30 (natural cytotoxicity triggering receptor 3), NKp46 (natural cytotoxicity triggering receptor 1), NKG2D (natural killer group 2D) and DNAM-1 (DNAX accessory molecule-1) compared with healthy controls (Costello et al., 2002; Fauriat et al., 2007; Khaznadar et al., 2015; Sanchez-Correa et al., 2011, 2012; Tang et al., 2020). All four receptors recognize surface ligands expressed on virus infected or tumorigenic cells and are critical for the activation of NK cells and the clearance of target cells. The expression of NKp30 and NKp46 is down-regulated in patients at diagnosis, but higher during complete remission, connecting the presence of AML blasts with the down-regulation of these receptors (Fauriat et al., 2007). Also, the functional response of NK cells towards a target cell line and autologous leukemia cells was found strongly impaired in AML patients compared with age matched controls, but partly restored during remission (Stringaris et al., 2014). The reduced expression of activating receptors correlated with the overall survival and relapse risk of AML patients (Fauriat et al., 2007; Khaznadar et al., 2015).

However, the regulatory mechanism behind the dysfunctional phenotype and reduced effector functions of NK cells in AML is insufficiently understood. We therefore hypothesized that AML blasts have a direct suppressive effect on NK cells. The aim of this second part of the study was to shed light on immune suppressive mechanisms in AML.

3.3.1 NK cells in AML are low responsive and have reduced activating receptor expression

To verify previously published results, the expression levels of NKp30, NKp46, NKG2D and DNAM-1 were measured in NK cells ($CD3^- CD56^+$) derived from AML patient blood and compared with healthy controls via flow cytometry. As expected, AML patient-derived NK cells expressed lower surface levels of all four activating receptors (Figure 13A). To test for functionality, NK cells from patients and healthy controls were stimulated with K562, an immortalized myeloid leukemia cell line that is highly susceptible to NK-cell mediated killing. Due to the high expression of MICA/B and ULBP1-6 (ligands of NKG2D), CD112 and CD155 (ligands of DNAM-1) and B7-H6 (ligand of NKp30) together with low expression of HLA-class I molecules (ligands of inhibitory KIR receptors) K562 cells trigger multiple stimulatory NK cell receptors and represent a suited model to study NK cell effector functions against tumor cells (Bae et al., 2012; Sabry et al., 2019; Tremblay-McLean et al., 2019). Stimulation with K562 cells induced synthesis of proinflammatory cytokines IFN-γ and TNF in healthy NK cells, but not in NK cells originating from AML patients (Figure 13B). Due to the low frequency of NK cells in AML peripheral blood (often reduced due to dysregulated hematopoiesis and excessive blast content) further comprehensive characterizations of patient NK cells are not feasible without cytokine-driven expansion (via IL-2, IL-12, IL-15 or IL-18). Therefore, an in vitro co-culture system was developed to study the effects of AML blasts on healthy NK cells. In this model, AML blasts are pre-cultivated on MS-5 feeder cells for 4 days as described by van Gosliga et al. (van Gosliga et al., 2007). Then, blasts are removed from the feeder layer and co-cultivated with allogenic, healthy donor-derived peripheral blood NK cells for additional 18h. Phenotypic, functional and metabolic characteristics of co-cultivated NK cells were comprehensively analyzed and compared to NK cells cultured in the absence of AML blasts.

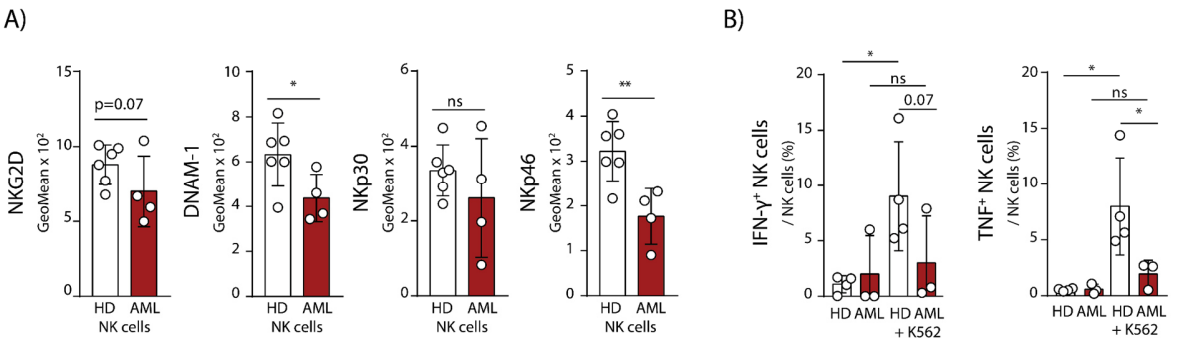

Figure 13: AML patient-derived NK cells are dysfunctional. A) Expression of NKG2D, DNAM-1, NKp30 or NKp46 was measured via flow cytometry in healthy donor-derived (HD) and AML patient-derived (AML) NK cells (gating on $CD3^- CD56^+$). Geo mean of staining is depicted (n = 4 biological replicates for AML and n = 6 for HD). **B)** Cells were stimulated for 4h with K562 or left unstimulated. The frequency of IFN-γ or TNF positive cells was assessed via flow cytometry (n = 3 biological replicates for AML

and n = 4 for HD). Statistical analysis: Unpaired (A) or paired (B) one-tailed student T test. *p<0.05; **p<0.01; ***p<0.001; ****p<0.0001.

3.3.2 AML blasts affect effector functions of NK cells

In commencing experiments, we tested if healthy NK cells acquired phenotypic and functional deficiencies in co-culture with AML blasts, comparable to AML patient NK cells. In overnight co-culture with AML blasts, healthy NK cells down-regulated NKG2D, DNAM-1 and NKp30, thereby phenotypically resembling AML patient NK cells (Figure 14A). The down-regulation of NKp46 was not reproduced in the overnight co-culture and we assume the receptor is regulated with slower time kinetics (Figure 14A). The down-regulation of NKG2D, DNAM-1 and NKp30 was observed for $CD3^-$ $CD56^{bright}$ and $CD3^-$ $CD56^{dim}$ NK cells, the two main sub-types of NK cells described in humans (not discriminated in the figure). Next, the recognition of AML blasts by NK cells was analyzed. Healthy NK cells are well suited to recognize allogenic tumor cells. Still, there was only induction of cytokine production in co-culture with K562 cells but not with AML blasts (Figure 14B). Additionally, the expression of CD69 and CD107a was measured, of which the latter is a surrogate marker for degranulation (Lorenzo-Herrero et al., 2019). Although, the early activation marker CD69 suggested simulation of NK cells by AML blasts, only a minor frequency of NK cells degranulated (Figure 14B). We wanted to know, if NK cells not only fail to recognize AML blasts, but are actively suppressed. To this end, NK cells were co-cultivated with AML blasts in different ratios (AML blasts:NK cells = 0.3:1, 1:1, 3:1, 10:1) followed by K562 stimulation. The production of IFN-γ and TNF by NK cells in response to K562 stimulation after contact with blasts decreased in a dose dependent manner (Figure 14C-E and J). To analyze target cell killing by NK cells, the frequency of apoptotic K562 cells was measured after a 3h stimulation period. In line with hampered cytokine production, lower frequencies of NK cells degranulated after co-culture with AML blasts and the killing of K562 cells was significantly impaired (Figure 14F-H and J). No effect on GzmB expression was observed, suggesting NK cells were armed with cytotoxic granules but not competent to degranulate (Figure 14I). The degree of suppression was not significantly correlated with a specific FAB subtype, the stage of disease (initial diagnosis or relapse) or specific mutations associated with AML (NPM1, FLT3-ITD, FLT3-TKD) (not shown). Multiple studies showed, that mTORC1 signaling is up-regulated upon NK cell activation and interconnected with NK cell effector functions (Donnelly et al., 2014; Jensen et al., 2017; Keating et al., 2016; Nandagopal et al., 2014). mTOR is the catalytic unit of mTORC1 and its kinase activity is responsible for metabolic down-stream effects. Interestingly, with AML blast co-cultured NK cells only had low mTOR phosphorylation, suggesting that NK cell metabolic reprogramming is affected by AML blasts (Figure 14J-K). Nonetheless, in the short period of stimulation

(4h) only minor adaptations of OXPHOS and glycolysis have been observed in NK cells stimulated with K562 and blocking mTOR signaling had no effect on NK cell effector functions (data not shown).

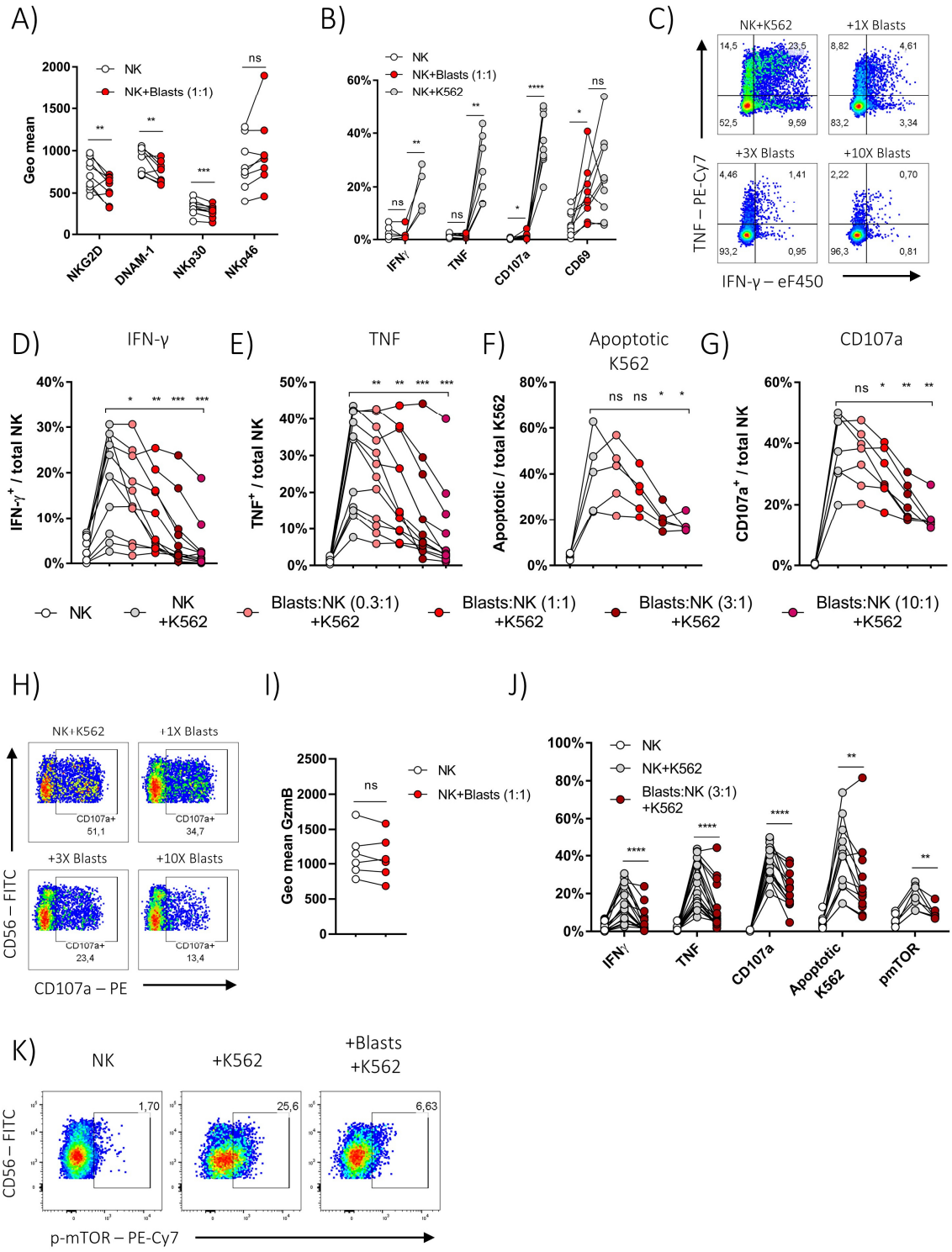

Figure 14: *In vitro* with AML blasts co-cultivated NK cells aquire functional defects of AML patient NK cells.The expression of NKG2D, DNAM-1, NKp30 or NKp46 was measured via flow cytometry and geo mean of staining is depicted (gate on NK cells). Connected data points depict NK cells from the same donor cultured alone (filled white circles) or with AML blasts in 1:1 ratio (filled red circles) overnight (n = 9 biological replicates). **B)** NK cells were stimulated with AML blasts or K562 cells. Cytokine production, degranulation (CD107a) and the activation marker CD69 was measured via flow cytometry (n = 5-9 biological replicates depending on readout). **C-E)** NK cells cultivated alone or with increasing numbers of AML blasts (0.3/1/3/10:1) were stimulated for 4h with K562. Representative plots (**C**, gate on NK cells) or frequency of IFN-γ (**D**; n = 11) and TNF (**E**; n = 12) positive cells is shown. Sets of connected data points depict one biological replicate from an independent experiment. **F-H)** NK cells were stimulated for 3h with K562 and frequency of apoptotic K562 (**F**; n = 5) or frequency of CD107a positive NK (**G**; n = 7) was assessed via flow cytometry. **H)** Representative plots showing CD107a expression (gate on NK cells). **I)** Geo mean of GzmB expression (n = 6 biological replicates). **J)** NK cells unstimulated (filled white circles) or K562 stimulated NK cells without (filled grey circle) or with 3:1 AML blasts in co-culture (filled dark red circles) (IFN: n = 18, TNF: n = 20, CD107a: n = 14, Killing: n = 12, pmTOR: n = 7). **K)** Representative FACS plot showing reduced phosphorylation of mTOR in stimulated NK cells co-cultivated with AML blasts. Statistical analysis: paired one-tailed student T test (A, B, I, J) or repeated measures one-way ANOVA (D-G). *p<0.05; **p<0.01; ***p<0.001; ****p<0.0001.

We tested if cell death was induced in NK cells in co-culture with AML blasts, accounting for reduced effector functions. The number of viable NK cells was equal in all tested co-culture conditions as measured with counting beads and live/dead staining in flow cytometry, excluding negative effects on NK cell viability (Figure 15A). Furthermore, it was tested if the observed suppressive effects of AML blasts on NK cells was also induced in co-culture with non-cancer cells. The addition of allogenic monocytes did not suppress NK cell effector functions towards K562, pointing towards an effect exclusive for pathogenic myeloid cells (Figure 15B). Together, these results demonstrate moderate loss of receptor expression, strong reduction of all major NK cell effector functions and reduced mTORC1 signaling after overnight-contact with AML blasts.

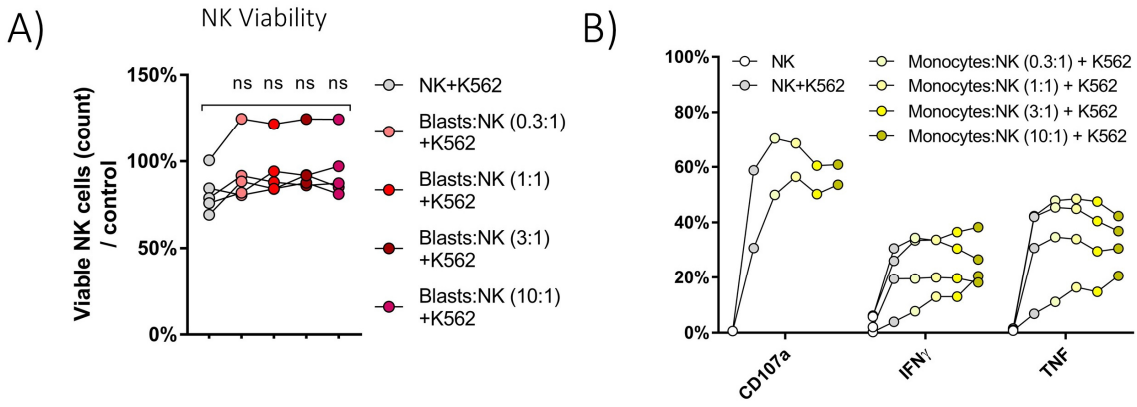

Figure 15. Controls of co-culture experiments. A) Viability of NK cells in co-culture normalized to NK cell count of control well (n = 5 biological replicates). **B)** NK cell effector functions in co-culture with allogenic monocytes, culture conditions as with AML blasts. Statistical analysis: One-way ANOVA with Dunnett correction (A). *p<0.05; **p<0.01; ***p<0.001; ****p<0.0001.

3.3.3 Amino acid metabolism of NK cells

We wondered if impaired mTOR phosphorylation is not the cause but rather a consequence of blast-mediated suppression. mTORC1 is a protein complex that integrates multiple metabolic signals (that is oxygen level, energy or ADP/ATP ratio, amino acid availability and growth factor signals) and regulates anabolic metabolism in mammalian cells (Laplante and Sabatini, 2009). Intracellular mTORC1 is stabilized by several amino acids, including the neutral amino acid L-leucine. NK cells activated in leucine-deficient medium are deficient for mTORC1 signaling (Loftus et al., 2018). In NK cells, glutamine is taken up shortly after stimulation via glutamine transporter SLC1A5 (solute carrier family 1 member 5). Glutamine is then exported via neutral amino acid antiporter CD98 in exchange for other neutral amino acids, including L-leucine. Influx of amino acids is not only important for mTORC1 stabilization, but also translation of cytokines and synthesis of the metabolic regulator c-myc (O'Brien and Finlay, 2019). In a study conducted by Jensen and co-workers, pharmacological blockade of SLC1A5 or CD98 suppressed IFN-γ production and degranulation of NKG2D-stimulated NK cells that were primed with IL-2, undermining the importance of amino acid availability for NK cell effector functions (Jensen et al., 2017). Furthermore, arginase-dependent depletion of L-arginine diminishes IL-12/IL-18-stimulated NK cell proliferation and IFN-γ secretion (Oberlies et al., 2009). Interestingly, in a study of Mussai expression of arginase II by AML blasts was detected and blocking arginase and iNOS activity prohibited the suppression of T cell proliferation (Mussai et al., 2013). We reasoned that L-arginine depletion could be connected to NK cell suppression. Accordingly, the arginase inhibitor nor-NOHA and the iNOS inhibitor L-NMMA were added to co-cultures, but no alleviation of blast-mediated suppression was detected (Figure 16A). In co-culture with MDSCs, $CD8^+$ T cells exhibited intracellular L-arginine deprivation that was attributed to methylglyoxal transfer. We therefore tested, if MGO is transferred from AML blasts to NK cells. However, the presence of the MGO scavenger DMBG could not rescue NK cells from blast-mediated suppression, excluding involvement of MGO transfer (Figure 16B). Not only targeted modes of amino acid depletion are associated with tumor cells, but also blast-mediated nutrient consumption could account for amino acid shortage in NK cells. To test this possibility, NK cells were re-isolated from blast co-culture and intracellular amino acids were analyzed via UHPLC-MS/MS.* Measurement of free amino acids in AML co-cultured NK cells did not indicate differences in the concentration of L-leucine, L-arginine, L-glutamine or any other amino acid, arguing against

interference with amino acid metabolism (Figure 16C). In summary, MGO transfer is not part of blast-mediated NK cell suppression and we fond neither evidence for enzymatic depletion of L-arginine, nor amino acid deprivation in co-cultures in general.

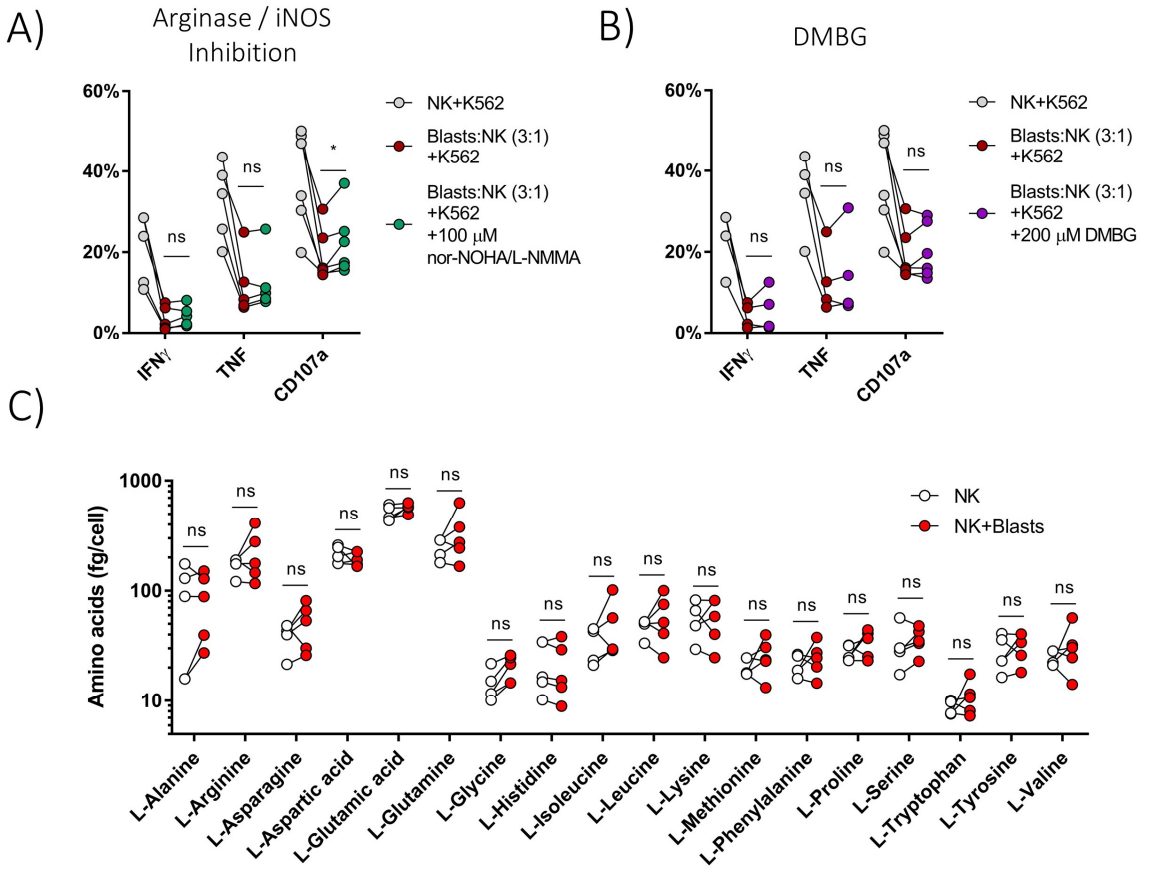

Figure 16: Amino acid metabolism of NK cells and methylglyoxal transfer. NK cells were co-cultured with AML blasts overnight. **A-B)** Addition of 100 µM nor-NOHA/L-NMMA (each) (**A**) or 200 µM DMBG (**B**) to NK-AML co-cultures did not alleviate the suppressive effect **C)** Measurement of intracellular amino acids via SIDA UHPLC-MS/MS_{MRM}. No significant difference in intracellular amino acid composition between NK cells cultured alone or with AML blasts (n = 5 biological replicates). Statistical analysis: student T test with Sidak-Holm correction for multiple comparisons (C) and paired one-tailed student T test (A, B). *p<0.05; **p<0.01; ***p<0.001; ****p<0.0001.

** Quantification of free amino acids and derivates via stable isotope dilution analysis (SIDA) UHPLC-MS/MS_{MRM} by Christian Schmid*
Food Chemistry and Molecular Sensory Science, TUM, Munich

3.3.4 TGF-β1, PD-L1 and adenosine

Since methylglyoxal and arginase / iNOS activity was not involved in blast-mediated NK cell suppression, we searched for alternative modes of NK cell regulation. In a study from 2017, Hong and others discovered AML-derived exosomes presenting surface-bound TGF-β1, PD-L1 and adenosine producing enzymes CD38 and CD73. Incubation of the NK cell line NK-92 with AML-derived exosomes suppressed K562 killing and addition of a TGF-β blocking antibody alleviated the suppressive effect partly (Hong et al., 2017).

Interestingly, the addition of blocking anti-TGF-β (clone 1D11) also increased primary NK cell effector functions in our AML blast co-cultures (Figure 17A). However, also in control settings without AML blasts, anti- TGF-β significantly increased IFN-γ and TNF production and degranulation in response to K562, suggesting autocrine secretion of TGF-β1 by NK cells or K562 cells (Figure 17B). Additionally, the expression level of TGFB1 (TGF-β1) mRNA was equal in monocytes and AML blasts (not shown). Also, blocking PD-L1 (Figure 17C) or the adenosine receptor A2AR via SCH 58621 (Figure 17D) did not significantly alleviate AML blast-mediated NK cell suppression. In conclusion, no evidence was found for the participation of TGF-β1, PD-L1 or adenosine in AML blast-mediated NK cell suppression.

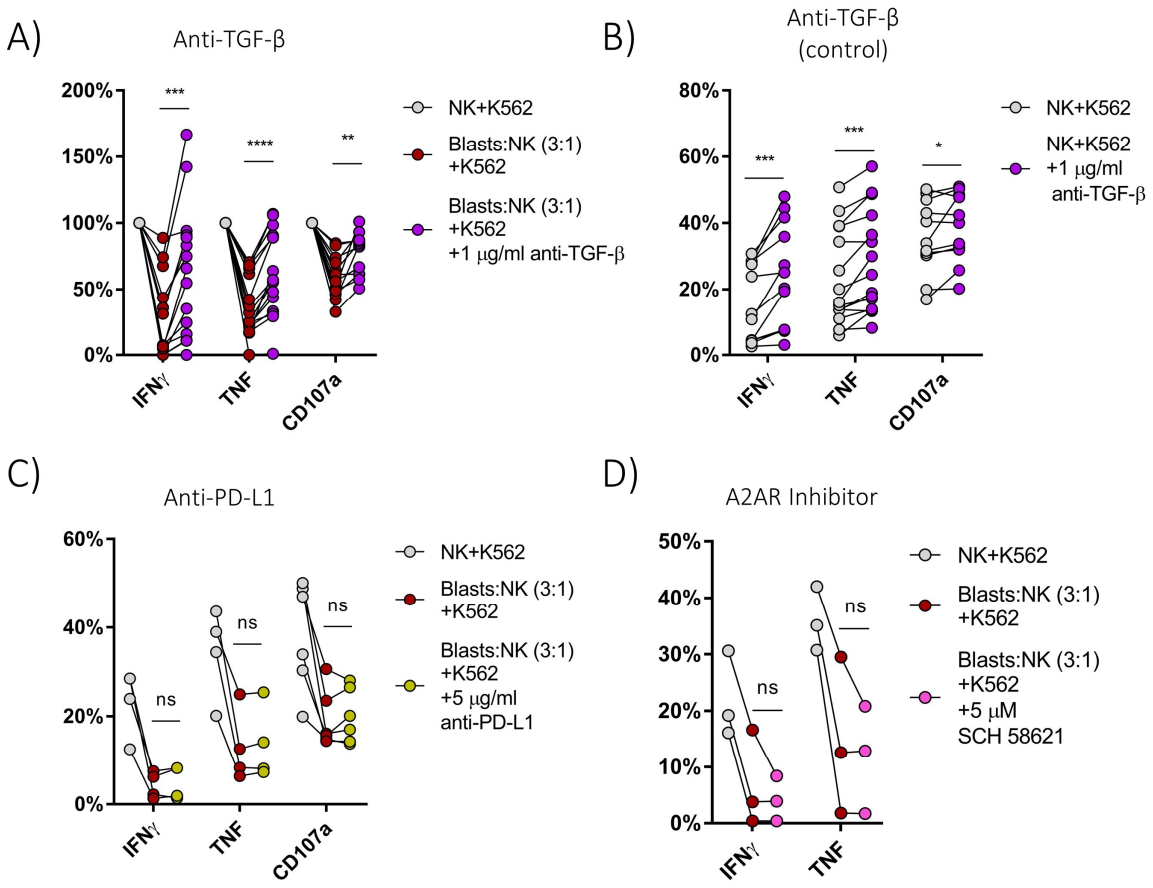

Figure 17: NK cell suppression is not mediated by TGF-β1, PD-L1 or adenosine. A-B) NK cells were co-cultured with or without AML blasts in the presence of 1 µg/ml blocking anti-TGF-β antibody (clone 1D11), then stimulated with K562 and effector functions were assessed via flow cytometry. **A)** NK cell effector functions are increased in AML co-cultures in the presence of anti-TGF-β (n = 14 for cytokines and n = 12 replicates for CD107a). **B)** In control settings without AML blasts, anti-TGF-β still increases NK cell effector functions against K562 cells (n = 12 for cytokines and n = 11 replicates for CD107a). **C-D)** The addition of 5 µg/ml anti-PD-L1 (**C**, n = 4 for cytokines and n = 6 replicates for CD107a) or 5 µM A2AR inhibitor SCH 58621 (**D**, n = 3 biological replicates) does not alleviate AML blast-mediated NK cell suppression. Statistical analysis: paired one-tailed student T test (A-D). *p<0.05; **p<0.01; ***p<0.001; ****p<0.0001.

3.3.5 AML blasts produce PGE2

Recently, Bonavita and colleagues demonstrated in a mouse melanoma model that tumor-derived prostaglandin E2 exerts strong immunomodulatory effects on NK cells, thereby shaping the whole tumor environment into an anti-inflammatory milieu (Bonavita et al., 2020). In the field of AML, to our knowledge, it was not investigated if PGE2 is produced by leukemia blasts, thereby possibly regulating NK cell functions. To test if PGE2 is produced by AML blasts, PGE2 concentrations were measured in the supernatant of AML blasts or healthy donor-derived monocytes. Monocytes only produced low amounts of PGE2 and did not suppress NK cells (Figure 15B, 18A). In contrast, the concentration of

PGE2 in blast supernatants was significantly higher and AML blasts expressed elevated levels of COX2 mRNA (Figure 18A-B). Of note, the concentration of PGE2 in blast supernatant from different patients was variable (Figure 18B). Addition of NK cells to AML blasts further increased the secretion of PGE2, suggesting up-regulation of PGE2 synthesis in the presence of NK cells (not shown). The concentration of PGE2 detected in blast supernatant from different AML patients correlated with their suppressive effect on NK cell effector functions, pointing towards PGE2-mediated suppression (Figure 18C).

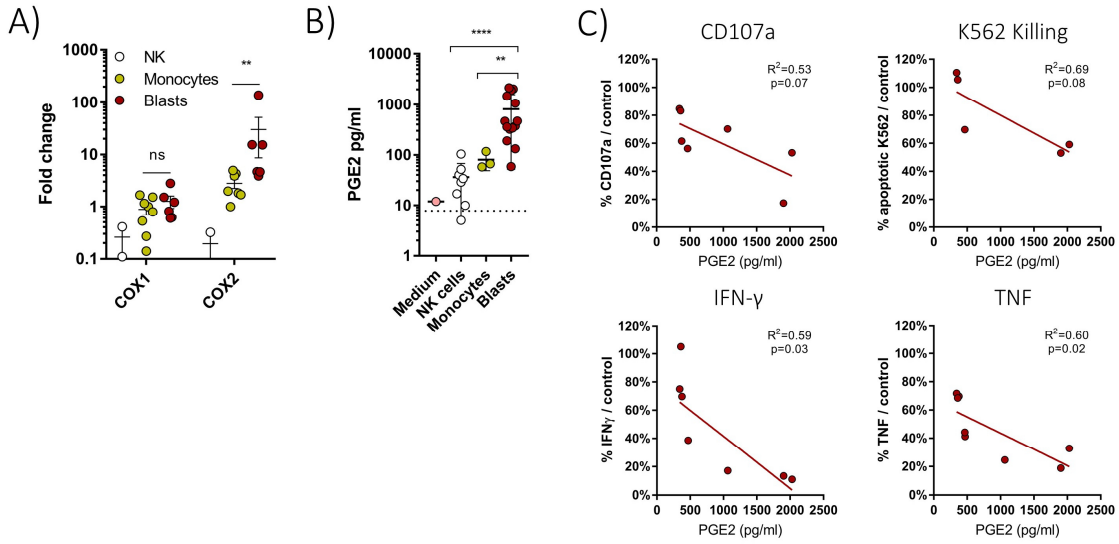

Figure 18: PGE2 secreted by AML blasts correlates with NK cell suppression. A) Expression of COX1 or COX2 mRNA in different cell types measured via qPCR. Delta Cp values calculated by substratction of house keeping gene Cp (ACTG1 and RSP18). Results were then normalized to monocyte donor #1 (n = 8 monocyte or n= 6 AML blast donors). **B)** Equal numbers of NK cells, monocytes or AML blasts were cultivated overnight, then supernatant (SN) was analyzed for PGE2 via ELISA (n = 8 NK, n = 3 monocyte or n = 14 AML blast donors). **C)** Degranulation (CD107a), K562 killing or cytokine (IFN-γ, TNF) secretion of K562-stimulated NK cells co-cultured with AML blasts normalized to blast-free control. Low percentages inidcate strong suppression of effector functions and vice versa. Negative correlation with PGE2 secreted by AML blasts (measured in SN via ELISA) indicates PGE2-dependent suppression of NK cells by AML blasts. Every circle depicts one biological replicate (n = 5-8 depending on readout). Statistical analysis: upaired one-tailed student T test (A-B) or linear regression analysis (C). *p<0.05; **p<0.01; ***p<0.001; ****p<0.0001.

3.3.6 NK cells are suppressed via blast-derived PGE2

Inhibition of the PGE2 generating enzyme COX2 via celecoxib effectively prevented the suppression of NK cell effector functions (Figure 19A-B). No effects on NK cells were observed when celecoxib was added to NK cells cultured without AML blasts (Figure 19A). The inhibitory effect of PGE2 on NK cells is mainly transmitted via its receptors EP2 and EP4 (Bonavita et al., 2020; Martinet et al., 2010; Park et al., 2018). Accordingly, pharmacologic blocking of EP2 and EP4 receptors (via PF 04418948 and L-161,982) also significantly alleviated the suppressive effect of AML-blasts (Figure 19C). We aimed to

understand how PGE2 affects human NK cells on a functional level *in vitro*. Adding increasing concentrations of PGE2 to NK cells overnight dose-dependently decreased degranulation, target cell killing and cytokine production (Figure 19D). PGE2 suppressed degranulation and K562 killing moderately, but strongly impaired cytokine production, thereby resembling dysfunctional NK cells after AML blast co-culture (Figure 14J and 19D). As anticipated, addition of EP2/4 inhibitors protected NK cells from PGE2-mediated suppression of TNF and IFN-γ production (Figure 19E).

In summary, we detected the secretion of the immune suppressive prostaglandin E2 by AML blasts and we identified PGE2 as mediator of NK cell suppression. Targeting PGE2 synthesis via celecoxib and related inhibitors might therefore represent a promising therapeutic option that can be combined with existing and future therapies in AML.

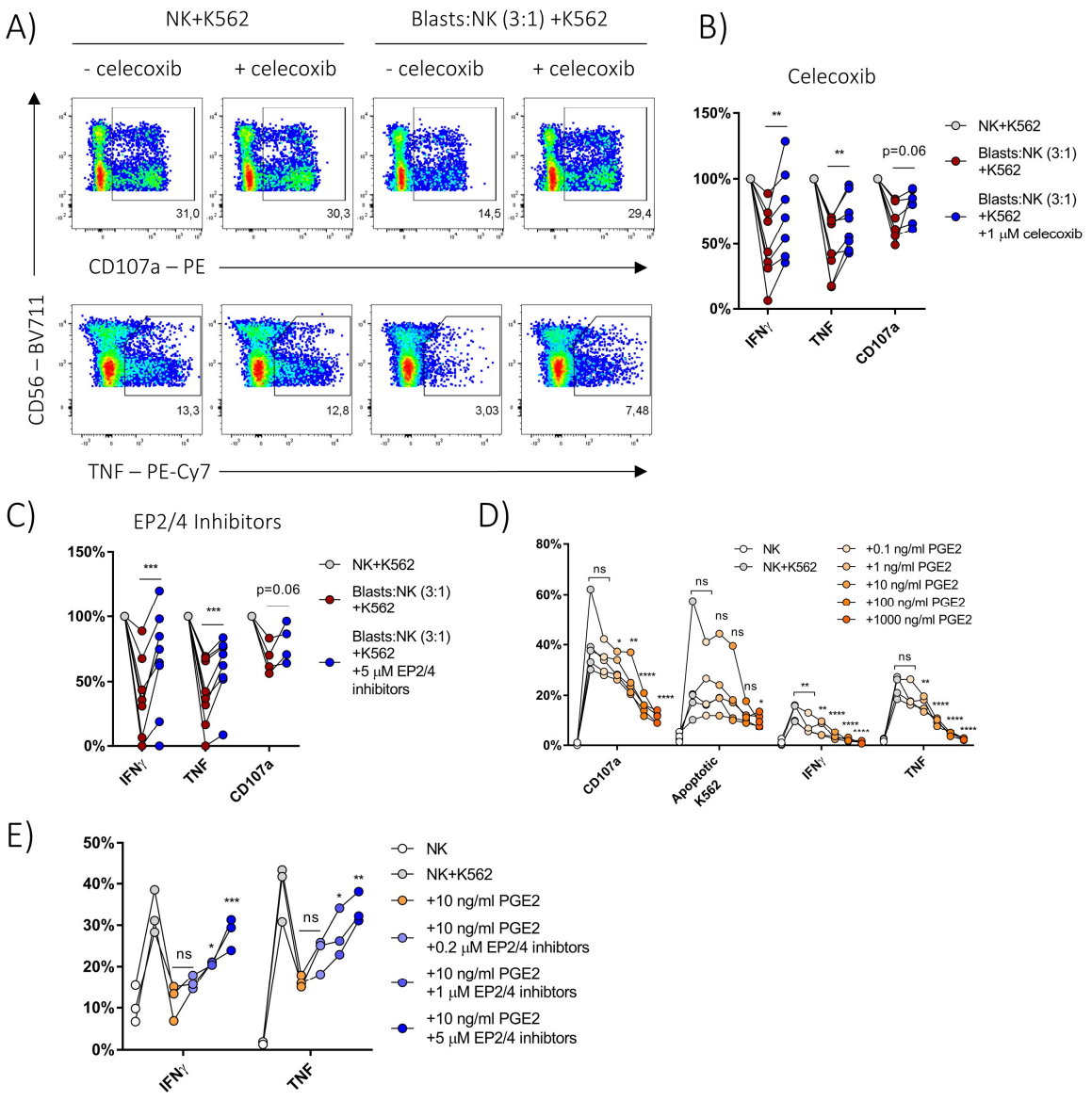

Figure 19: AML blasts suppress NK cell effector functions via PGE2 secretion. A-C) Addition of inhibitors targeting PGE2 to AML-NK co-cultures. COX2 inhibitor celecoxib (n = 6 for CD107a and n = 7 for cytokines) (**A, B**) or EP2/4 inhibitors (n = 4 for CD107a and n = 8 for cytokines) (**C**) to co-cultures alleviates the suppressive effect of AML blasts on NK cells. **D)** NK cells were treated with 0.1-1000 ng/ml PGE2 overnight, then cells were stimulated with K562 cells. Frequency of CD107a, IFN-γ or TNF positive NK cells and frequency of apoptotic K562 cells at the end of stimulation period depicted (n = 4 for cytokines, n = 5 for CD107a and killing). **E)** NK cells were treated with combinations of 0.2-5 µM PF 04418948 (EP2 inhibitor) and L-161,982 (EP4 inhibitor) for 30 min. PGE2 (10 ng/ml) was added to cultures with inhibitors overnight, then cells were stimulated with K562 and IFNγ or TNF was measured via flow cytometry (n = 3 biological replicates).. Statistical analysis: one-way ANOVA with Dunnett correction (D, E) or paired one-tailed student T test (B, C). *p<0.05; **p<0.01; ***p<0.001; ****p<0.0001.

4. Discussion

Tumor environments are often referred to as wounds that never heal and tumor-promoting inflammation as well as avoiding immune destruction are emerging hallmarks of cancer (Hanahan and Weinberg, 2011). In this thesis, mechanisms of immune evasion have been studied in the context of solid and hematological tumors that exemplify why immune cells often fail to respond appropriately to cancer cells in the tumor microenvironment (TME).

4.1 Immune regulation via methylglyoxal transfer

In the context of solid tumors, MDSCs are considered the most suppressive cell type often associated with $CD8^+$ T cell exhaustion and bad prognosis. Several suppressive mechanisms have been attributed to MDSCs as outlined in the introduction. We propose the direct transfer of methylglyoxal alongside cytosolic constituents from MDSCs to $CD8^+$ T cells as a new mechanism inducing metabolic dormancy and functional anergy.

4.1.1 Cytosolic transfer between immune cells

The intercellular communication of immune cells via exchange of cytosolic constituents, cell organelles or pathogens is a growing field of interest. In principal, two major routes of communication have been described: (1) the exchange of low molecular weight (<1kDa) compounds via gap junctions (GJs) in close-contact (Gleisner et al., 2017) and (2) the transfer of cytosolic constituents, cell organelles or pathogens via thin (<1 µm), tubular, membrane channels termed tunneling nanotubes (TNTs) over medium to long distances (up to 500 µM in tumor tissues) (Pinto et al., 2020). Distinct from secreted signal molecules, gap junctions and TNTs address only one neighboring or distant cell partner, respectively. Both types of communication are non-exclusive for immune cells and rather seem to have ubiquitous biological functions that are still insufficiently understood.

TNTs are tubular structures containing actin (and sometimes microtubule) that connect two distant cells with each other without adhering to the substratum. Different from other membrane protrusions, they are open ended allowing the uni- or bidirectional exchange of cytosolic molecules (e.g. proteins, dyes, nucleic acids, Ca^{2+}), cell organelles (mitochondria, lysosomes, autophagosomes) or pathogens (HIV, bacteria, prions) (Pinto et al., 2020). TNTs have been described between many different cell types, including cancer cells and most leukocytes. TNTs are mostly studied between cells of one type, but heterotypic connections between immune cells (e.g. DCs and macrophages) have also been observed

(Dupont et al., 2018). Although most experimental evidence for TNTs is derived from *in vitro* studies due to technical challenges in detection, TNTs have also been imaged *in vivo* between putative dendritic cells (DCs) in mouse cornea (Chinnery et al., 2008). On a functional level, the effects of TNT communication between myeloid cells have been punctually uncovered and comprise the spread of HIV, bacteria or prions, the intercellular exchange of antigens or the transmission of calcium signals (Dupont et al., 2018). In different cancer types, tumor cells seem to spread chemotherapy resistance and acquire survival advantage and invasiveness via TNT communication (Pinto et al., 2020). However, many additional functions of TNT communication are conceivable.

Gap junctions (GJs) on the other hand are open plasma channels between two adjacent cells that allow the exchange of small molecules, including immunologically relevant molecules like cyclic adenosine monophosphate (cAMP), cyclic guanosine monophosphate-adenosine monophosphate (cGAMP), inositol triphosphate (IP3), Ca^{2+}, microRNAs and small peptides (Sáez et al., 2014). GJs are composed of connexins, a family of molecules ubiquitously expressed. Almost all cell types of the immune system including T cells and monocytes, cancer cells and cells of the tumor stroma express one or more connexin isoform, with connexin 43kDa (Cx43) most frequently reported in immune cells (Neijssen et al., 2007). Gap junctions have been implicated in a plethora of immunological processes, including immune tolerance, antigen cross-presentation and lymphocyte activity (Gleisner et al., 2017). For example, GJs allow for cAMP transfer from regulatory T cells (T_{reg}) to $CD4^+$ T cells or DCs, thereby suppressing IL-2 expression or co-stimulation, respectively (Bopp et al., 2007; Weber et al., 2013). On the other hand, gap junctions assembled at the immune synapse between $CD4^+$ T cells and DCs are implicated in $CD4^+$ T cell activation (Elgueta et al., 2009; Mendoza-Naranjo et al., 2011) and the expression of Cx43 is upregulated by anti-CD3/28 stimulation (Oviedo-Orta et al., 2010). It is conceivable though, that monocytes and MDSCs communicate with antigen-experienced $CD8^+$ T cells through gap junctions with either stimulatory or regulatory outcome, respectively.

The nature of the mechanism of cytosolic transfer from MDSCs to $CD8^+$ T cells could not be unequivocally determined and was beyond the scope of this thesis. In confocal microscopy, membranous connections between myeloid cells and between myeloid cells and $CD8^+$ T cells have been visualized (data not shown). Serum starvation and other stress signals induce the formation of TNTs (Kretschmer et al., 2019; Lou et al., 2012) and we observed that human plasma reduced the transfer of MitoTracker green. However, addition of actin inhibitors (cytochalasin B and latrunculin B) did not inhibit transfer of the dye (data not shown). Confocal time lapse microscopy indicated that the transfer of MitoTracker green dye happens in proximity between myeloid cells and $CD8^+$ T cells, pointing

towards GJ-mediated communication. Connexins are up-regulated in response to pro-inflammatory cytokines and T cell stimulation, which could explain the preferential transfer to antigen experienced $CD8^+$ T cells. Since myeloid cells have been shown to engage in both, TNT- and GJ-mediated intercellular communication, it is also conceivable that both mechanisms are employed in parallel by MDSCs and monocytes in a redundant fashion.

The composition of transferred cargo from MDSCs or monocytes, respectively, remains largely elusive. Most immune cells circulate in the body between the lymph compartment, blood and tissue, each of which comprise highly distinct metabolic environments. It can be speculated, that immune cells employ cytosolic transfer of metabolic enzymes and metabolites to allow incoming cells rapid adaptation to the new environment. At sites of chronic inflammation characterized by hypoxia, acidity and nutrient depletion the metabolic imprint might rather be detrimental for immune cells whereas in the spleen or in lymph nodes antigen presenting cells might boost the initiation of an anabolic metabolism in TCR-stimulated T cells. Clearly, further studies are needed on the role of intercellular communication via cytosolic transfer to increase our understanding of the highly coordinated immune defense against cancer.

4.1.2 SSAO and the origin of MGO

In our studies, we identified MGO as crucial mediator of suppression and scavenging of MGO via DMBG prevented MDSC-mediated suppression of $CD8^+$ T cells. For the induction of MDSCs, peripheral blood monocytes were pre-cultivated three days on the hepatic stellate cell line LX2, which can be replaced by primary, activated hepatic stellate cells (HSC) (Höchst et al., 2013). The origin of MGO was traced to the enzymatic activity of SSAO and inhibition of SSAO during the pre-cultivation period rendered MDSCs non-suppressive or in other words prevented MDSC induction. Additionally, stable isotope labelling experiments with $^{13}C_6$-glucose indicated MGO production from acetyl-CoA and glycine, substrates of SSAO-mediated MGO synthesis. Last, the expression of SSAO was increased in MDSCs compared with monocytes, as determined by q-PCR.

SSAO is a protein with dual functions, which is amine oxidase activity (production of MGO) and cell adhesion. Due to its expression on endothelium, SSAO is alternatively termed vascular adhesion protein 1 (VAP-1). In a study of 2015, Weston and co-workers investigated the expression of SSAO / VAP-1 in livers of patients suffering from non-alcoholic fatty liver disease (NAFLD) (Weston et al., 2015). NAFLD comprises a spectrum of liver diseases ranging from steatosis to non-alcoholic steatohepatitis (NASH) and cirrhosis. Chronic inflammation in NASH and liver cirrhosis often paves the way for the

development of hepatocellular carcinoma (HCC). Interestingly, the expression of SSAO / VAP-1 was detected in liver stromal cells (α-SMA$^+$ and CD90$^+$) and was up-regulated in NAFLD compared with healthy controls. Both activated hepatic stellate cells (HSC) and LX2 cells expressed SSAO, which was located at the cell membrane and in intracellular vesicles. Deletion of AOC3 (the gene coding SSAO / VAP-1) or blocking the catalytic amine oxidase activity prevented the development of fibrosis in several mouse models of severe steatohepatitis. This effect was attributed to reduced leukocyte infiltration (T, NKT and myeloid cells) (Weston et al., 2015).

Apart from NAFLD, SSAO / VAP-1 is expressed on the endothelium of tumor- and metastasis vasculature and assists lymphocyte and myeloid cell extravasation (Ferjančič et al., 2013; Irjala et al., 2001; Li et al., 2013; Marttila-Ichihara et al., 2009, 2010; Yoong et al., 1998). In two consecutive studies, Marttila-Ichihara and co-workers analyzed the functional implications of SSAO / VAP-1 expression on tumor endothelium. Whereas antibody-mediated blocking of VAP-1 prevented the extravasation of anti-tumorigenic CD8$^+$ T cells, inhibition or deletion of SSAO oxidase activity reduced the number of GR1$^+$ CD11b$^+$ MDSCs in mouse models of melanoma and lymphoma. Not surprisingly, only SSAO inhibition / deletion but not anti-VAP-1 treatment retarded tumor growth in both models (Marttila-Ichihara et al., 2009, 2010). Similar results have been reported for HCC (Li et al., 2013). The tumor-promoting role of SSAO found in those studies is in line with our data linking SSAO activity with MDSC-mediated suppression via MGO. Considering the data presented in this thesis, we propose that not only extravasation of MDSCs was affected by SSAO inhibition, but induction of MDSCs from non-suppressive myeloid cells and the acquisition of suppressive capacity.

It is unclear how stimulatory monocytes transdifferentiate into suppressive MDSCs after contact with LX2 or activated HSCs. Dependency on CD44 expression has been demonstrated, but the exact mechanism is still unknown (Höchst et al., 2013). Likely, the expression of SSAO / VAP-1 on activated HSCs or LX2 is connected to the induction of MDSCs. SSAO is an ectoenzyme expressed on the cell surface but was also found in intracellular vesicles of activated liver stromal cells (Weston et al., 2015). To our knowledge it was not demonstrated to date, whether MGO is produced extracellularly or intracellularly, either accumulated inside vesicles or in the cytosol. To allow for intracellular transfer, accumulation in the cytosol or in vesicles is mandatory. MBo staining of MDSCs indicated intracellular MGO, but cellular localization of MGO could not be pinpointed via flow cytometry. The accumulation of MGO in MDSCs can be explained by several modes of action. First, vesicular SSAO could be transferred from LX2 to monocytes (via TNTs), allowing for an immediate start of MGO production and consequent acquisition of suppressive potential. Second, MGO could be originally produced by LX2 or

other stromal cells and transferred to monocytes (via GJ or TNTs), making MDSCs a transmitter of suppressive cargo. Both theories are along the idea, that incoming immune cells are metabolically changed by tissue resident cells. Additionally, signals from LX2 could induce the up-regulation of SSAO on MDSCs, which is in line with the increased expression of AOC3 mRNA on stromal-cell induced MDSCs compared with monocytes. In any case, cells of the tumor microenvironment or stromal cells of chronically infected tissue could produce SSAO / MGO that contributes to the conversion of arriving, non-suppressive myeloid cells into MDSCs. Accumulation of MGO by MDSCs could account for the three days of induction period in the *in vitro* system. Loaded with MGO, MDSCs would then be able to rapidly transfer large quantities to $CD8^+$ T cells for immediate suppression of effector functions, thereby hindering tumor clearance.

4.1.3 Cell intrinsic effects of MGO

Irrespective of the exact origin of MGO, it can be speculated how MGO affects $CD8^+$ T cell biology. There are no data available on the exact behavior of MGO inside cells. *In vitro* studies demonstrated binding to guanidine containing molecules, including L-arginine (Lo et al., 1994). Considering the pivotal role of L-arginine in T cell activation and metabolism (Bronte et al., 2003; Geiger et al., 2016; Rodriguez et al., 2002), intracellular depletion of L-arginine and concomitant increase in L-arginine-derivates MG-H1 and argpyrimidine suggested L-arginine deprivation as underlying reason for the suppression of $CD8^+$ T cell effector functions. However, there is room for speculations on additional modes of action. MGO is constantly produced during glycolysis via spontaneous de-phosphorylation of DHAP. Immediate and irreversible binding of MGO to L-arginine or arginine residues in vicinity would make it impossible for cells to detoxicate via the glyoxalase system. Also, there would be no unbound MGO that can be transferred from MDSCs to $CD8^+$ T cells. Re-isolated $CD8^+$ T cells recovered from MDSC-mediated suppression within 4h (possibly glyoxalase-mediated), but this period was shortened to 1h after addition of DMBG. DMBG only binds to free MGO, therefore unbound DMBG must have been available in $CD8^+$ T cells after re-isolation. Likely, intracellular MGO is in an equilibrium of unbound and (arginine-)bound MGO. Indeed, studies from the early 90s suggested that more than 99% of MGO is reversibly bound to cysteine-, lysine- and arginine residues of proteins and peptides under physiological conditions (Lo et al., 1994). Multiple studies support the idea, that MGO might not be a chemical radical that covalently modifies peptides and proteins without selectivity, but rather represents a post-translational modification with regulatory effect on many cellular processes.

MGO has been shown to modify histones in the same order of magnitude as arginine methylation with implications on DNA transcription (Galligan et al., 2018). In a study of Nokin and colleagues, tumor cell derived MGO lead to sustained nuclear localization of YAP, a transcriptional co-activator involved in tumor growth and invasion (Nokin et al., 2016). Additionally, MGO affects heat shock protein 27 and 90 (Hsp27 and Hsp90) activity, which are important chaperones involved in tumorigenicity, metastatic potential and chemoresistance (Bellahcène et al., 2017). On a metabolic level, MGO interferes with respiratory complex I and possible other mitochondrial proteins, thereby reducing mitochondrial membrane potential and intracellular ATP levels (de Arriba et al., 2007; Ghosh et al., 2011; Rosca et al., 2002). Interestingly, some but not all glycolytic enzymes are targets of inhibiting MGO modification (Leoncini et al., 1989; Sibbersen et al., 2018). Among those, the activity of fructose-1,6-bisphosphate aldolase and glyceraldehyde 3-phosphate dehydrogenase (GAPDH) were inactivated the fastest, with 2.7 and 19.8 minutes half-inactivation times, respectively (Leoncini et al., 1989). Catalytically inactive GAPDH has been shown to bind to the untranslated region of IFN-γ mRNA in T cells, thereby suppressing its translation (Chang et al., 2013). Accordingly, inhibition of GAPDH can account for both, functional and metabolic deficiency of $CD8^+$ T cells. Inhibition of glycolytic flux and consequent shortage of acetyl-CoA would force $CD8^+$ T cells to feed the tricarboxylic acid cycle (TCA) with glutamine-derived α-ketoglutarate and glutamine deprivation has been observed for suppressed $CD8^+$ T cells in our study. Like the metabolite acetate, MGO could regulate transcription and metabolism via posttranslational modifications with widespread effects on cellular biology. Such molecular regulation could also contribute to the transition of monocytes to MDSCs.

4.1.4 Combination of suppressive effects exerted by MDSCs to dampen immunity

Human and mouse MDSCs have been extensively studied in the past and several modes of action contributing to $CD8^+$ T cell suppression have been reported, that can be roughly divided into four categories: (1) the release of reactive molecule species (H_2O_2, peroxynitrite) impairing TCR and IL-2 signaling, (2) the depletion of essential amino acids (L-arginine, L-cysteine), (3) the expansion of regulatory T cells (Treg) and (4) the interference with T cell migration (Gabrilovich et al., 2012). The transfer of methylglyoxal alongside cytosolic constituents represents a 5^{th} category of mechanisms mediating suppression of immunity, with putative connections to other modes of action. MGO was found to be associated with oxidative stress in different cell types, possibly due to detrimental effects on mitochondrial respiration (de Arriba et al., 2007; Chang et al., 2005; Kikuchi et al., 1999; Rosca et al., 2002). Reactive oxygen species (ROS) on the other hand have been shown to be inducer of tunneling

nanotubes, thereby possibly facilitating methylglyoxal transfer from MDSCs to $CD8^+$ T cells (Pinto et al., 2020). Arginase 1 (Arg1) and inducible nitric oxide synthase (iNOS) are key enzymes connected to the production of reactive oxygen species, the consumption of extracellular L-arginine and consequently the suppressive effect of MDSCs. Frequently used inhibitors against Arg1 and iNOS comprise chemical derivates of L-arginine, like nor-NOHA (Nω-hydroxy-nor-arginine) and L-NMMA (L-NG-monomethyl arginine). In high concentrations, these inhibitors likely react with MGO, therefore effects solely attributed to Arg1 and iNOS inhibition in previous studies might be partly connected to MGO scavenging. Besides, extracellular depletion of L-arginine via Arg1 and iNOS activity might synergize with intracellular depletion of L-arginine via MGO transfer to rapidly deplete $CD8^+$ T cells of all available L-arginine. Additionally, ROS-mediated oxidation of reduced glutathione (GSH) together with extracellular depletion of the GSH precursor cysteine / cystine (Srivastava et al., 2010) prevents efficient MGO detoxification via the glyoxalase system in MDSCs and $CD8^+$ T cells. In summary, different modes of suppression employed by MDSCs might act in concert to deplete $CD8^+$ T cells from essential amino acids and to prevent $CD8^+$ T cell activation and metabolic reprogramming in immune challenging environments.

4.1.5 The potential of DMBG in anti-cancer treatment

DMBG is a licensed drug affecting glucose metabolism and its effect on cancer risk and survival has been studied frequently and compared to other anti-diabetic drugs. Epidemiological studies suggest a reduced risk of HCC development in type 2 diabetes (T2D) patients infected with hepatitis C virus (HCV) receiving DMBG (Harris and Smith, 2013). Similarly, in T2D patients receiving DMBG, HCC risk is reduced compared to treatment with insulin or sulphonylureas (Donadon et al., 2010). These observations were corroborated in a mouse model that develops chemically-induced liver fibrosis, cirrhosis and finally HCC. DMBG treatment prevented HCC development and this effect was attributed to reduced activation of hepatic stellate cells (Shankaraiah et al., 2019). The liver is the primary site of action of DMBG and several known effects of the drug could contribute to HCC prevention, for example inhibition of hepatic gluconeogenesis and AMP-activated kinase (AMPK) activation. However, DMBG has been demonstrated protective in other cancer entities as well, including breast cancer (Bodmer et al., 2010), gastric cancer (Cheung et al., 2019; Kim et al., 2020), colorectal cancer (Yang et al., 2020), lung cancer (Tseng, 2017; Zhang et al., 2014) and nasopharyngeal cancer (Tseng, 2018). Apart from reported direct effects of DMBG on tumor cell survival and metabolism, effects of DMBG on immune-mediated tumor control have been investigated previously. In a study of Pereira and co-workers, DMBG

treatment of mice that were inoculated with B16F10 melanoma cells reduced lung metastasis. In the treatment group, $GR1^+$ $CD11b^+$ MDSCs were decreased in the spleen and infiltration of the lung with $CD8^+$ effector cells increased. In mouse strains lacking functional T cells ($Rag^{-/-}$ or NSG) or antibody T cell depleted wild types (WT) no protective effect of DMBG was detected, pointing towards a T cell dependent anti-metastatic effect of DMBG (Pereira et al., 2018). In another study, DMBG enabled $CD8^+$ T cell dependent rejection of solid tumors in different mouse models (Eikawa et al., 2015). DMBG treatment post tumor implantation (beginning day 7) increased the number of multifunctional (IFN-γ^+, TNF^+ and IL-2^+) tumor infiltrating lymphocytes (TIL) and shifted the balance from central memory (CM) to effector memory (EM) $CD8^+$ T cells in the TME (Eikawa et al., 2015). The effects were attributed to improved TIL survival upon DMBG treatment and effects were partly dependent on the activation of the DMBG target AMPK in TILs.

Here, we add a completely new mechanism to the growing list of anti-tumorigenic effects of DMBG. Scavenging of MGO via DMBG rendered MDSCs non-suppressive and protected $CD8^+$ T cells from metabolic and functional exhaustion. It is increasingly recognized that lymphocytes undergo drastic metabolic adaptations (glycolytic switch) upon activation and that the metabolic environment might serve as a fourth signal of activation, on one level with T cell receptor (TCR) stimulation, perception of co-stimulatory cytokines and co-stimulatory ligands. Interference with the metabolic environment in tumors might open new avenues in anti-cancer therapies. The abundant detection of MDSCs in multiple cancer entities and the correlation of MDSC presence with bad prognosis suggests a broad potential of DMBG in the treatment of cancer. Epidemiological studies already suggest protective effects of DMBG on tumor development. In line, DMBG alleviated the suppressive effect of MDSCs in a pre-clinical mouse melanoma model and improved T cell mediated tumor control in combination with anti-PD-1 treatment. In melanoma, only sub-populations of patients respond to ICB therapy with long lasting remission or even cure (Gauci et al., 2019). The presence of MDSCs has been associated with non-responsiveness to current immune therapies (Gebhardt et al., 2015; Martens et al., 2016; Meyer et al., 2014; Sade-Feldman et al., 2016; Weber et al., 2016), therefore combination treatment with DMBG might increase the frequency of therapy response among patients. However, randomized controlled trials are needed to further elucidate the efficacy of DMBG treatment and ICB therapy in cancer. Currently, a combination of DMBG with Nivolumab, a blocking PD-1 antibody, is tested in a phase 2 study in patients with non-small cell lung cancer (ClinicalTrials.gov NCT03048500). The results of such studies are eagerly awaited and promise better immune control of solid tumors in the future.

4.2 PGE2-mediated suppression of NK cells in AML

Acute myeloid leukemia (AML) is a deadly disease with insufficient therapeutic options to date. Here, we found that AML blasts actively suppressed natural killer cell effector functions, thereby contributing to immune evasion. Several possible modes of suppression were considered, including MGO transfer, TGF-β1 secretion, adenosine production, PD-L1 transmitted suppression or enzyme mediated amino acid depletion, but only for the involvement of prostaglandin E2 comprehensive evidence was found. Secretion of PGE2 impaired the production of IFN-γ and TNF strongly and inhibited degranulation and target cell killing of the K562 cell line. Inhibition of COX2 via celecoxib or blockade of EP2/4 receptors protected NK cells from AML-blast mediated suppression and might represent a promising treatment that can be combined with existing and future immunotherapies.

4.2.1 Regulation of surface receptors in AML NK cells

In AML, NK cells have been found to express low levels of activating receptors NKp30, NKp46, NKG2D and DNAM-1 (Costello et al., 2002; Fauriat et al., 2007; Khaznadar et al., 2015; Sanchez-Correa et al., 2011, 2012; Szczepanski et al., 2010; Tang et al., 2020) and some studies reported higher expression levels of the inhibiting receptors CD94/NKG2A or members of the killer immunoglobulin-like receptor (KIR / CD158) family (Sandoval-Borrego et al., 2016; Stringaris et al., 2014) whereas others could not find such effect (Sanchez-Correa et al., 2011; Tang et al., 2020). Such phenotype likely represents cells with an elevated activation threshold compared with healthy donor-derived NK cells. The reduced expression of activating receptors correlated with the overall survival and relapse risk of AML patients (Fauriat et al., 2007; Khaznadar et al., 2015), stressing the clinical significance of NK cells in AML. It is of relevance, whether the regulation of NK cell receptors is a consequence of the disease or if individuals with low responsive NK cells are of higher risk to develop AML. In our *in vitro* model, healthy donor-derived NK cells co-cultivated with patient-derived AML blasts down-regulated NKp30, DNAM-1 and NKG2D expression within overnight culture, arguing for a causal relationship between the presence of AML blasts and the regulation of these receptors. The same has been observed by others in similar experimental settings with primary AML blasts or AML cell lines (Fauriat et al., 2007; Khaznadar et al., 2014). In two studies the NK cell receptor expression in AML patients at different stages of disease was measured. In line with our data, the expression of NKp30 and NKp46 recovered during complete remission, further indicating that the physical presence of AML blasts induced the dysfunctional phenotype of AML NK cells (Fauriat et al., 2007; Stringaris et al., 2014). Constant

perception of activating ligands can be the cause of receptor down-regulation and hypo-responsiveness in NK cells (Champsaur and Lanier, 2010; Oppenheim et al., 2005). Interestingly, Sanchez-Correa and colleagues tested the expression of NK cell activating ligands on AML blasts and found expression of the NKG2D ligands MICA/B, the DNAM-1 ligands CD112 and CD155, and the co-stimulatory ligand CD166 (Braun et al., 2011) that were expressed on blasts of a majority of AML patients (Sanchez-Correa et al., 2011, 2012). Correlation of high DNAM-1 ligand expression on AML blasts and low DNAM-1 receptor expression on matched AML NK cells suggested ligand-mediated down-regulation of the receptor in AML patients (Sanchez-Correa et al., 2011, 2012). Likewise for NKG2D, the expression of one or more ligands has been detected on blasts of 70% of all analyzed AML patients in a comparative analysis of different leukemia types (Hilpert et al., 2012). However, others found overall low expression of activating ligands on AML blasts (Nowbakht et al., 2005). Moreover, the shedding of NKG2D ligands was reported for AML and other types of cancer and might contribute to immune evasion in AML (Champsaur and Lanier, 2010; Salih et al., 2003). Of note, leukemia stemness was associated with the absence of NKG2D ligands and consequent NK cell evasion in AML mouse models (Paczulla et al., 2019). It is of debate if AML blasts express significant amounts of activating ligands for NK cell mediated killing and if receptor down-regulation is induced by constant perception of activating ligands. Alternatively, the regulation of NKG2D and NKp30 is associated with PGE2 (Park et al., 2018) and we confirmed reduced expression of both receptors after overnight culture in medium containing PGE2 (not shown). Also, TGF-β1 down-regulates the expression of both receptors but no TGF-β1 was detected in our experiments (Castriconi et al., 2003; Crane et al., 2010; Lee et al., 2004; Park et al., 2011).

Not only activating ligands but also the expression of inhibiting ligands on AML blasts determines the degree of NK cell activation. Inhibitory ligands comprise CD94/NKG2A ligand HLA-E and other ligands from HLA-class I family binding to KIR receptors (Ljunggren and Malmberg, 2007). In mixed co-cultures with AML blasts and K562 cells, the target cell line K562 was still lysed and effector functions of NK cells were induced, even though with lower intensity as compared to control wells without AML blasts. In line, blasts from leukemia patients were found to express HLA-class I molecules and the expression of HLA-E was further increased in response to IFN-γ (Baessler et al., 2010; Nguyen et al., 2009; Sanchez-Correa et al., 2011), whereas K562 cells are low in HLA-class I expression (Bae et al., 2012; Sabry et al., 2019).

It is unclear, to what extent the down-regulation of NKp30, NKG2D and DNAM-1 is attributed to ligand perception, PGE2 signaling or other modes of regulation. But likely, the low expression of activating receptors on NK cells in AML contributes to evasion from NK cell mediated clearance.

4.2.2 Local environment of NK cell suppression

The interaction of AML blasts with NK cells is likely connected to the degree of NK cell activation, since surface receptors expressed on activated NK cells might be absent or lower expressed on unstimulated NK. We therefore wondered how NK cell stimulatory cytokines (IL-2, IL-12, IL-15) are concentrated in AML. Studies on the cytokine composition of AML patients are sparse, but some groups have addressed this question via multiplex technology. Not surprisingly, the overall cytokine composition of MDS and AML patients differs from normal controls in the bone marrow and in the blood (Kornblau et al., 2010; Moudra et al., 2016; Sanchez-Correa et al., 2013). In a comparison of low risk MDS, high risk MDS and AML with healthy donors the concentration of IL-12 in the bone marrow of all patient groups was found decreased, whereas no data was collected on IL-2 or IL-15 (Moudra et al., 2016). IL-12 concentrations in AML patient blood was found increased on average for elderly patients (>65 years) and not significantly different for younger patients (Sanchez-Correa et al., 2013). In a different study, on average increased IL-12 concentrations in AML patient blood was confirmed, but most individual values were in the range of healthy controls (Kornblau et al., 2010). The same was true for IL-15, even though IL-15 trans-presented on antigen presenting cells could not be estimated with the applied methodology (Kornblau et al., 2010). No significant difference in the concentration of IL-2 was found in blood from MDS or AML patients compared with healthy controls (Kornblau et al., 2010; Sanchez-Correa et al., 2013). Although the picture on cytokine expression in AML, especially in the bone marrow, is incomplete, we presume, that studies conducted with high-dose cytokine-primed NK cells or cells pre-expanded on feeder cells might overestimate the degree of NK cell activation present in AML. Consequently, we chose to conduct our studies with unstimulated NK cells that were co-cultured with AML blasts directly after isolation *ex vivo*. Such NK cells have neither received excessive cytokine stimulation, nor target cell contact. We imagine that first contact and suppression of NK cells by myeloid blasts takes place in the bone marrow of MDS and AML patients and that this is a critical step in the transition from MDS to AML. In line, NK cells in high-risk MDS are already dysfunctional (Daher et al., 2017). However, more studies on the bone marrow microenvironment of MDS and AML patients and the dynamics of NK cell suppression in those pathologies are warranted.

4.2.3 Dysfunction of NK cells in AML-Patients

There is controversy, if NK cell counts in AML are equal to healthy controls or reduced and if the proportion of $CD56^{bright}CD16^{-}$ to $CD56^{dim}CD16^{+}$ NK cell population is increased (Sanchez-Correa et al., 2016). In contrast, it is evident that NK cells from AML patients are dysfunctional in response to stimulation. NK cells isolated from AML patients produce significantly less pro-inflammatory cytokines and have impaired degranulation in response to K562 target cell stimulation (Stringaris et al., 2014). Furthermore, only minor effector functions are induced in co-cultures of AML blasts with autologous or healthy donor derived NK cells (Khaznadar et al., 2014; Stringaris et al., 2014). Even in experimental settings, where polyclonal, activated AML NK cells were used at effector to target ratios of 10:1, only dismal cytolytic activity against autologous blasts was measured that could be increased by using antagonistic anti-HLA-class I antibodies or antibodies stimulating NKp44 or NKp46, demonstrating the weak immunogenicity and/or strong suppressive effect of AML blasts on NK cells (Costello et al., 2002).

We confirmed diminished cytokine production of AML NK cells in response to K562 cells. Also, healthy donor derived NK cells responded with strongly decreased IFN-γ, TNF secretion, degranulation and K562 lysis after overnight co-culture with AML blasts dose-dependently. Apparently, cytokine production was more sensitive towards inhibition as compared with degranulation since degranulation could not be suppressed completely in co-culture with any AML donor tested. No induction of effector functions was measured in co-culture with AML blasts in absence of K562 cells. Since the viability of NK cells was unaffected by AML blasts, we speculated that cell intrinsic defects account for impaired effector functions.

To our knowledge, the regulation of NK cell metabolism and signaling in AML patients or AML blast co-cultures has not been studied to date. Interestingly, AML blasts negatively affected the metabolic regulator mTOR in K562-stimulated NK cells and we wondered if this is connected to the suppression of effector functions. mTORC1 activity has been connected to metabolic reprogramming and IFN-γ production of cytokine-primed NK cells previously (Jensen et al., 2017; Keating et al., 2016). In a study of Keating and co-workers, human NK cells strongly upregulated glycolysis and oxidative phosphorylation and produced IFN-γ in response to 18h culture in high dose IL-2 (500 IU/ml) or high dose IL-12+IL-15 (30 ng/ml IL-12+100 ng/ml IL-15) (Keating et al., 2016). Blocking mTORC1 via rapamycin, a well studied inhibitor of mTORC1 (Laplante and Sabatini, 2009), prevented IL-2-induced but not IL-12+IL-15-induced metabolic reprogramming and IFN-γ production. Similarly, in another study, IL-2 primed (200 IU/ml) NK cells were susceptible to mTORC1-inhibition via rapamycin and

produced less IFN-γ in response to NKG2D stimulation (Jensen et al., 2017). We tested if mTORC1 activity also regulates effector functions of unprimed, target-cell stimulated NK cells. Cells were cultured overnight in low dose IL-2 (25 IU/ml), treated for 1h with rapamycin (0.2-200 nM) and stimulated with K562 for additional 3-4h. However, rapamycin treatment did not impair NK cell cytokine secretion or degranulation of K562-stimulated NK cells, despite reducing mTOR and down-stream target S6 phosphorylation, suggesting independence of acute effector functions from mTORC1 signaling (not shown). In contrast to NK cells primed in high-concentrated cytokines, K562 stimulation did not induce strong metabolic changes as indicated by 2-NBDG uptake assay (not shown). This difference can be explained by a bimodal model proposed by Gardiner and Finlay. In a first phase of activation NK cells are mainly stimulated via innate cytokines (IL-12, IL-15, IL-18) and target cell contact. NK cells rapidly respond in this first phase without the need for substantial metabolic reprogramming. In a second phase of activation, high concentrated IL-2 mainly produced by T cells more strongly stimulate metabolic reprogramming of NK cells which is mandatory for NK cell activity over extended time periods (Gardiner and Finlay, 2017). Possibly the impaired kinase activity of mTORC1 is irrelevant for short-term culture but critical in situations of sustained NK cell activation mediated by IL-2. We furthermore considered that amino acid metabolism of NK cells is affected by AML blasts due to metabolic competition or enzymatic depletion of L-arginine, thereby limiting the efficacy of cytokine translation and negatively affecting mTORC1 stabilization. However, no evidence was found for dysregulated amino acid metabolism since the concentration of all measured intracellular amino acids was equal in culture conditions with or without AML blasts.

4.2.4 Mechanism of blast-mediated suppression

Suppression of NK cell effector functions in AML is critical for disease progression, since the cytolytic activity and cytokine production of autologous NK cells is a sensitive predictor of relapse and disease-free survival in patients achieving complete remission (Lowdell et al., 2002; Tajima et al., 1996; Tratkiewicz and Szer, 1990). Consequently, it is important to understand the process leading to NK cell dysfunction and to develop treatments counteracting this mechanism. Multiple suppressive modes have been proposed to play a role in NK cell regulation mediated by AML blasts and several treatments have been suggested.

In an early study by Bergman and co-workers, expression of TGF-β1/2 mRNA and secretion of TGF-β1/2 protein was detected in cultures of AML blasts und supernatants from such cultures inhibited the cytotoxicity of lymphocytes (Bergmann et al., 1995). In a more recent study, TGF-β1 bound to

exosomes was found in plasma from AML patients and addition of such exosomes to the NK cell line NK-92 inhibited lysis of K562 cells (Hong et al., 2017). In both studies, blocking anti-TGF-β antibodies alleviated the suppressive effect. Similarly, membrane-bound TGF-β1 was implicated in NK cell suppression mediated by blasts from patients with myelodysplastic syndrome (MDS), which describes a pathological condition that arises from the growth and spread of mutated hematopoietic stem cells in the bone marrow and often evolves into AML (Cazzola, 2020; Daher et al., 2017). In contrast, other groups did not detect TGF-β1 in blast supernatants and even found reduced concentrations of TGF-β1 in AML patient blood and bone marrow aspirates compared with healthy controls (Fauriat et al., 2007; Sanchez-Correa et al., 2013; Stringaris et al., 2014; WU et al., 2012). In our co-culture experiments, the addition of anti-TGF-β increased NK cell effector functions. However, this effect was irrespective of the presence of blasts and no TGF-β1 was detected in blast supernatants after overnight culture (not shown). Furthermore, AML blasts from several patients were stained with antibodies directed against TGF-β1 or latency associated peptide (LAP), which is part of the latent TGF-β1 complex and associated with TGF-β1 before conversion into the active form (Khalil, 1999). Both targets were not detected on AML blasts and TGFB1 mRNA was expressed lower compared with non-suppressive monocytes (not shown). In summary, we found no experimental evidence that TGF-β1 is produced by AML blasts or that it mediates the suppressive effect on NK cells.

Frequently connected to immune suppression in cancer are immune checkpoints like PD-1 and its ligand PD-L1. Although found located on AML blasts and exosomes isolated from some AML patients (Hong et al., 2017; Zajac et al., 2016), blocking PD-L1 did not protect NK cells from blast-mediated suppression. This is in accordance with a recent article, demonstrating that NK cells in contrast to T cells hardly express PD-1 even after various modes of stimulation (Judge et al., 2020). Nonetheless, expression of PD-L1 might contribute to suppression of T cells in AML.

Most studies on NK cell dysfunction in AML suggest contact-dependent mediation of defects (Baessler et al., 2010; Fauriat et al., 2007; Khaznadar et al., 2014), whereas only one group found suppression of NK cells in transwell co-cultures (Stringaris et al., 2014). Baessler and co-workers detected the expression of CD137L (also known as 4-1BB) on a fraction of AML patients (35%) and suggested its participation in NK cell suppression (Baessler et al., 2010). The study was performed with polyclonal, 10 days expanded NK cells derived from healthy donors. Such NK cells expressed CD137, the receptor of CD137L, whereas unstimulated NK cells were devoid of CD137. Also, variable frequencies of NK cells isolated from AML patients expressed CD137. Blocking CD137-CD137L interaction between $CD137L^{+}$

blasts and NK cells increased degranulation, lysis of such blasts and IFN-γ secretion (Baessler et al., 2010). However, CD137 was not detected in overnight cultured NK cells in our *in vitro* setting (not shown) which is in line with data from Baessler and colleagues. Furthermore, monocytes and other myeloid cells from healthy donors express substantial levels of CD137L and we did not measure suppression of NK cells in co-culture with allogenic monocytes. As pointed out by the authors, their experimental system mimics a situation of adoptive cell transfer, where allogenic NK cells are usually expanded *ex vivo* in high-dosed cytokines. In such therapeutic settings, patient specific CD137L assessment and possible treatment with anti-CD137L might be a promising option. Also, such AML patients in which most NK cells express CD137 might benefit from the therapy.

In another study, a cell intrinsic marker higher expressed in AML NK cells was detected. In a comparison of pre-expanded patient NK and healthy donor NK cells, Parameswaran and colleagues found elevated expression of the kinase GSK3 in AML NK cells, possibly connected to NK cell dysfunction (Parameswaran et al., 2016). Blocking GSK3 activity in AML NK cells increased cytotoxic activity against AML cell lines and autologous blast and this effect was mediated by NF-κB induced TNF secretion. Up-regulation of LFA-1 on NK cells and ICAM-1 on tumor cells, of which the latter was regulated by TNF, improved the formation of a cytolytic synapse. The authors suggest GSK3 inhibition as possible therapy against AML. However, the mechanism leading to GSK3 expression in AML NK cells was not elucidated in the study (Parameswaran et al., 2016). Of note, others found proper conjugation between NK cells and AML blasts or cell lines and correct actin reorganization, but lytic granules were not polarized (Khaznadar et al., 2014). The authors speculated, that improper CD3ζ signaling, which is a the signal unit of NKp30, NKp46 and CD16 receptors, might be responsible for this defect (Khaznadar et al., 2014).

There is consensus that NK cells from AML patients are dysfunctional and many studies suggested that AML blasts directly suppress NK cell functions. However, different modes of suppression have been described and might be relevant at different stages of the disease for different cell types or in response to different treatments. For example, while PD-L1 expression might not affect NK cells it likely diminishes T cell responses. Furthermore, CD137L expression does not affect unstimulated NK cells but in settings where stimulated NK cells are adoptively transferred or in patients that have high frequencies of $CD137^+$ NK cells this mechanism might add to the suppression of NK cells. And although we could not confirm TGF-β1 mediated suppression of NK cells in our system it cannot be excluded that AML blasts express (surface bound) TGF-β1 in the local environment of the bone marrow.

4.2.5 PGE2-mediated suppression of NK cells in AML

In co-cultures of AML blasts with unstimulated NK cells directly *ex vivo*, we found no experimental evidence for some of the previously reported mechanism of NK cell suppression. Instead, we detected expression of COX2 and secretion of prostaglandin E2 by AML blasts that mediated NK cells suppression. PGE2 concentrations were measured via PGE2 ELISA and found increased in blasts compared with monocytes. In line, monocytes did not suppress NK cell effector functions in co-culture. Additionally, PGE2 concentrations in the supernatant of blasts correlated with the degree of NK cell suppression and blocking PGE2 perception or production alleviated the regulatory effect.

It is unclear, how NK cell effector functions are regulated by PGE2. Although cytokine secretion of NK cells is more sensitive towards PGE2 mediated inhibition in our hands, degranulation and lysis of target cells is also impaired at high concentrations. In a study of Martinet and co-workers, NK cell mediated lysis of target cells coated with agonistic antibodies was impaired for each of the activating receptors tested (NKG2D, CD16, NKp30, NKp44, NKp46) upon PGE2 treatment, indicating that PGE2 induces cell intrinsic defects. In the same study, the suppressive effect of PGE2 on γδ T cells was investigated and a defect in early TCR signaling mediated by protein kinase A (PKA) type I was proposed by the authors (Martinet et al., 2010). In a different study, reduced signaling via MAPK-ERK and NF-κB was connected to PGE2 treatment (Park et al., 2018). While NKG2D, CD16, NKp30 and NKp46 rely on various proximal signal chains (DAP10, FcεRI-γ or CD3ζ), the activation of the PI3K/AKT/mTOR pathway, MAPK/ERK pathway and calcium influx is common. While calcium influx mainly regulates degranulation, NF-κB and MAPK-ERK signaling is associated with cytokine response (Lanier, 2008). Successive experiments will address the question, which transcriptional and post-transcriptional (phosphorylation) events impair NK cell degranulation and cytokine secretion, respectively. Considering our data and published experiments it is hypothesized, that NK cell signal transduction is regulated by PGE2 leading to strong impairment of cytokine production with moderate effects on degranulation and killing. Additionally, down-regulation of activating receptors likely increases the activation threshold for PGE2 regulated NK cells.

PGE2 is perceived by EP1-4 receptors, of which EP2 and EP4 are relevant for suppression of NK cell effector functions in mice and human (Bonavita et al., 2020; Martinet et al., 2010). PGE2 receptors EP2 and EP4 are detected on mRNA and protein level by almost all peripheral blood NK cells freshly after isolation and after IL-2 stimulation (Martinet et al., 2010). We found that high concentration of PGE2 (1000 ng/ml) blocked the production of TNF and IFN-γ by NK cells completely, underlining that at least

all NK cells competent to secrete cytokines express PGE2 receptors. The secretion of PGE2 by AML blasts therefore likely targets NK cells independent of the state of activation and represents a potent mode of suppression. It has been demonstrated that the local environment of solid tumors is shaped by IFN-γ secretion of NK cells and that blocking IFN-γ secretion via PGE2 prevents the induction of anti-cancer immunity (Bonavita et al., 2020). Similarly, blocking cytokine production of infiltrating or locally maturing NK cells in the bone marrow might be critical to prevent the induction of successful anti-cancer immunity in AML. Blocking PGE2 production via COX2 inhibitor celecoxib or PGE2 perception via EP2/4 inhibitors protected NK cells from AML mediated-suppression partly. Since PGE2 production and the effect of blockade was heterogenous among patients, it is likely that additional mechanisms of suppression are employed by AML blasts and that some patients could benefit more from PGE2 targeting therapy than others. We suggest evaluating the integration of celecoxib or related inhibitors into AML maintenance therapy in the future.

4.2.6 Immunotherapies against AML

We tested, if AML blasts were recognized and killed by allogenic NK cells that were not primed with cytokines or stimulated by other means, but no degranulation or production of cytokines was detected. This is in accordance with other studies, that showed minor effector functions of autologous or allogenic NK cells against primary AML blasts (Khaznadar et al., 2014; Stringaris et al., 2014). Considering the presented data, we propose that AML blasts evade NK cell mediated killing with a dual strategy. On the one hand, AML blasts express surface ligands favoring immune evasion. This is obvious, since K562 cells are still recognized and killed in mixed cultures of AML blasts and NK cells whereas in co-cultures of AML blasts and NK cells no induction of effector functions was observed. Although the expression of surface receptors on NK cells is decreased, likely AML blasts express high levels of inhibiting ligands like HLA-class I to counterbalance stimulatory ligands (Baessler et al., 2010; Nguyen et al., 2009). On the other hand, NK effector functions are actively suppressed via secretion of PGE2. Due to the broad immune dampening effect of this prostaglandin (Bonavita et al., 2020; Böttcher et al., 2018; Martinet et al., 2010; Snijdewint et al., 1993), the induction of T cell mediated immunity is likely impaired as well. We therefore propose a therapeutic strategy, in which patients during complete remission receive celecoxib for maintenance therapy to prevent remodeling of the bone marrow into an anti-inflammatory environment by regrowing leukemia cells, as frequently observed for solid tumors (Bonavita et al., 2020). In addition, treatments increasing activating ligand expression, decreasing NKG2D ligand shedding or facilitating AML blast recognition (e.g. anti-CD33 and related

BiKE, TriKE) are promising ideas for combination treatments (Xu and Niu, 2020). Furthermore, CAR-NK cells should be engineered to lack EP2 and EP4 receptors to reduce immune suppression by AML blasts. Counteracting PGE2 mediated suppression in AML might improve therapeutic success of existing and future immunotherapies. However, pre-clinical and clinical trials are required to validate the efficacy of celecoxib *in vivo*.

4.3 Conclusion

A common hallmark of cancer is the evasion from immune-mediated destruction, which is often achieved via active suppression of critical immune cell populations (Hanahan and Weinberg, 2011). Our data provide evidence that such immune evasion is achieved by both, primary tumor cells (as seen by AML blasts) and regulatory cells of the tumor microenvironment (as demonstrated for MDSCs). Repurposing of the anti-diabetic drug DMBG alleviated the suppressive capacity of MDSCs in a mouse melanoma model via scavenging of MGO and had strong anti-tumor effects in combination with anti-PD-1 therapy. The broad safety profile of DMBG in humans opens new opportunities for targeted immune therapies against solid tumors. Differently, AML blasts suppressed NK cells directly via secretion of prostaglandin E2. PGE2 strongly impaired the ability of NK cells to produce pro-inflammatory cytokines and reduced NK cell cytotoxicity. PGE2 is secreted by many tumor types and there is growing scientific evidence that PGE2 is a main player in the suppression of various critical immune cell populations in the TME (Bonavita et al., 2020; Böttcher et al., 2018). Inhibitors of the PGE2 producing enzyme COX2 are frequently used anti-pain medications. Diagnostic screening of each patients individual TME for biomarkers of immune suppressive cells (MDSC counts, SSAO staining in IHC, PGE2 concentrations or COX signatures, as proposed by Bonavita and colleagues) and targeted treatment dependent on the results might strongly improve the efficacy of anti-cancer therapies in the future.

5. Bibliography

Ahmed, N., Argirov, O.K., Minhas, H.S., Cordeiro, C.A.A., and Thornalley, P.J. (2002). Assay of advanced glycation endproducts (AGEs): surveying AGEs by chromatographic assay with derivatization by 6-aminoquinolyl-N-hydroxysuccinimidyl-carbamate and application to Nepsilon-carboxymethyl-lysine- and Nepsilon-(1-carboxyethyl)lysine-modified albumin. Biochem J *364*, 1–14.

Ahrends, T., and Borst, J. (2018). The opposing roles of CD4+ T cells in anti-tumour immunity. Immunology *154*, 582–592.

Ai, L., Mu, S., Wang, Y., Wang, H., Cai, L., Li, W., and Hu, Y. (2018). Prognostic role of myeloid-derived suppressor cells in cancers: a systematic review and meta-analysis. BMC Cancer *18*.

Alberts, B., Johnson, A., Lewis, J., Raff, M., Roberts, K., and Walter, P. (2008). Molecular Biology of the Cell (Garland Science).

de Arriba, S.G., Stuchbury, G., Yarin, J., Burnell, J., Loske, C., and Münch, G. (2007). Methylglyoxal impairs glucose metabolism and leads to energy depletion in neuronal cells—protection by carbonyl scavengers. Neurobiology of Aging *28*, 1044–1050.

Asseman, C., Mauze, S., Leach, M.W., Coffman, R.L., and Powrie, F. (1999). An Essential Role for Interleukin 10 in the Function of Regulatory T Cells That Inhibit Intestinal Inflammation. Journal of Experimental Medicine *190*, 995–1004.

Bae, D.S., Hwang, Y.K., and Lee, J.K. (2012). Importance of NKG2D-NKG2D ligands interaction for cytolytic activity of natural killer cell. Cellular Immunology *276*, 122–127.

Baessler, T., Charton, J.E., Schmiedel, B.J., Grünebach, F., Krusch, M., Wacker, A., Rammensee, H.-G., and Salih, H.R. (2010). CD137 ligand mediates opposite effects in human and mouse NK cells and impairs NK-cell reactivity against human acute myeloid leukemia cells. Blood *115*, 3058–3069.

Balsamo, M., Manzini, C., Pietra, G., Raggi, F., Blengio, F., Mingari, M.C., Varesio, L., Moretta, L., Bosco, M.C., and Vitale, M. (2013). Hypoxia downregulates the expression of activating receptors involved in NK-cell-mediated target cell killing without affecting ADCC. Eur J Immunol *43*, 2756–2764.

Barry, K.C., Hsu, J., Broz, M.L., Cueto, F.J., Binnewies, M., Combes, A.J., Nelson, A.E., Loo, K., Kumar, R., Rosenblum, M.D., et al. (2018). A natural killer–dendritic cell axis defines checkpoint therapy–responsive tumor microenvironments. Nat Med *24*, 1178–1191.

Baumann, T., Dunkel, A., Schmid, C., Schmitt, S., Hiltensperger, M., Lohr, K., Laketa, V., Donakonda, S., Ahting, U., Lorenz-Depiereux, B., et al. (2020). Regulatory myeloid cells paralyze T cells through cell–cell transfer of the metabolite methylglyoxal. Nature Immunology *21*, 555–566.

Beisswenger, P., and Ruggiero-Lopez, D. (2003). Metformin inhibition of glycation processes. Diabetes & Metabolism *29*, 6S95-6S103.

5. Bibliography

Bellahcène, A., Nokin, M.-J., Castronovo, V., and Schalkwijk, C. (2017). Methylglyoxal-derived stress: An emerging biological factor involved in the onset and progression of cancer. Seminars in Cancer Biology.

Bergmann, L., Schui, D.K., Brieger, J., Weidmann, E., Mitrou, P.S., and Hoelzer, D. (1995). The inhibition of lymphokine-activated killer cells in acute myeloblastic leukemia is mediated by transforming growth factor-beta 1. Exp. Hematol. *23*, 1574–1580.

Binnewies, M., Roberts, E.W., Kersten, K., Chan, V., Fearon, D.F., Merad, M., Coussens, L.M., Gabrilovich, D.I., Ostrand-Rosenberg, S., Hedrick, C.C., et al. (2018). Understanding the tumor immune microenvironment (TIME) for effective therapy. Nat Med *24*, 541–550.

Bodmer, M., Meier, C., Krähenbühl, S., Jick, S.S., and Meier, C.R. (2010). Long-term metformin use is associated with decreased risk of breast cancer. Diabetes Care *33*, 1304–1308.

Bonavita, E., Bromley, C.P., Jonsson, G., Pelly, V.S., Sahoo, S., Walwyn-Brown, K., Mensurado, S., Moeini, A., Flanagan, E., Bell, C.R., et al. (2020). Antagonistic Inflammatory Phenotypes Dictate Tumor Fate and Response to Immune Checkpoint Blockade. Immunity *0*.

Bopp, T., Becker, C., Klein, M., Klein-Heßling, S., Palmetshofer, A., Serfling, E., Heib, V., Becker, M., Kubach, J., Schmitt, S., et al. (2007). Cyclic adenosine monophosphate is a key component of regulatory T cell–mediated suppression. J Exp Med *204*, 1303–1310.

Böttcher, J.P., and Reis e Sousa, C. (2018). The Role of Type 1 Conventional Dendritic Cells in Cancer Immunity. Trends Cancer *4*, 784–792.

Böttcher, J.P., Bonavita, E., Chakravarty, P., Blees, H., Cabeza-Cabrerizo, M., Sammicheli, S., Rogers, N.C., Sahai, E., Zelenay, S., and Reis e Sousa, C. (2018). NK Cells Stimulate Recruitment of cDC1 into the Tumor Microenvironment Promoting Cancer Immune Control. Cell *172*, 1022-1037.e14.

Brand, A., Singer, K., Koehl, G.E., Kolitzus, M., Schoenhammer, G., Thiel, A., Matos, C., Bruss, C., Klobuch, S., Peter, K., et al. (2016). LDHA-Associated Lactic Acid Production Blunts Tumor Immunosurveillance by T and NK Cells. Cell Metabolism *24*, 657–671.

Braun, M., Müller, B., ter Meer, D., Raffegerst, S., Simm, B., Wilde, S., Spranger, S., Ellwart, J., Mosetter, B., Umansky, L., et al. (2011). The CD6 scavenger receptor is differentially expressed on a CD56 natural killer cell subpopulation and contributes to natural killer-derived cytokine and chemokine secretion. J Innate Immun *3*, 420–434.

Brimnes, M.K., Vangsted, A.J., Knudsen, L.M., Gimsing, P., Gang, A.O., Johnsen, H.E., and Svane, I.M. (2010). Increased level of both CD4+FOXP3+ regulatory T cells and CD14+HLA-DR$^-$/low myeloid-derived suppressor cells and decreased level of dendritic cells in patients with multiple myeloma. Scand. J. Immunol. *72*, 540–547.

Bronte, V., Serafini, P., Mazzoni, A., Segal, D.M., and Zanovello, P. (2003). L-arginine metabolism in myeloid cells controls T-lymphocyte functions. Trends in Immunology *24*, 301–305.

5. Bibliography

Bronte, V., Brandau, S., Chen, S.-H., Colombo, M.P., Frey, A.B., Greten, T.F., Mandruzzato, S., Murray, P.J., Ochoa, A., Ostrand-Rosenberg, S., et al. (2016). Recommendations for myeloid-derived suppressor cell nomenclature and characterization standards. Nature Communications *7*, 12150.

Butte, M.J., Keir, M.E., Phamduy, T.B., Freeman, G.J., and Sharpe, A.H. (2007). PD-L1 interacts specifically with B7-1 to inhibit T cell proliferation. Immunity *27*, 111–122.

Carr, E.L., Kelman, A., Wu, G.S., Gopaul, R., Senkevitch, E., Aghvanyan, A., Turay, A.M., and Frauwirth, K.A. (2010). Glutamine uptake and metabolism are coordinately regulated by ERK/MAPK during T lymphocyte activation. J Immunol *185*, 1037–1044.

Castriconi, R., Cantoni, C., Chiesa, M.D., Vitale, M., Marcenaro, E., Conte, R., Biassoni, R., Bottino, C., Moretta, L., and Moretta, A. (2003). Transforming growth factor β1 inhibits expression of NKp30 and NKG2D receptors: Consequences for the NK-mediated killing of dendritic cells. PNAS *100*, 4120–4125.

Cazzola, M. (2020). Myelodysplastic Syndromes. N Engl J Med *383*, 1358–1374.

Chakraborty, S., Karmakar, K., and Chakravortty, D. (2014). Cells producing their own nemesis: Understanding methylglyoxal metabolism: Cause and Consequences of Methylglyoxal Metabolism. IUBMB Life *66*, 667–678.

Cham, C.M., Driessens, G., O'Keefe, J.P., and Gajewski, T.F. (2008). Glucose Deprivation Inhibits Multiple Key Gene Expression Events and Effector Functions in CD8+ T Cells. Eur J Immunol *38*, 2438–2450.

Champsaur, M., and Lanier, L.L. (2010). Effect of NKG2D ligand expression on host immune responses. Immunol Rev *235*, 267–285.

Chang, C.-H., Curtis, J.D., Maggi, L.B., Faubert, B., Villarino, A.V., O'Sullivan, D., Huang, S.C.-C., van der Windt, G.J.W., Blagih, J., Qiu, J., et al. (2013). Posttranscriptional Control of T Cell Effector Function by Aerobic Glycolysis. Cell *153*, 1239–1251.

Chang, C.-H., Qiu, J., O'Sullivan, D., Buck, M.D., Noguchi, T., Curtis, J.D., Chen, Q., Gindin, M., Gubin, M.M., van der Windt, G.J.W., et al. (2015). Metabolic Competition in the Tumor Microenvironment Is a Driver of Cancer Progression. Cell *162*, 1229–1241.

Chang, T., Wang, R., and Wu, L. (2005). Methylglyoxal-induced nitric oxide and peroxynitrite production in vascular smooth muscle cells. Free Radic Biol Med *38*, 286–293.

Cheung, K.S., Chan, E.W., Wong, A.Y.S., Chen, L., Seto, W.K., Wong, I.C.K., and Leung, W.K. (2019). Metformin Use and Gastric Cancer Risk in Diabetic Patients After Helicobacter pylori Eradication. J Natl Cancer Inst *111*, 484–489.

Chiesa, M.D., Carlomagno, S., Frumento, G., Balsamo, M., Cantoni, C., Conte, R., Moretta, L., Moretta, A., and Vitale, M. (2006). The tryptophan catabolite l-kynurenine inhibits the surface expression of NKp46- and NKG2D-activating receptors and regulates NK-cell function. Blood *108*, 4118–4125.

Chinnery, H.R., Pearlman, E., and McMenamin, P.G. (2008). Cutting Edge: Membrane Nanotubes In Vivo: A Feature of MHC Class II+ Cells in the Mouse Cornea. J Immunol *180*, 5779–5783.

5. Bibliography

Costello, R.T., Sivori, S., Marcenaro, E., Lafage-Pochitaloff, M., Mozziconacci, M.-J., Reviron, D., Gastaut, J.-A., Pende, D., Olive, D., and Moretta, A. (2002). Defective expression and function of natural killer cell–triggering receptors in patients with acute myeloid leukemia. Blood *99*, 3661–3667.

Crane, C.A., Han, S.J., Barry, J.J., Ahn, B.J., Lanier, L.L., and Parsa, A.T. (2010). TGF-beta downregulates the activating receptor NKG2D on NK cells and CD8+ T cells in glioma patients. Neuro-Oncology *12*, 7–13.

Daher, M., Basar, R., Shaim, H., Gokdemir, E., Uprety, N., Kontoyiannis, A., Mendt, M.C., Imahashi, N., Kerbauy, L.N., Lim, F.L.W.I., et al. (2017). The TGF-β/SMAD Signaling Pathway As a Mediator of NK Cell Dysfunction and Immune Evasion in Myelodysplastic Syndrome. Blood *130*, 53–53.

De Rosa, V., Galgani, M., Porcellini, A., Colamatteo, A., Santopaolo, M., Zuchegna, C., Romano, A., De Simone, S., Procaccini, C., La Rocca, C., et al. (2015). Glycolysis controls the induction of human regulatory T cells by modulating the expression of FOXP3 exon 2 splicing variants. Nat Immunol *16*, 1174–1184.

DeBerardinis, R.J., and Chandel, N.S. (2020). We need to talk about the Warburg effect. Nature Metabolism *2*, 127–129.

Diaz-Montero, C.M., Salem, M.L., Nishimura, M.I., Garrett-Mayer, E., Cole, D.J., and Montero, A.J. (2009). Increased circulating myeloid-derived suppressor cells correlate with clinical cancer stage, metastatic tumor burden, and doxorubicin–cyclophosphamide chemotherapy. Cancer Immunol Immunother *58*, 49–59.

Donadon, V., Balbi, M., Mas, M.D., Casarin, P., and Zanette, G. (2010). Metformin and reduced risk of hepatocellular carcinoma in diabetic patients with chronic liver disease. Liver Int *30*, 750–758.

Donkor, M.K., Lahue, E., Hoke, T.A., Shafer, L.R., Coskun, U., Solheim, J.C., Gulen, D., Bishay, J., and Talmadge, J.E. (2009). Mammary tumor heterogeneity in the expansion of myeloid-derived suppressor cells. Int Immunopharmacol *9*, 937–948.

Donnelly, R.P., Loftus, R.M., Keating, S.E., Liou, K.T., Biron, C.A., Gardiner, C.M., and Finlay, D.K. (2014). mTORC1-Dependent Metabolic Reprogramming Is a Prerequisite for NK Cell Effector Function. J.I. *193*, 4477–4484.

Dupont, M., Souriant, S., Lugo-Villarino, G., Maridonneau-Parini, I., and Vérollet, C. (2018). Tunneling Nanotubes: Intimate Communication between Myeloid Cells. Front Immunol *9*.

Eikawa, S., Nishida, M., Mizukami, S., Yamazaki, C., Nakayama, E., and Udono, H. (2015). Immune-mediated antitumor effect by type 2 diabetes drug, metformin. Proc Natl Acad Sci U S A *112*, 1809–1814.

Elgueta, R., Tobar, J.A., Shoji, K.F., De Calisto, J., Kalergis, A.M., Bono, M.R., Rosemblatt, M., and Sáez, J.C. (2009). Gap junctions at the dendritic cell-T cell interface are key elements for antigen-dependent T cell activation. J Immunol *183*, 277–284.

5. Bibliography

El-Mir, M.Y., Nogueira, V., Fontaine, E., Avéret, N., Rigoulet, M., and Leverve, X. (2000). Dimethylbiguanide inhibits cell respiration via an indirect effect targeted on the respiratory chain complex I. J Biol Chem *275*, 223–228.

Fauriat, C., Just-Landi, S., Mallet, F., Arnoulet, C., Sainty, D., Olive, D., and Costello, R.T. (2007). Deficient expression of NCR in NK cells from acute myeloid leukemia: evolution during leukemia treatment and impact of leukemia cells in NCRdull phenotype induction. Blood *109*, 323–330.

Ferjančič, Š., Gil-Bernabé, A.M., Hill, S.A., Allen, P.D., Richardson, P., Sparey, T., Savory, E., McGuffog, J., and Muschel, R.J. (2013). VCAM-1 and VAP-1 recruit myeloid cells that promote pulmonary metastasis in mice. Blood *121*, 3289–3297.

Fink, T., Ebbesen, P., Koppelhus, U., and Zachar, V. (2003). Natural killer cell-mediated basal and interferon-enhanced cytotoxicity against liver cancer cells is significantly impaired under in vivo oxygen conditions. Scand J Immunol *58*, 607–612.

Freeman, G.J., Long, A.J., Iwai, Y., Bourque, K., Chernova, T., Nishimura, H., Fitz, L.J., Malenkovich, N., Okazaki, T., Byrne, M.C., et al. (2000). Engagement of the PD-1 immunoinhibitory receptor by a novel B7 family member leads to negative regulation of lymphocyte activation. J Exp Med *192*, 1027–1034.

Fridman, W.H., Pagès, F., Sautès-Fridman, C., and Galon, J. (2012). The immune contexture in human tumours: impact on clinical outcome. Nat Rev Cancer *12*, 298–306.

Frumento, G., Rotondo, R., Tonetti, M., Damonte, G., Benatti, U., and Ferrara, G.B. (2002). Tryptophan-derived Catabolites Are Responsible for Inhibition of T and Natural Killer Cell Proliferation Induced by Indoleamine 2,3-Dioxygenase. J Exp Med *196*, 459–468.

Gabrilovich, D.I. (2017). Myeloid-Derived Suppressor Cells. Cancer Immunology Research *5*, 3–8.

Gabrilovich, D.I., Ostrand-Rosenberg, S., and Bronte, V. (2012). Coordinated regulation of myeloid cells by tumours. Nature Reviews Immunology *12*, 253–268.

Galligan, J.J., Wepy, J.A., Streeter, M.D., Kingsley, P.J., Mitchener, M.M., Wauchope, O.R., Beavers, W.N., Rose, K.L., Wang, T., Spiegel, D.A., et al. (2018). Methylglyoxal-derived posttranslational arginine modifications are abundant histone marks. PNAS *115*, 9228–9233.

Gardiner, C.M., and Finlay, D.K. (2017). What Fuels Natural Killers? Metabolism and NK Cell Responses. Front Immunol *8*.

Gauci, M.-L., Lanoy, E., Champiat, S., Caramella, C., Ammari, S., Aspeslagh, S., Varga, A., Baldini, C., Bahleda, R., Gazzah, A., et al. (2019). Long-Term Survival in Patients Responding to Anti-PD-1/PD-L1 Therapy and Disease Outcome upon Treatment Discontinuation. Clin Cancer Res *25*, 946–956.

Gebhardt, C., Sevko, A., Jiang, H., Lichtenberger, R., Reith, M., Tarnanidis, K., Holland-Letz, T., Umansky, L., Beckhove, P., Sucker, A., et al. (2015). Myeloid Cells and Related Chronic Inflammatory Factors as Novel Predictive Markers in Melanoma Treatment with Ipilimumab. Clin. Cancer Res. *21*, 5453–5459.

5. Bibliography

Geiger, R., Rieckmann, J.C., Wolf, T., Basso, C., Feng, Y., Fuhrer, T., Kogadeeva, M., Picotti, P., Meissner, F., Mann, M., et al. (2016). L-Arginine Modulates T Cell Metabolism and Enhances Survival and Anti-tumor Activity. Cell *167*, 829-842.e13.

Gentles, A.J., Newman, A.M., Liu, C.L., Bratman, S.V., Feng, W., Kim, D., Nair, V.S., Xu, Y., Khuong, A., Hoang, C.D., et al. (2015). The prognostic landscape of genes and infiltrating immune cells across human cancers. Nat Med *21*, 938–945.

Ghosh, A., Bera, S., Ghosal, S., Ray, S., Basu, A., and Ray, M. (2011). Differential inhibition/inactivation of mitochondrial complex I implicates its alteration in malignant cells. Biochemistry Moscow *76*, 1051.

Giebel, S., Locatelli, F., Lamparelli, T., Velardi, A., Davies, S., Frumento, G., Maccario, R., Bonetti, F., Wojnar, J., Martinetti, M., et al. (2003). Survival advantage with KIR ligand incompatibility in hematopoietic stem cell transplantation from unrelated donors. Blood *102*, 814–819.

Gleisner, M.A., Navarrete, M., Hofmann, F., Salazar-Onfray, F., and Tittarelli, A. (2017). Mind the Gaps in Tumor Immunity: Impact of Connexin-Mediated Intercellular Connections. Front. Immunol. *8*.

Goh, S.-Y., and Cooper, M.E. (2008). The Role of Advanced Glycation End Products in Progression and Complications of Diabetes. The Journal of Clinical Endocrinology & Metabolism *93*, 1143–1152.

Goh, C.C., Roggerson, K.M., Lee, H.-C., Golden-Mason, L., Rosen, H.R., and Hahn, Y.S. (2016). Hepatitis C Virus-Induced Myeloid-Derived Suppressor Cells Suppress NK Cell IFN-γ Production by Altering Cellular Metabolism via Arginase-1. J. Immunol. *196*, 2283–2292.

Gorelik, L., and Flavell, R.A. (2001). Immune-mediated eradication of tumors through the blockade of transforming growth factor-β signaling in T cells. Nat Med *7*, 1118–1122.

van Gosliga, D., Schepers, H., Rizo, A., van der Kolk, D., Vellenga, E., and Schuringa, J.J. (2007). Establishing long-term cultures with self-renewing acute myeloid leukemia stem/progenitor cells. Experimental Hematology *35*, 1538–1549.

Griessinger, E., Moschoi, R., Biondani, G., and Peyron, J.-F. (2017). Mitochondrial Transfer in the Leukemia Microenvironment. Trends in Cancer *3*, 828–839.

Gubser, P.M., Bantug, G.R., Razik, L., Fischer, M., Dimeloe, S., Hoenger, G., Durovic, B., Jauch, A., and Hess, C. (2013). Rapid effector function of memory $CD8^+$ T cells requires an immediate-early glycolytic switch. Nature Immunology *14*, 1064–1072.

Guerra, L., Bonetti, L., and Brenner, D. (2020). Metabolic Modulation of Immunity: A New Concept in Cancer Immunotherapy. Cell Reports *32*, 107848.

Hanahan, D., and Weinberg, R.A. (2011). Hallmarks of cancer: the next generation. Cell *144*, 646–674.

Hanson, E.M., Clements, V.K., Sinha, P., Ilkovitch, D., and Ostrand-Rosenberg, S. (2009). Myeloid-derived suppressor cells down-regulate L-selectin expression on CD4+ and CD8+ T cells. J Immunol *183*, 937–944.

5. Bibliography

Hargadon, K.M., Johnson, C.E., and Williams, C.J. (2018). Immune checkpoint blockade therapy for cancer: An overview of FDA-approved immune checkpoint inhibitors. Int Immunopharmacol *62*, 29–39.

Harmon, C., Robinson, M.W., Hand, F., Almuaili, D., Mentor, K., Houlihan, D.D., Hoti, E., Lynch, L., Geoghegan, J., and O'Farrelly, C. (2019). Lactate-Mediated Acidification of Tumor Microenvironment Induces Apoptosis of Liver-Resident NK Cells in Colorectal Liver Metastasis. Cancer Immunol Res *7*, 335–346.

Harris, K., and Smith, L. (2013). Safety and efficacy of metformin in patients with type 2 diabetes mellitus and chronic hepatitis C. Ann Pharmacother *47*, 1348–1352.

Hashemi Goradel, N., Najafi, M., Salehi, E., Farhood, B., and Mortezaee, K. (2019). Cyclooxygenase-2 in cancer: A review. J Cell Physiol *234*, 5683–5699.

Hayakawa, K., Esposito, E., Wang, X., Terasaki, Y., Liu, Y., Xing, C., Ji, X., and Lo, E.H. (2016). Transfer of mitochondria from astrocytes to neurons after stroke. Nature *535*, 551–555.

Hilpert, J., Grosse-Hovest, L., Grünebach, F., Buechele, C., Nuebling, T., Raum, T., Steinle, A., and Salih, H.R. (2012). Comprehensive Analysis of NKG2D Ligand Expression and Release in Leukemia: Implications for NKG2D-Mediated NK Cell Responses. The Journal of Immunology *189*, 1360–1371.

Ho, P.-C., Bihuniak, J.D., Macintyre, A.N., Staron, M., Liu, X., Amezquita, R., Tsui, Y.-C., Cui, G., Micevic, G., Perales, J.C., et al. (2015). Phosphoenolpyruvate Is a Metabolic Checkpoint of Anti-tumor T Cell Responses. Cell *162*, 1217–1228.

Höchst, B., Schildberg, F.A., Sauerborn, P., Gäbel, Y.A., Gevensleben, H., Goltz, D., Heukamp, L.C., Türler, A., Ballmaier, M., Gieseke, F., et al. (2013). Activated human hepatic stellate cells induce myeloid derived suppressor cells from peripheral blood monocytes in a CD44-dependent fashion. Journal of Hepatology *59*, 528–535.

Hoechst, B., Ormandy, L.A., Ballmaier, M., Lehner, F., Krüger, C., Manns, M.P., Greten, T.F., and Korangy, F. (2008). A new population of myeloid-derived suppressor cells in hepatocellular carcinoma patients induces CD4(+)CD25(+)Foxp3(+) T cells. Gastroenterology *135*, 234–243.

Hoechst, B., Voigtlaender, T., Ormandy, L., Gamrekelashvili, J., Zhao, F., Wedemeyer, H., Lehner, F., Manns, M.P., Greten, T.F., and Korangy, F. (2009). Myeloid derived suppressor cells inhibit natural killer cells in patients with hepatocellular carcinoma via the NKp30 receptor. Hepatology *50*, 799–807.

Hoechst, B., Gamrekelashvili, J., Manns, M.P., Greten, T.F., and Korangy, F. (2011). Plasticity of human Th17 cells and iTregs is orchestrated by different subsets of myeloid cells. Blood *117*, 6532–6541.

Hong, C.-S., Sharma, P., Yerneni, S.S., Simms, P., Jackson, E.K., Whiteside, T.L., and Boyiadzis, M. (2017). Circulating exosomes carrying an immunosuppressive cargo interfere with cellular immunotherapy in acute myeloid leukemia. Sci Rep *7*, 14684.

Hsu, K.C., Keever-Taylor, C.A., Wilton, A., Pinto, C., Heller, G., Arkun, K., O'Reilly, R.J., Horowitz, M.M., and Dupont, B. (2005). Improved outcome in HLA-identical sibling hematopoietic stem-cell

transplantation for acute myelogenous leukemia predicted by KIR and HLA genotypes. Blood *105*, 4878–4884.

Huang, B., Pan, P.-Y., Li, Q., Sato, A.I., Levy, D.E., Bromberg, J., Divino, C.M., and Chen, S.-H. (2006). Gr-1+CD115+ immature myeloid suppressor cells mediate the development of tumor-induced T regulatory cells and T-cell anergy in tumor-bearing host. Cancer Res *66*, 1123–1131.

Husain, Z., Huang, Y., Seth, P., and Sukhatme, V.P. (2013). Tumor-Derived Lactate Modifies Antitumor Immune Response: Effect on Myeloid-Derived Suppressor Cells and NK Cells. The Journal of Immunology *191*, 1486–1495.

Irjala, H., Salmi, M., Alanen, K., Grénman, R., and Jalkanen, S. (2001). Vascular Adhesion Protein 1 Mediates Binding of Immunotherapeutic Effector Cells to Tumor Endothelium. The Journal of Immunology *166*, 6937–6943.

Jensen, H., Potempa, M., Gotthardt, D., and Lanier, L.L. (2017). Cutting Edge: IL-2–Induced Expression of the Amino Acid Transporters SLC1A5 and CD98 Is a Prerequisite for NKG2D-Mediated Activation of Human NK Cells. The Journal of Immunology *199*, 1967–1972.

Jordan, K.R., Amaria, R.N., Ramirez, O., Callihan, E.B., Gao, D., Borakove, M., Manthey, E., Borges, V.F., and McCarter, M.D. (2013). Myeloid-derived suppressor cells are associated with disease progression and decreased overall survival in advanced-stage melanoma patients. Cancer Immunol Immunother *62*, 1711–1722.

Judge, S.J., Dunai, C., Aguilar, E.G., Vick, S.C., Sturgill, I.R., Khuat, L.T., Stoffel, K.M., Dyke, J.V., Longo, D.L., Darrow, M.A., et al. (2020). Minimal PD-1 expression in mouse and human NK cells under diverse conditions. J Clin Invest *130*, 3051–3068.

Keating, S.E., Zaiatz-Bittencourt, V., Loftus, R.M., Keane, C., Brennan, K., Finlay, D.K., and Gardiner, C.M. (2016). Metabolic Reprogramming Supports IFN-γ Production by CD56bright NK Cells. The Journal of Immunology *196*, 2552–2560.

Kender, Z., Fleming, T., Kopf, S., Torzsa, P., Grolmusz, V., Herzig, S., Schleicher, E., Rácz, K., Reismann, P., and Nawroth, P. (2014). Effect of Metformin on Methylglyoxal Metabolism in Patients with Type 2 Diabetes. Experimental and Clinical Endocrinology & Diabetes *122*, 316–319.

Khalil, N. (1999). TGF-β: from latent to active. Microbes and Infection *1*, 1255–1263.

Khalil, D.N., Smith, E.L., Brentjens, R.J., and Wolchok, J.D. (2016). The future of cancer treatment: immunomodulation, CARs and combination immunotherapy. Nat Rev Clin Oncol *13*, 273–290.

Khaznadar, Z., Henry, G., Setterblad, N., Agaugue, S., Raffoux, E., Boissel, N., Dombret, H., Toubert, A., and Dulphy, N. (2014). Acute myeloid leukemia impairs natural killer cells through the formation of a deficient cytotoxic immunological synapse. European Journal of Immunology *44*, 3068–3080.

Khaznadar, Z., Boissel, N., Agaugué, S., Henry, G., Cheok, M., Vignon, M., Geromin, D., Cayuela, J.-M., Castaigne, S., Pautas, C., et al. (2015). Defective NK Cells in Acute Myeloid Leukemia Patients at Diagnosis Are Associated with Blast Transcriptional Signatures of Immune Evasion. J.I. *195*, 2580–2590.

5. Bibliography

Kikuchi, S., Shinpo, K., Moriwaka, F., Makita, Z., Miyata, T., and Tashiro, K. (1999). Neurotoxicity of methylglyoxal and 3-deoxyglucosone on cultured cortical neurons: synergism between glycation and oxidative stress, possibly involved in neurodegenerative diseases. J Neurosci Res *57*, 280–289.

Kim, J., and DeBerardinis, R.J. (2019). Mechanisms and Implications of Metabolic Heterogeneity in Cancer. Cell Metab *30*, 434–446.

Kim, J., Hyun, H.-J., Choi, E.-A., Kim, Y., Bae, Y.-J., and Kang, H.-T. (2020). Metformin use reduced the risk of stomach cancer in diabetic patients in Korea: an analysis of Korean NHIS-HEALS database. Gastric Cancer *23*, 1075–1083.

Kinsky, O.R., Hargraves, T.L., Anumol, T., Jacobsen, N.E., Dai, J., Snyder, S.A., Monks, T.J., and Lau, S.S. (2016). Metformin Scavenges Methylglyoxal To Form a Novel Imidazolinone Metabolite in Humans. Chem Res Toxicol *29*, 227–234.

Kornblau, S.M., McCue, D., Singh, N., Chen, W., Estrov, Z., and Coombes, K.R. (2010). Recurrent expression signatures of cytokines and chemokines are present and are independently prognostic in acute myelogenous leukemia and myelodysplasia. *116*, 12.

Kretschmer, A., Zhang, F., Somasekharan, S.P., Tse, C., Leachman, L., Gleave, A., Li, B., Asmaro, I., Huang, T., Kotula, L., et al. (2019). Stress-induced tunneling nanotubes support treatment adaptation in prostate cancer. Sci Rep *9*.

Krummel, M.F., and Allison, J.P. (1996). CTLA-4 engagement inhibits IL-2 accumulation and cell cycle progression upon activation of resting T cells. J Exp Med *183*, 2533–2540.

Ku, A.W., Muhitch, J.B., Powers, C.A., Diehl, M., Kim, M., Fisher, D.T., Sharda, A.P., Clements, V.K., O'Loughlin, K., Minderman, H., et al. (2016). Tumor-induced MDSC act via remote control to inhibit L-selectin-dependent adaptive immunity in lymph nodes. Elife *5*.

Kusmartsev, S., Nefedova, Y., Yoder, D., and Gabrilovich, D.I. (2004). Antigen-specific inhibition of CD8+ T cell response by immature myeloid cells in cancer is mediated by reactive oxygen species. J Immunol *172*, 989–999.

Kusmartsev, S.A., Li, Y., and Chen, S.H. (2000). Gr-1+ myeloid cells derived from tumor-bearing mice inhibit primary T cell activation induced through CD3/CD28 costimulation. J Immunol *165*, 779–785.

Lanier, L.L. (2008). Up on the tightrope: natural killer cell activation and inhibition. Nat Immunol *9*, 495–502.

Laplante, M., and Sabatini, D.M. (2009). mTOR signaling at a glance. Journal of Cell Science *122*, 3589–3594.

Latchman, Y., Wood, C.R., Chernova, T., Chaudhary, D., Borde, M., Chernova, I., Iwai, Y., Long, A.J., Brown, J.A., Nunes, R., et al. (2001). PD-L2 is a second ligand for PD-1 and inhibits T cell activation. Nat Immunol *2*, 261–268.

Lee, G.K., Park, H.J., Macleod, M., Chandler, P., Munn, D.H., and Mellor, A.L. (2002). Tryptophan deprivation sensitizes activated T cells to apoptosis prior to cell division. Immunology *107*, 452–460.

5. Bibliography

Lee, J.-C., Lee, K.-M., Kim, D.-W., and Heo, D.S. (2004). Elevated TGF-β1 Secretion and Down-Modulation of NKG2D Underlies Impaired NK Cytotoxicity in Cancer Patients. The Journal of Immunology *172*, 7335–7340.

Leoncini, G., Maresca, M., and Buzzi, E. (1989). Inhibition of the glycolytic pathway by methylglyoxal in human platelets. Cell Biochemistry and Function *7*, 65–70.

Li, H., Han, Y., Guo, Q., Zhang, M., and Cao, X. (2009). Cancer-Expanded Myeloid-Derived Suppressor Cells Induce Anergy of NK Cells through Membrane-Bound TGF-β1. J Immunol *182*, 240–249.

Li, R., Li, H., Luo, H.-J., Lin, Z.-X., Jiang, Z.-W., and Luo, W.-H. (2013). SSAO inhibitors suppress hepatocellular tumor growth in mice. Cellular Immunology *283*, 61–69.

Li, S., Liu, S., and Ho, C.-T. (2018). Safety issues of methylglyoxal and potential scavengers. Frontiers of Agricultural Science and Engineering *0*, 0.

Liu, C., Yu, S., Kappes, J., Wang, J., Grizzle, W.E., Zinn, K.R., and Zhang, H.-G. (2007a). Expansion of spleen myeloid suppressor cells represses NK cell cytotoxicity in tumor-bearing host. Blood *109*, 4336–4342.

Liu, C.-Y., Wang, Y.-M., Wang, C.-L., Feng, P.-H., Ko, H.-W., Liu, Y.-H., Wu, Y.-C., Chu, Y., Chung, F.-T., Kuo, C.-H., et al. (2010). Population alterations of L-arginase- and inducible nitric oxide synthase-expressed CD11b+/CD14$^-$/CD15+/CD33+ myeloid-derived suppressor cells and CD8+ T lymphocytes in patients with advanced-stage non-small cell lung cancer. J. Cancer Res. Clin. Oncol. *136*, 35–45.

Liu, V.C., Wong, L.Y., Jang, T., Shah, A.H., Park, I., Yang, X., Zhang, Q., Lonning, S., Teicher, B.A., and Lee, C. (2007b). Tumor Evasion of the Immune System by Converting CD4+CD25− T Cells into CD4+CD25+ T Regulatory Cells: Role of Tumor-Derived TGF-β. The Journal of Immunology *178*, 2883–2892.

Ljunggren, H.-G., and Malmberg, K.-J. (2007). Prospects for the use of NK cells in immunotherapy of human cancer. Nat Rev Immunol *7*, 329–339.

Lo, T.W., Westwood, M.E., McLellan, A.C., Selwood, T., and Thornalley, P.J. (1994). Binding and modification of proteins by methylglyoxal under physiological conditions. A kinetic and mechanistic study with N alpha-acetylarginine, N alpha-acetylcysteine, and N alpha-acetyllysine, and bovine serum albumin. J Biol Chem *269*, 32299–32305.

Loftus, R.M., Assmann, N., Kedia-Mehta, N., O'Brien, K.L., Garcia, A., Gillespie, C., Hukelmann, J.L., Oefner, P.J., Lamond, A.I., Gardiner, C.M., et al. (2018). Amino acid-dependent cMyc expression is essential for NK cell metabolic and functional responses in mice. Nat Commun *9*, 2341.

Lorenzo-Herrero, S., Sordo-Bahamonde, C., Gonzalez, S., and López-Soto, A. (2019). CD107a Degranulation Assay to Evaluate Immune Cell Antitumor Activity. In Cancer Immunosurveillance: Methods and Protocols, A. López-Soto, and A.R. Folgueras, eds. (New York, NY: Springer), pp. 119–130.

5. Bibliography

Lou, E., Fujisawa, S., Morozov, A., Barlas, A., Romin, Y., Dogan, Y., Gholami, S., Moreira, A.L., Manova-Todorova, K., and Moore, M.A.S. (2012). Tunneling Nanotubes Provide a Unique Conduit for Intercellular Transfer of Cellular Contents in Human Malignant Pleural Mesothelioma. PLoS One *7*.

Lowdell, M.W., Craston, R., Samuel, D., Wood, M.E., O'Neill, E., Saha, V., and Prentice, H.G. (2002). Evidence that continued remission in patients treated for acute leukaemia is dependent upon autologous natural killer cells. British Journal of Haematology *117*, 821–827.

Lu, T., Ramakrishnan, R., Altiok, S., Youn, J.-I., Cheng, P., Celis, E., Pisarev, V., Sherman, S., Sporn, M.B., and Gabrilovich, D. (2011). Tumor-infiltrating myeloid cells induce tumor cell resistance to cytotoxic T cells in mice. J Clin Invest *121*, 4015–4029.

Mahvi, D.A., Liu, R., Grinstaff, M.W., Colson, Y.L., and Raut, C.P. (2018). Local Cancer Recurrence: The Realities, Challenges, and Opportunities for New Therapies. CA Cancer J Clin *68*, 488–505.

Martens, A., Wistuba-Hamprecht, K., Geukes Foppen, M., Yuan, J., Postow, M.A., Wong, P., Romano, E., Khammari, A., Dreno, B., Capone, M., et al. (2016). Baseline Peripheral Blood Biomarkers Associated with Clinical Outcome of Advanced Melanoma Patients Treated with Ipilimumab. Clin. Cancer Res. *22*, 2908–2918.

Martinet, L., Jean, C., Dietrich, G., Fournié, J.-J., and Poupot, R. (2010). PGE2 inhibits natural killer and γδ T cell cytotoxicity triggered by NKR and TCR through a cAMP-mediated PKA type I-dependent signaling. Biochemical Pharmacology *80*, 838–845.

Marttila-Ichihara, F., Auvinen, K., Elima, K., Jalkanen, S., and Salmi, M. (2009). Vascular adhesion protein-1 enhances tumor growth by supporting recruitment of Gr-1+CD11b+ myeloid cells into tumors. Cancer Res. *69*, 7875–7883.

Marttila-Ichihara, F., Castermans, K., Auvinen, K., Egbrink, M.G.A. oude, Jalkanen, S., Griffioen, A.W., and Salmi, M. (2010). Small-Molecule Inhibitors of Vascular Adhesion Protein-1 Reduce the Accumulation of Myeloid Cells into Tumors and Attenuate Tumor Growth in Mice. The Journal of Immunology *184*, 3164–3173.

Mazzoni, A., Bronte, V., Visintin, A., Spitzer, J.H., Apolloni, E., Serafini, P., Zanovello, P., and Segal, D.M. (2002). Myeloid suppressor lines inhibit T cell responses by an NO-dependent mechanism. J Immunol *168*, 689–695.

Mehta, M.M., Weinberg, S.E., and Chandel, N.S. (2017). Mitochondrial control of immunity: beyond ATP. Nature Reviews Immunology *17*, 608–620.

Mendoza-Naranjo, A., Bouma, G., Pereda, C., Ramírez, M., Webb, K.F., Tittarelli, A., López, M.N., Kalergis, A.M., Thrasher, A.J., Becker, D.L., et al. (2011). Functional gap junctions accumulate at the immunological synapse and contribute to T cell activation. J Immunol *187*, 3121–3132.

Menk, A.V., Scharping, N.E., Moreci, R.S., Zeng, X., Guy, C., Salvatore, S., Bae, H., Xie, J., Young, H.A., Wendell, S.G., et al. (2018). Early TCR Signaling Induces Rapid Aerobic Glycolysis Enabling Distinct Acute T Cell Effector Functions. Cell Reports *22*, 1509–1521.

5. Bibliography

Metelli, A., Salem, M., Wallace, C.H., Wu, B.X., Li, A., Li, X., and Li, Z. (2018). Immunoregulatory functions and the therapeutic implications of GARP-TGF-β in inflammation and cancer. Journal of Hematology & Oncology *11*, 24.

Meyer, C., Cagnon, L., Costa-Nunes, C.M., Baumgaertner, P., Montandon, N., Leyvraz, L., Michielin, O., Romano, E., and Speiser, D.E. (2014). Frequencies of circulating MDSC correlate with clinical outcome of melanoma patients treated with ipilimumab. Cancer Immunol. Immunother. *63*, 247–257.

Mezrich, J.D., Fechner, J.H., Zhang, X., Johnson, B.P., Burlingham, W.J., and Bradfield, C.A. (2010). An interaction between kynurenine and the aryl hydrocarbon receptor can generate regulatory T cells. J Immunol *185*, 3190–3198.

Millet, P., Vachharajani, V., McPhail, L., and McCall, C.E. GAPDH Binding to TNF-α mRNA Contributes to Posttranscriptional Repression in Monocytes: A Novel Mechanism of Communication between Inflammation and Metabolism. 12.

Moon, J.-S., Hisata, S., Park, M.-A., DeNicola, G.M., Ryter, S.W., Nakahira, K., and Choi, A.M.K. (2015). mTORC1-Induced HK1-Dependent Glycolysis Regulates NLRP3 Inflammasome Activation. Cell Reports *12*, 102–115.

Moses, K., and Brandau, S. Human neutrophils: Their role in cancer and relation to myeloid-derived suppressor cells. Seminars in Immunology.

Moudra, A., Hubackova, S., Machalova, V., Vancurova, M., Bartek, J., Reinis, M., Hodny, Z., and Jonasova, A. (2016). Dynamic alterations of bone marrow cytokine landscape of myelodysplastic syndromes patients treated with 5-azacytidine. Oncoimmunology *5*.

Murray, L.M.A., and Krasnodembskaya, A.D. (2019). Concise Review: Intercellular Communication Via Organelle Transfer in the Biology and Therapeutic Applications of Stem Cells: Intercellular Communication Via Organelle Transfer. Stem Cells *37*, 14–25.

Mussai, F., De Santo, C., Abu-Dayyeh, I., Booth, S., Quek, L., McEwen-Smith, R.M., Qureshi, A., Dazzi, F., Vyas, P., and Cerundolo, V. (2013). Acute myeloid leukemia creates an arginase-dependent immunosuppressive microenvironment. Blood *122*, 749–758.

Nagaraj, S., Gupta, K., Pisarev, V., Kinarsky, L., Sherman, S., Kang, L., Herber, D.L., Schneck, J., and Gabrilovich, D.I. (2007). Altered recognition of antigen is a mechanism of CD8+ T cell tolerance in cancer. Nat Med *13*, 828–835.

Nakaya, M., Xiao, Y., Zhou, X., Chang, J.-H., Chang, M., Cheng, X., Blonska, M., Lin, X., and Sun, S.-C. (2014). Inflammatory T cell responses rely on amino acid transporter ASCT2 facilitation of glutamine uptake and mTORC1 kinase activation. Immunity *40*, 692–705.

Nandagopal, N., Ali, A.K., Komal, A.K., and Lee, S.-H. (2014). The Critical Role of IL-15–PI3K–mTOR Pathway in Natural Killer Cell Effector Functions. Front Immunol *5*.

Neijssen, J., Pang, B., and Neefjes, J. (2007). Gap junction-mediated intercellular communication in the immune system. Progress in Biophysics and Molecular Biology *94*, 207–218.

5. Bibliography

Nguyen, S., Beziat, V., Dhedin, N., Kuentz, M., Vernant, J.P., Debre, P., and Vieillard, V. (2009). HLA-E upregulation on IFN-γ-activated AML blasts impairs CD94/NKG2A-dependent NK cytolysis after haplo-mismatched hematopoietic SCT. Bone Marrow Transplant *43*, 693–699.

Nishimura, H., Nose, M., Hiai, H., Minato, N., and Honjo, T. (1999). Development of lupus-like autoimmune diseases by disruption of the PD-1 gene encoding an ITIM motif-carrying immunoreceptor. Immunity *11*, 141–151.

Nishimura, H., Okazaki, T., Tanaka, Y., Nakatani, K., Hara, M., Matsumori, A., Sasayama, S., Mizoguchi, A., Hiai, H., Minato, N., et al. (2001). Autoimmune dilated cardiomyopathy in PD-1 receptor-deficient mice. Science *291*, 319–322.

Nokin, M.-J., Durieux, F., Peixoto, P., Chiavarina, B., Peulen, O., Blomme, A., Turtoi, A., Costanza, B., Smargiasso, N., Baiwir, D., et al. (2016). Methylglyoxal, a glycolysis side-product, induces Hsp90 glycation and YAP-mediated tumor growth and metastasis. ELife Sciences *5*, e19375.

Nowbakht, P., Ionescu, M.-C.S., Rohner, A., Kalberer, C.P., Rossy, E., Mori, L., Cosman, D., Libero, G.D., and Wodnar-Filipowicz, A. (2005). Ligands for natural killer cell–activating receptors are expressed upon the maturation of normal myelomonocytic cells but at low levels in acute myeloid leukemias. Blood *105*, 3615–3622.

Oberlies, J., Watzl, C., Giese, T., Luckner, C., Kropf, P., Müller, I., Ho, A.D., and Munder, M. (2009). Regulation of NK Cell Function by Human Granulocyte Arginase. The Journal of Immunology *182*, 5259–5267.

O'Brien, K.L., and Finlay, D.K. (2019). Immunometabolism and natural killer cell responses. Nat Rev Immunol *19*, 282–290.

Okazaki, T., and Honjo, T. (2007). PD-1 and PD-1 ligands: from discovery to clinical application. International Immunology *19*, 813–824.

O'Neill, L.A.J., Kishton, R.J., and Rathmell, J. (2016). A guide to immunometabolism for immunologists. Nature Reviews Immunology *16*, 553.

Opitz, C.A., Litzenburger, U.M., Sahm, F., Ott, M., Tritschler, I., Trump, S., Schumacher, T., Jestaedt, L., Schrenk, D., Weller, M., et al. (2011). An endogenous tumour-promoting ligand of the human aryl hydrocarbon receptor. Nature *478*, 197–203.

Oppenheim, D.E., Roberts, S.J., Clarke, S.L., Filler, R., Lewis, J.M., Tigelaar, R.E., Girardi, M., and Hayday, A.C. (2005). Sustained localized expression of ligand for the activating NKG2D receptor impairs natural cytotoxicity in vivo and reduces tumor immunosurveillance. Nat. Immunol. *6*, 928–937.

Ostrand-Rosenberg, S., and Fenselau, C. (2018). Myeloid-Derived Suppressor Cells: Immune-Suppressive Cells That Impair Antitumor Immunity and Are Sculpted by Their Environment. J.I. *200*, 422–431.

OuYang, L.-Y., Wu, X.-J., Ye, S.-B., Zhang, R., Li, Z.-L., Liao, W., Pan, Z.-Z., Zheng, L.-M., Zhang, X.-S., Wang, Z., et al. (2015). Tumor-induced myeloid-derived suppressor cells promote tumor progression through oxidative metabolism in human colorectal cancer. J Transl Med *13*.

Oviedo-Orta, E., Perreau, M., Evans, W.H., and Potolicchio, I. (2010). Control of the proliferation of activated CD4+ T cells by connexins. J Leukoc Biol *88*, 79–86.

Paczulla, A.M., Rothfelder, K., Raffel, S., Konantz, M., Steinbacher, J., Wang, H., Tandler, C., Mbarga, M., Schaefer, T., Falcone, M., et al. (2019). Absence of NKG2D ligands defines leukaemia stem cells and mediates their immune evasion. Nature *572*, 254–259.

Palsson-McDermott, E.M., Curtis, A.M., Goel, G., Lauterbach, M.A.R., Sheedy, F.J., Gleeson, L.E., van den Bosch, M.W.M., Quinn, S.R., Domingo-Fernandez, R., Johnston, D.G.W., et al. (2015). Pyruvate kinase M2 regulates Hif-1α activity and IL-1β induction and is a critical determinant of the warburg effect in LPS-activated macrophages. Cell Metab. *21*, 65–80.

Pandiyan, P., Zheng, L., Ishihara, S., Reed, J., and Lenardo, M.J. (2007). CD4+CD25+Foxp3+ regulatory T cells induce cytokine deprivation–mediated apoptosis of effector CD4+ T cells. Nat Immunol *8*, 1353–1362.

Parameswaran, R., Ramakrishnan, P., Moreton, S.A., Xia, Z., Hou, Y., Lee, D.A., Gupta, K., deLima, M., Beck, R.C., and Wald, D.N. (2016). Repression of GSK3 restores NK cell cytotoxicity in AML patients. Nature Communications *7*, 1–11.

Park, S.-M., and Youn, J.-I. (2019). Role of myeloid-derived suppressor cells in immune checkpoint inhibitor therapy in cancer. Arch. Pharm. Res. *42*, 560–566.

Park, A., Lee, Y., Kim, M.S., Kang, Y.J., Park, Y.-J., Jung, H., Kim, T.-D., Lee, H.G., Choi, I., and Yoon, S.R. (2018). Prostaglandin E2 Secreted by Thyroid Cancer Cells Contributes to Immune Escape Through the Suppression of Natural Killer (NK) Cell Cytotoxicity and NK Cell Differentiation. Front. Immunol. *9*, 1859.

Park, Y.P., Choi, S.-C., Kiesler, P., Gil-Krzewska, A., Borrego, F., Weck, J., Krzewski, K., and Coligan, J.E. (2011). Complex regulation of human NKG2D-DAP10 cell surface expression: opposing roles of the γc cytokines and TGF-β1. Blood *118*, 3019–3027.

Parry, R.V., Chemnitz, J.M., Frauwirth, K.A., Lanfranco, A.R., Braunstein, I., Kobayashi, S.V., Linsley, P.S., Thompson, C.B., and Riley, J.L. (2005). CTLA-4 and PD-1 Receptors Inhibit T-Cell Activation by Distinct Mechanisms. Mol Cell Biol *25*, 9543–9553.

Pearce, E.L., and Pearce, E.J. (2013). Metabolic Pathways in Immune Cell Activation and Quiescence. Immunity *38*, 633–643.

Pearce, E.L., Poffenberger, M.C., Chang, C.-H., and Jones, R.G. (2013). Fueling Immunity: Insights into Metabolism and Lymphocyte Function. Science *342*, 1242454.

Pereira, F.V., Melo, A.C.L., Low, J.S., de Castro, Í.A., Braga, T.T., Almeida, D.C., de Lima, A.G.U.B., Hiyane, M.I., Correa-Costa, M., Andrade-Oliveira, V., et al. (2018). Metformin exerts antitumor

activity via induction of multiple death pathways in tumor cells and activation of a protective immune response. Oncotarget *9*.

Pinto, G., Brou, C., and Zurzolo, C. (2020). Tunneling Nanotubes: The Fuel of Tumor Progression? Trends in Cancer *6*, 874–888.

Porembka, M.R., Mitchem, J.B., Belt, B.A., Hsieh, C.-S., Lee, H.-M., Herndon, J., Gillanders, W.E., Linehan, D.C., and Goedegebuure, P. (2012). Pancreatic adenocarcinoma induces bone marrow mobilization of myeloid-derived suppressor cells which promote primary tumor growth. Cancer Immunol. Immunother. *61*, 1373–1385.

Pötzl, J., Roser, D., Bankel, L., Hömberg, N., Geishauser, A., Brenner, C.D., Weigand, M., Röcken, M., and Mocikat, R. (2017). Reversal of tumor acidosis by systemic buffering reactivates NK cells to express IFN-γ and induces NK cell-dependent lymphoma control without other immunotherapies. Int J Cancer *140*, 2125–2133.

Rachidi, S., Metelli, A., Riesenberg, B., Wu, B.X., Nelson, M.H., Wallace, C., Paulos, C.M., Rubinstein, M.P., Garrett-Mayer, E., Hennig, M., et al. (2017). Platelets subvert T cell immunity against cancer via GARP-TGF axis. SCIENCE IMMUNOLOGY 13.

Robert, C. (2020). A decade of immune-checkpoint inhibitors in cancer therapy. Nature Communications *11*, 3801.

Robert, C., Ribas, A., Hamid, O., Daud, A., Wolchok, J.D., Joshua, A.M., Hwu, W.-J., Weber, J.S., Gangadhar, T.C., Joseph, R.W., et al. (2017). Durable Complete Response After Discontinuation of Pembrolizumab in Patients With Metastatic Melanoma. JCO *36*, 1668–1674.

Rodriguez, P.C., Zea, A.H., Culotta, K.S., Zabaleta, J., Ochoa, J.B., and Ochoa, A.C. (2002). Regulation of T cell receptor CD3zeta chain expression by L-arginine. J Biol Chem *277*, 21123–21129.

Rodriguez, P.C., Hernandez, C.P., Quiceno, D., Dubinett, S.M., Zabaleta, J., Ochoa, J.B., Gilbert, J., and Ochoa, A.C. (2005). Arginase I in myeloid suppressor cells is induced by COX-2 in lung carcinoma. J Exp Med *202*, 931–939.

Rodriguez, P.C., Quiceno, D.G., and Ochoa, A.C. (2007). L-arginine availability regulates T-lymphocyte cell-cycle progression. Blood *109*, 1568–1573.

Rosca, M.G., Monnier, V.M., Szweda, L.I., and Weiss, M.F. (2002). Alterations in renal mitochondrial respiration in response to the reactive oxoaldehyde methylglyoxal. American Journal of Physiology - Renal Physiology *283*, F52–F59.

Ruggeri, L., Capanni, M., Urbani, E., Perruccio, K., Shlomchik, W.D., Tosti, A., Posati, S., Rogaia, D., Frassoni, F., Aversa, F., et al. (2002). Effectiveness of Donor Natural Killer Cell Alloreactivity in Mismatched Hematopoietic Transplants. Science *295*, 2097–2100.

Sabry, M., Zubiak, A., Hood, S.P., Simmonds, P., Arellano-Ballestero, H., Cournoyer, E., Mashar, M., Pockley, A.G., and Lowdell, M.W. (2019). Tumor- and cytokine-primed human natural killer cells exhibit distinct phenotypic and transcriptional signatures. PLoS One *14*.

5. Bibliography

Sade-Feldman, M., Kanterman, J., Klieger, Y., Ish-Shalom, E., Olga, M., Saragovi, A., Shtainberg, H., Lotem, M., and Baniyash, M. (2016). Clinical Significance of Circulating CD33+CD11b+HLA-DR- Myeloid Cells in Patients with Stage IV Melanoma Treated with Ipilimumab. Clin. Cancer Res. *22*, 5661–5672.

Sáez, P.J., Shoji, K.F., Aguirre, A., and Sáez, J.C. (2014). Regulation of Hemichannels and Gap Junction Channels by Cytokines in Antigen-Presenting Cells. Mediators Inflamm *2014*.

Salih, H.R., Antropius, H., Gieseke, F., Lutz, S.Z., Kanz, L., Rammensee, H.-G., and Steinle, A. (2003). Functional expression and release of ligands for the activating immunoreceptor NKG2D in leukemia. Blood *102*, 1389–1396.

Salmon, H., Idoyaga, J., Rahman, A., Leboeuf, M., Remark, R., Jordan, S., Casanova-Acebes, M., Khudoynazarova, M., Agudo, J., Tung, N., et al. (2016). Expansion and Activation of CD103 + Dendritic Cell Progenitors at the Tumor Site Enhances Tumor Responses to Therapeutic PD-L1 and BRAF Inhibition. Immunity *44*, 924–938.

Salomón, T., Sibbersen, C., Hansen, J., Britz, D., Svart, M.V., Voss, T.S., Møller, N., Gregersen, N., Jørgensen, K.A., Palmfeldt, J., et al. (2017). Ketone Body Acetoacetate Buffers Methylglyoxal via a Non-enzymatic Conversion during Diabetic and Dietary Ketosis. Cell Chem Biol *24*, 935-943.e7.

Sanchez-Correa, B., Morgado, S., Gayoso, I., Bergua, J.M., Casado, J.G., Arcos, M.J., Bengochea, M.L., Duran, E., Solana, R., and Tarazona, R. (2011). Human NK cells in acute myeloid leukaemia patients: analysis of NK cell-activating receptors and their ligands. Cancer Immunol. Immunother. *60*, 1195–1205.

Sanchez-Correa, B., Gayoso, I., Bergua, J.M., Casado, J.G., Morgado, S., Solana, R., and Tarazona, R. (2012). Decreased expression of DNAM-1 on NK cells from acute myeloid leukemia patients. Immunol Cell Biol *90*, 109–115.

Sanchez-Correa, B., Bergua, J.M., Campos, C., Gayoso, I., Arcos, M.J., Bañas, H., Morgado, S., Casado, J.G., Solana, R., and Tarazona, R. (2013). Cytokine profiles in acute myeloid leukemia patients at diagnosis: Survival is inversely correlated with IL-6 and directly correlated with IL-10 levels. Cytokine *61*, 885–891.

Sanchez-Correa, B., Campos, C., Pera, A., Bergua, J.M., Arcos, M.J., Bañas, H., Casado, J.G., Morgado, S., Duran, E., Solana, R., et al. (2016). Natural killer cell immunosenescence in acute myeloid leukaemia patients: new targets for immunotherapeutic strategies? Cancer Immunol Immunother *65*, 453–463.

Sandoval-Borrego, D., Moreno-Lafont, M.C., Vazquez-Sanchez, E.A., Gutierrez-Hoya, A., López-Santiago, R., Montiel-Cervantes, L.A., Ramírez-Saldaña, M., and Vela-Ojeda, J. (2016). Overexpression of CD158 and NKG2A Inhibitory Receptors and Underexpression of NKG2D and NKp46 Activating Receptors on NK Cells in Acute Myeloid Leukemia. Arch. Med. Res. *47*, 55–64.

Sarkar, S., Germeraad, W.T.V., Rouschop, K.M.A., Steeghs, E.M.P., van Gelder, M., Bos, G.M.J., and Wieten, L. (2013). Hypoxia induced impairment of NK cell cytotoxicity against multiple myeloma can be overcome by IL-2 activation of the NK cells. PLoS One *8*, e64835.

5. Bibliography

Savani, B.N., Mielke, S., Adams, S., Uribe, M., Rezvani, K., Yong, A.S.M., Zeilah, J., Kurlander, R., Srinivasan, R., Childs, R., et al. (2007). Rapid natural killer cell recovery determines outcome after T-cell-depleted HLA-identical stem cell transplantation in patients with myeloid leukemias but not with acute lymphoblastic leukemia. Leukemia *21*, 2145–2152.

Schlecker, E., Stojanovic, A., Eisen, C., Quack, C., Falk, C.S., Umansky, V., and Cerwenka, A. (2012). Tumor-infiltrating monocytic myeloid-derived suppressor cells mediate CCR5-dependent recruitment of regulatory T cells favoring tumor growth. J Immunol *189*, 5602–5611.

Schumacher, T.N., Scheper, W., and Kvistborg, P. (2019). Cancer Neoantigens. Annu Rev Immunol *37*, 173–200.

Serafini, P., Mgebroff, S., Noonan, K., and Borrello, I. (2008). Myeloid-derived suppressor cells promote cross-tolerance in B-cell lymphoma by expanding regulatory T cells. Cancer Res *68*, 5439–5449.

Sethna, M.P., van Perijs, L., Sharpe, A.H., Abbas, A.K., and Freemant, G.J. (1994). A negative regulatory function of B7 revealed in B7-1 transgenic mice. Immunity *1*, 415–421.

Shallis, R.M., Wang, R., Davidoff, A., Ma, X., and Zeidan, A.M. (2019). Epidemiology of acute myeloid leukemia: Recent progress and enduring challenges. Blood Reviews *36*, 70–87.

Shankaraiah, R.C., Callegari, E., Guerriero, P., Rimessi, A., Pinton, P., Gramantieri, L., Silini, E.M., Sabbioni, S., and Negrini, M. (2019). Metformin prevents liver tumourigenesis by attenuating fibrosis in a transgenic mouse model of hepatocellular carcinoma. Oncogene *38*, 7035–7045.

Sharma, S., Yang, S.-C., Zhu, L., Reckamp, K., Gardner, B., Baratelli, F., Huang, M., Batra, R.K., and Dubinett, S.M. (2005). Tumor cyclooxygenase-2/prostaglandin E2-dependent promotion of FOXP3 expression and CD4+ CD25+ T regulatory cell activities in lung cancer. Cancer Res *65*, 5211–5220.

Shyer, J.A., Flavell, R.A., and Bailis, W. (2020). Metabolic signaling in T cells. Cell Research *30*, 649–659.

Sibbersen, C., Schou Oxvig, A.-M., Bisgaard Olesen, S., Nielsen, C.B., Galligan, J.J., Jørgensen, K.A., Palmfeldt, J., and Johannsen, M. (2018). Profiling of Methylglyoxal Blood Metabolism and Advanced Glycation End-Product Proteome Using a Chemical Probe. ACS Chem. Biol. *13*, 3294–3305.

Snijdewint, F.G., Kaliński, P., Wierenga, E.A., Bos, J.D., and Kapsenberg, M.L. (1993). Prostaglandin E2 differentially modulates cytokine secretion profiles of human T helper lymphocytes. J Immunol *150*, 5321–5329.

Srivastava, M.K., Sinha, P., Clements, V.K., Rodriguez, P., and Ostrand-Rosenberg, S. (2010). Myeloid-derived suppressor cells inhibit T-cell activation by depleting cystine and cysteine. Cancer Res *70*, 68–77.

Stringaris, K., Sekine, T., Khoder, A., Alsuliman, A., Razzaghi, B., Sargeant, R., Pavlu, J., Brisley, G., Lavallade, H. de, Sarvaria, A., et al. (2014). Leukemia-induced phenotypic and functional defects in natural killer cells predict failure to achieve remission in acute myeloid leukemia. Haematologica *99*, 836.

5. Bibliography

Surman, D.R., Dudley, M.E., Overwijk, W.W., and Restifo, N.P. (2000). Cutting edge: CD4+ T cell control of CD8+ T cell reactivity to a model tumor antigen. J Immunol *164*, 562–565.

Szczepanski, M.J., Szajnik, M., Welsh, A., Foon, K.A., Whiteside, T.L., and Boyiadzis, M. (2010). Interleukin-15 enhances natural killer cell cytotoxicity in patients with acute myeloid leukemia by upregulating the activating NK cell receptors. Cancer Immunol Immunother *59*, 73–79.

Tajima, F., Kawatani, T., Endo, A., and Kawasaki, H. (1996). Natural killer cell activity and cytokine production as prognostic factors in adult acute leukemia. Leukemia *10*, 478–482.

Takahashi, T., Tagami, T., Yamazaki, S., Uede, T., Shimizu, J., Sakaguchi, N., Mak, T.W., and Sakaguchi, S. (2000). Immunologic Self-Tolerance Maintained by CD25ƨCD4ƨ Regulatory T Cells Constitutively Expressing Cytotoxic T Lymphocyte–associated Antigen 4. 7.

Talmadge, J.E., and Gabrilovich, D.I. (2013). History of myeloid-derived suppressor cells. Nat Rev Cancer *13*, 739–752.

Tanaka, A., and Sakaguchi, S. (2017). Regulatory T cells in cancer immunotherapy. Cell Research *27*, 109–118.

Tang, L., Wu, J., Li, C.-G., Jiang, H.-W., Xu, M., Du, M., Yin, Z., Mei, H., and Hu, Y. (2020). Characterization of Immune Dysfunction and Identification of Prognostic Immune-related Risk Factors in Acute Myeloid Leukemia. Clin Cancer Res clincanres.3003.2019.

Tannahill, G.M., Curtis, A.M., Adamik, J., Palsson-McDermott, E.M., McGettrick, A.F., Goel, G., Frezza, C., Bernard, N.J., Kelly, B., Foley, N.H., et al. (2013). Succinate is an inflammatory signal that induces IL-1β through HIF-1α. Nature *496*, 238–242.

Teeter, M.E., Baginsky, M.L., and Hatefi, Y. (1969). Ectopic inhibition of the complexes of the electron transport system by rotenone, piericidin A, demerol and antimycin A. Biochim Biophys Acta *172*, 331–333.

Tesi, R.J. (2019). MDSC; the Most Important Cell You Have Never Heard Of. Trends in Pharmacological Sciences *40*, 4–7.

Thomas, D.A., and Massagué, J. (2005). TGF-β directly targets cytotoxic T cell functions during tumor evasion of immune surveillance. Cancer Cell *8*, 369–380.

Tivol, E.A., Borriello, F., Schweitzer, A.N., Lynch, W.P., Bluestone, J.A., and Sharpe, A.H. (1995). Loss of CTLA-4 leads to massive lymphoproliferation and fatal multiorgan tissue destruction, revealing a critical negative regulatory role of CTLA-4. Immunity *3*, 541–547.

Tratkiewicz, J.A., and Szer, J. (1990). Loss of natural killer activity as an indicator of relapse in acute leukaemia. Clinical & Experimental Immunology *80*, 241–246.

Tremblay-McLean, A., Coenraads, S., Kiani, Z., Dupuy, F.P., and Bernard, N.F. (2019). Expression of ligands for activating natural killer cell receptors on cell lines commonly used to assess natural killer cell function. BMC Immunol *20*.

Tseng, C.-H. (2017). Metformin and lung cancer risk in patients with type 2 diabetes mellitus. Oncotarget *8*, 41132–41142.

Tseng, C.-H. (2018). Metformin and risk of developing nasopharyngeal cancer in patients with type 2 diabetes mellitus. Metabolism *85*, 223–226.

Viel, S., Marçais, A., Guimaraes, F.S.-F., Loftus, R., Rabilloud, J., Grau, M., Degouve, S., Djebali, S., Sanlaville, A., Charrier, E., et al. (2016). TGF-β inhibits the activation and functions of NK cells by repressing the mTOR pathway. Sci. Signal. *9*, ra19–ra19.

Vuk-Pavlović, S., Bulur, P.A., Lin, Y., Qin, R., Szumlanski, C.L., Zhao, X., and Dietz, A.B. (2010). Immunosuppressive CD14+HLA-DRlow/− monocytes in prostate cancer. The Prostate *70*, 443–455.

Wang, L., Chang, E.W.Y., Wong, S.C., Ong, S.-M., Chong, D.Q.Y., and Ling, K.L. (2013a). Increased myeloid-derived suppressor cells in gastric cancer correlate with cancer stage and plasma S100A8/A9 proinflammatory proteins. J. Immunol. *190*, 794–804.

Wang, T., Douglass, E.F., Fitzgerald, K.J., and Spiegel, D.A. (2013b). A "Turn-On" Fluorescent Sensor for Methylglyoxal. J. Am. Chem. Soc. *135*, 12429–12433.

Waterhouse, P., Penninger, J.M., Timms, E., Wakeham, A., Shahinian, A., Lee, K.P., Thompson, C.B., Griesser, H., and Mak, T.W. (1995). Lymphoproliferative disorders with early lethality in mice deficient in Ctla-4. Science *270*, 985–988.

Weber, J., Gibney, G., Kudchadkar, R., Yu, B., Cheng, P., Martinez, A.J., Kroeger, J., Richards, A., McCormick, L., Moberg, V., et al. (2016). Phase I/II Study of Metastatic Melanoma Patients Treated with Nivolumab Who Had Progressed after Ipilimumab. Cancer Immunol Res *4*, 345–353.

Weber, M., Lupp, C., Stein, P., Kreft, A., Bopp, T., Wehler, T.C., Schmitt, E., Schild, H., and Radsak, M.P. (2013). Mechanisms of Cyclic Nucleotide Phosphodiesterases in Modulating T Cell Responses in Murine Graft-versus-Host Disease. PLoS One *8*.

Weber, R., Fleming, V., Hu, X., Nagibin, V., Groth, C., Altevogt, P., Utikal, J., and Umansky, V. (2018). Myeloid-Derived Suppressor Cells Hinder the Anti-Cancer Activity of Immune Checkpoint Inhibitors. Front. Immunol. *9*.

Weide, B., Martens, A., Zelba, H., Stutz, C., Derhovanessian, E., Giacomo, A.M.D., Maio, M., Sucker, A., Schilling, B., Schadendorf, D., et al. (2014). Myeloid-Derived Suppressor Cells Predict Survival of Patients with Advanced Melanoma: Comparison with Regulatory T Cells and NY-ESO-1- or Melan-A–Specific T Cells. Clin Cancer Res *20*, 1601–1609.

Weiskirchen, R., Weimer, J., Meurer, S.K., Kron, A., Seipel, B., Vater, I., Arnold, N., Siebert, R., Xu, L., Friedman, S.L., et al. (2013). Genetic characteristics of the human hepatic stellate cell line LX-2. PLoS ONE *8*, e75692.

Weston, C.J., Shepherd, E.L., Claridge, L.C., Rantakari, P., Curbishley, S.M., Tomlinson, J.W., Hubscher, S.G., Reynolds, G.M., Aalto, K., Anstee, Q.M., et al. (2015). Vascular adhesion protein-1 promotes liver inflammation and drives hepatic fibrosis. J Clin Invest *125*, 501–520.

5. Bibliography

Wheaton, W.W., Weinberg, S.E., Hamanaka, R.B., Soberanes, S., Sullivan, L.B., Anso, E., Glasauer, A., Dufour, E., Mutlu, G.M., Budigner, G.S., et al. (2014). Metformin inhibits mitochondrial complex I of cancer cells to reduce tumorigenesis. Elife *3*, e02242.

Wong, S.B.J., Bos, R., and Sherman, L.A. (2008). Tumor-specific CD4+ T cells render the tumor environment permissive for infiltration by low-avidity CD8+ T cells. J Immunol *180*, 3122–3131.

World Health Organization (2020). Cancer Fact Sheet (International Agency for Research on Cancer).

Worthington, J.J., Kelly, A., Smedley, C., Bauché, D., Campbell, S., Marie, J.C., and Travis, M.A. (2015). Integrin αvβ8-Mediated TGF-β Activation by Effector Regulatory T Cells Is Essential for Suppression of T-Cell-Mediated Inflammation. Immunity *42*, 903–915.

WU, H., LI, P., SHAO, N., MA, J., JI, M., SUN, X., MA, D., and JI, C. (2012). Aberrant expression of Treg-associated cytokine IL-35 along with IL-10 and TGF-β in acute myeloid leukemia. Oncol Lett *3*, 1119–1123.

Xu, J., and Niu, T. (2020). Natural killer cell-based immunotherapy for acute myeloid leukemia. J Hematol Oncol *13*.

Yang, W.-T., Yang, H.-J., Zhou, J.-G., and Liu, J.-L. (2020). Relationship between metformin therapy and risk of colorectal cancer in patients with diabetes mellitus: a meta-analysis. Int J Colorectal Dis *35*, 2117–2131.

Yoong, K.F., McNab, G., Hübscher, S.G., and Adams, D.H. (1998). Vascular Adhesion Protein-1 and ICAM-1 Support the Adhesion of Tumor-Infiltrating Lymphocytes to Tumor Endothelium in Human Hepatocellular Carcinoma. The Journal of Immunology *160*, 3978–3988.

Young, M.R., Wright, M.A., Matthews, J.P., Malik, I., and Prechel, M. (1996). Suppression of T cell proliferation by tumor-induced granulocyte-macrophage progenitor cells producing transforming growth factor-beta and nitric oxide. J Immunol *156*, 1916–1922.

Zaiatz-Bittencourt, V., Finlay, D.K., and Gardiner, C.M. (2018). Canonical TGF-β Signaling Pathway Represses Human NK Cell Metabolism. J.I. *200*, 3934–3941.

Zajac, M., Zaleska, J., Dolnik, A., Siwiec, A., Jankowska-Lecka, O., Mlak, R., Ciesielka, M., Gromek, T., Sokolowska, B., Grzasko, N., et al. (2016). Analysis of the PD-1/PD-L1 Axis Points to Association of Unfavorable Recurrent Mutations with PD-L1 Expression in AML. Blood *128*, 1685–1685.

Zhang, Z.-J., Bi, Y., Li, S., Zhang, Q., Zhao, G., Guo, Y., and Song, Q. (2014). Reduced risk of lung cancer with metformin therapy in diabetic patients: a systematic review and meta-analysis. Am J Epidemiol *180*, 11–14.

6. Appendix

6.1 Table of Figures

6.2 Table of Abbreviations

Abbreviation	Definition
2-DG	2-deoxy-D-glucose
2-NBDG	2-N-(7-Nitrobenz-2-oxa-1,3-diazol-4yl)-Amino)-2-Deoxyglucose
7-AAD	7-Aminoactinomycin D
AA	Amino acids
AGPs	Advanced glycation end products
AKT	Proteinkinase B
AML	Acute myeloid leukemia
AMPK	AMP-activated protein kinase
AOC3	Gene coding for SSAO
APC	Antigen presenting cell
ARG1	Arginase 1
ATP	Adenosine triphosphate
cAMP	cyclic adenosine monophosphate
CAR (T cell)	Chimeric antigen receptor (T cell)
CD(X)	Cluster of differentiation (X)
cDC1	Conventional type 1 dendritic cells
CFSE	Carboxyfluorescein succinimidyl ester
cGAMP	cyclic guanosine monophosphate-adenosine monophosphate
CM (T cell)	Central memory (T cell)
COX1/2	Cyclooxygenase 1/2
CTLA-4	Cytotoxic T-lymphocyte-associated protein 4
Cx43	Connexin 43kDa
DAMP	Damage-associated molecular pattern
DHAP	Dihydroxyacetone phosphate
DilC1(5)	1,1’,3,3,3’,3’-Hexamethylindodicarbocyanine iodide
DMBG	Dimethylbiguanide
DNA	Deoxyribonucleic acid
DNAM-1	DNAX accessory molecule-1
ECAR	Extracellular acidification rate
ELISA	Enzyme-linked immunosorbent assay
EM (T cell)	Effector memory (T cell)
ERK1/2	Extracellular regulated kinase-1/2
FACS	Fluorescent-activated cell sorting
FAO	Fatty acid oxidation
FAS	Fatty acid synthesis
FBS	Fetal bovine serum
FDA	Food and Drug Administration (US)
FOXP3	Forkhead box P3

FSC	Forward scatter (in flow cytometry)
GAPDH	Glyceraldehyde 3-phosphate dehydrogenase
G-CSF	Granulocyte colony stimulating factor
GFP	Green fluorescent protein
GJ	Gab junction
GLO1	Gene coding for glyoxalase 1
Glut-1	Glucose transporter type 1
GM-CSF	Granulocyte macrophage colony stimulating factor
GSH	Reduced glutathione
GSSG	Oxidized glutathione
GzmB	Granzyme B
HCC	Hepatocellular carcinoma
HCV	Hepatitis C virus
HIF1α	hypoxia inducible factor 1
HIV	Human immunodeficiency virus
HLA	Human leukocyte antigen
HMGB1	High mobility group box protein 1
HSC	Hepatic stellate cells
Hsp27/90	Heat shock protein 27/90
ICB	Immune checkpoint blockade (therapy)
ICS	Intracellular cytokine staining
IDO	Indoleamine-2,3-dioxygenase
IFN-γ	Interferon gamma
IHC	Immunohistochemistry
IL-(X)	Interleukin (X)
iNOS	Inducible nitric oxid synthase
IP3	inositol triphosphate
kDA	Kilodalton
KIR	Killer immunoglobulin-like receptors
LAP	Latency-associated peptide
LCK	Lymphocyte-specific protein tyrosine kinase
LDH	Lactate dehydrogenase
L-NMMA	L-NG-monomethyl arginine
MACS	Magnetic activated cell sorting
MBo	Methyl diaminobenzene-BODIPY
MCT	Monocarboxylate transporters
MDSC	Myeloid-derived suppressor cell
MG-H1	Methylglyoxal 5-hydro-5-methylimidazolones
MGO	Methylglyoxal
M-MDSC	Monocytic myeloid-derived suppressor cell
mRNA	Messenger RNA

MT green	MitoTracker green
mTOR	Mammalian target of rapamycin
mTORC1	mTOR complex 1
MYC	(Cellular) myelocytomatosis
NAFLD	Non-alcoholic fatty liver disease
NASH	Non-alcoholic steatohepatitis
NK (cell)	Natural killer (cell)
NKG2D	Natural killer group 2D
NKp30 / NCR3	Natural cytotoxicity triggering receptor 3
NKp46 / NCR1	Natural cytotoxicity triggering receptor 1
NKT (cell)	Natural killer T (cell)
NO	Nitric oxide
Nor-NOHA	N-Hydroxy-nor-arginine
OCR	Oxygen consumption rate
OVA	Ovalbumin
OXPHOS	Oxidative phosphorylation
PBMCs	Peripheral blood mononuclear cells
PBS	Phosphate buffered saline
PD-1	Programmed cell death protein 1
PD-L1	Programmed cell death ligand 1
PEP	Phosphoenolpyruvate
pERK	Phosphorylated ERK
PGE2	Prostaglandin E2
PI	Propidium Iodide
PKM2	Pyruvate kinase M2
PMN-MDSCs	Polymorphonuclear myeloid-derived suppressor cells
pmTOR	Phosphorylated mTOR
PPAR-γ	Peroxisome proliferator-activated receptor gamma
PPP	Pentose phosphate pathway
pS6	Phosphorylated S6
qPCR	Quantitative polymerase chain reaction
RNA	Ribonucleic acid
ROS	Reactive oxygen species
S6	Ribosomal protein S6
SLC1A5	Solute carrier family 1 member 5
SRC	Spare respiratory capacity
SSAO	Semicarbazide-sensitive amine oxidase (= VAP-1)
SSC	Side scatter (in flow cytometry)
T2D	Type 2 diabetes mellitus
TCA	Tricarboxylic acid cycle
TCR	T cell receptor

TETD	Tetraethylthiuram disulfide
TGF-β	Transforming growth factor beta
T_H1/2/17	T helper cell type 1/2/17
TILs	Tumor-infiltrating lymphocytes
TLR	Toll-like receptor
TMB	Tumor mutational burden
TME	Tumor microenvironment
TNF	Tumor necrosis factor
TNT	Tunneling Nanutube
Treg	Regulatory T cell
UHPLC-TOF-DIA-MS/MS	Ultrahigh performance liquid chromatography with time-of-flight tandem mass spectrometry and data independent acquisition
UTR	Untranslated region (mRNA)
UV	Ultraviolet (light)
VAP-1	Vascular adehsion protein 1 (= SSAO)
VEGF	Vascular endothelial growth factor
WHO	World Health Organization
WT	Wild type (mice)
ZAP70	Zeta chain of T cell receptor associated protein kinase 70kDa
αGalCer	alpha-Galactosylceramide
αSMA	Alpha smooth muscle actin

6.3 Publications

Baumann, T., Dunkel, A., Schmid, C., Schmitt, S., Hiltensperger, M., Lohr, K., Laketa, V., Donakonda, S., Ahting, U., Lorenz-Depiereux, B., et al. (2020). Regulatory myeloid cells paralyze T cells through cell–cell transfer of the metabolite methylglyoxal. Nature Immunology *21*, 555–566.

Chen, S., Kammerl, I.E., Vosyka, O., Baumann, T., Yu, Y., Wu, Y., Irmler, M., Overkleeft, H.S., Beckers, J., Eickelberg, O., et al. (2016). Immunoproteasome dysfunction augments alternative polarization of alveolar macrophages. Cell Death and Differentiation.

6.4 Poster presentations

Baumann T., Krupka C., Lindl B., Knolle P. A., Marion Subklewe M., Höchst B. "Investigation on the suppressive effect of AML blasts on NK cells". Poster presentation on DGfI Meeting 2017, Erlangen, Germany

Heine A. Flores C., Gevensleben H., Diehl L., Heikenwalder M., Ringelhan M., Janssen K-P., Nitsche U., Garbi N., Brossart P., Baumann T., Knolle P.A., Kurts C. and Höchst B. "Targeting myeloid derived suppressor cells with all-trans retinoic acid is highly time-dependent in therapeutic tumor vaccination". Poster presentation on ECI Meeting 2018, Amsterdam, Netherlands